

The Riemann problem for fluid flow of real materials

Ralph Menikoff

Theoretical Division, Los Alamos National Laboratory, Los Alamos, New Mexico 87545

Bradley J. Plohr

Computer Sciences Department and Center for the Mathematical Sciences, University of Wisconsin, Madison, Wisconsin 53706

The Riemann problem for fluid flow of real materials is examined. An arbitrary equation of state is allowed, subject only to the physical requirements of thermodynamics. The properties of the isentropes and the shock Hugoniot loci that follow from conditions imposed on the equation of state are reviewed systematically. Important properties of these wave curves are determined by three dimensionless variables characterizing the equation of state: the adiabatic exponent γ , the Grüneisen coefficient Γ , and the fundamental derivative \mathcal{G} . Standard assumptions on these variables break down near phase transitions. The result is an anomalous wave structure: either shock waves split into multiple waves, or composite waves form. Additional questions related to shock stability and nonuniqueness of the solution of the Riemann problem are discussed.

CONTENTS

I. Introduction	75
II. Mathematical Formulation and Physical Constraints	77
A. Dynamical equations	77
B. Equation of state	77
C. Thermodynamic constraints	79
D. Domain of state space	80
E. Asymptotic conditions	82
F. Incomplete equation of state	83
III. One-Dimensional Scale-Invariant Flows	84
A. Rarefaction waves	84
B. Shock waves and contact discontinuities	86
C. Composite and split waves	87
D. Wave curves and the Riemann problem	89
IV. Properties of Shock Curves	90
A. Local structure	91
B. Asymptotic properties	92
C. Monotonicity properties	94
V. Anomalous Wave Structure Caused by Phase Transition	99
A. Behavior of isentropes and Hugoniot loci at saturation boundaries	100
B. Anomalous wave structure caused by kinks	102
C. Anomalous wave structure caused by smooth loss of convexity	105
D. Overlap of isentropes in the P - V plane	108
E. Summary of anomalies	109
VI. Shock Instabilities and Nonuniqueness of Solutions	109
VII. A Model Equation of State	113
VIII. Summary	117
Acknowledgments	118
Appendix A: Thermodynamic Identities	118
Appendix B: Wave Curves for General Conservation Laws	121
Appendix C: Shock Profiles and Admissibility Conditions	124
References	128

I. INTRODUCTION

Fluid dynamics has been the paradigm for systems of hyperbolic conservation laws since the pioneering work of Riemann (1860). It provides the motivation for many of the central ideas in the analysis of quasilinear hyperbolic partial differential equations. Among them are the

following. (1) The need to consider discontinuous solutions. Even with smooth initial data, the solution may develop discontinuities within a finite time. (2) The need to impose "entropy" conditions. Without such conditions, the initial value problem has multiple discontinuous solutions. (3) The advantage in viewing solutions of conservation laws in terms of elementary wave patterns, such as shock and rarefaction waves. As a prototypical example, fluid dynamics has inspired the important work of Lax (1957) in generalizing concepts from fluid dynamics to systems of hyperbolic conservation laws. It has raised many interesting mathematical questions about quasilinear partial differential equations (see, e.g., Gelfand, 1959; Oleinik, 1965; and Lax, 1972).

The dynamical evolution of a fluid is determined by the principles of conservation of mass, momentum, and energy. To obtain a complete mathematical description, however, the conservation laws must be supplemented by constitutive relations that characterize the material properties of the fluid. Material properties strongly influence the structure and dynamics of waves in any continuum-mechanical system; this influence is the focus of study in this paper. Constitutive relations are understood at the most fundamental level for fluids, where they are embodied in an equilibrium equation of state (EOS), because physical principles of thermodynamics impose stringent constraints on the equation of state. Therefore it is important to explore the full range of physical phenomena that occur in fluid dynamics and to discern the implications for general systems of conservation laws.

Riemann studied fluid dynamics through the shock-tube experiment. More generally, a Riemann problem for a system of conservation laws is an initial value problem such that the initial data are scale invariant (i.e., constant on rays). Riemann problems play a key role in understanding the wave structure of hyperbolic partial differential equations. They are important also for numerical algorithms for solving these equations, such as the Godunov method (Godunov, 1959) and its descendants (van Leer, 1979; Colella and Woodward, 1984;

Colella, 1985), the random choice method (Glimm, 1965; Moler and Smoller, 1970; Chorin, 1976; Plohr, 1988a), and the front tracking method (Chern *et al.*, 1985; Glimm *et al.*, 1985; Chern and Colella, 1987). This is because general fluid flows may be pictured as nonlinear superpositions of Riemann solutions. These solutions, in turn, are composed of elementary waves that propagate as separate entities. Elementary waves, whose interactions are determined by Riemann problems, also reflect the asymptotic behavior of general solutions. Therefore the influence of an equation of state on the structure of waves may be studied through Riemann problems.

In the simplest case, a polytropic ideal gas, the structure of elementary waves and the solutions of Riemann problems can be determined analytically (Courant and Friedrichs, 1948; Landau and Lifshitz, 1959). Bethe (1942) and Weyl (1949) have extended this analysis to include more general equations of state. Physical principles of thermodynamics require the equation of state to satisfy certain convexity constraints and to have appropriate asymptotic properties. In the standard analysis, however, certain conditions are imposed on the equation of state beyond the demands of thermodynamics. Weyl's conditions require the isentropes to be convex and not to intersect in the pressure-volume plane; Bethe's conditions are slightly weaker. For fluids satisfying the standard assumptions, a solution of a Riemann problem for one-dimensional flow consists of a left-facing shock or rarefaction wave, a right-facing shock or rarefaction wave, and a contact discontinuity separating them. The waves in a solution may be determined graphically by intersecting wave curves in the pressure-velocity plane. It follows from asymptotic properties of the equation of state that a solution of a Riemann problem always exists. Bethe imposed an additional condition on the equation of state that is sufficient to guarantee uniqueness of the Riemann solution. More generally, uniqueness of solutions depends on the monotonicity of the wave curves; conditions on the equation of state that are necessary and sufficient for uniqueness of solutions have been analyzed by Smith (1979).

Even though the standard assumptions are valid for real materials in most of the state space, they are not universally valid. In particular, experiments (Duvall and Graham, 1977) have shown that the additional assumptions of the standard theory are not satisfied by materials near a phase transition. Without the standard assumptions, the wave propagation speed may not vary monotonically along a wave curve, which results in anomalous wave structures; waves that are composites of shock and rarefaction waves (Wendroff, 1972) and shock waves that split into multiple waves (Rice *et al.*, 1958). Similar wave structures arise in scalar conservation laws (Gelfand, 1959; Oleinik, 1959), and their occurrence in general systems of conservation laws has been studied (Liu, 1975). Thus several interesting physical effects are excluded when the standard assumptions are imposed. This is an important point because many numerical algorithms for solving Riemann problems (see, e.g., Colella

and Glaz, 1985; Dukowicz, 1985) make these, or stronger, assumptions. Furthermore, numerical errors in the equation of state are sometimes indistinguishable from real physical effects, such as phase transitions.

This paper describes the wave structure in fluids governed by the most general equations of state allowed by thermodynamics. It offers a comprehensive synthesis of the existing theory, together with several extensions. The emphasis is on providing physical motivation for the mathematical assumptions made about the equation of state, and on clarifying the profound influence that the EOS has on the qualitative structure of wave solutions. The discussion includes relaxing the hypotheses in the classical Bethe-Weyl analysis of shock waves; unifying and extending the treatment of monotonicity properties for shock curves and the relationship with uniqueness for the Riemann problem; analyzing wave curves at points where they suffer kinks caused by phase transitions; extending the Bethe-Wendroff theorem to composite waves and applying it to wave speed diagrams; relating nonuniqueness for one-dimensional Riemann problems to instability of multidimensional shock fronts, as well as identifying a thermodynamic criterion for stability; and analyzing a model EOS that exhibits anomalous behavior.

We begin in Sec. II with the mathematical description of fluid flow and the constraints imposed by physical principles. Included is a detailed analysis of the equation of state: its characterization by dimensionless parameters, the structure of its domain, and its local and asymptotic properties. Of particular importance is the relationship between convexity and phase transitions. In Sec. III the elementary waves that occur in fluids (the standard rarefaction and shock waves, and the anomalous composite and split waves) are defined. Then we describe how one-parameter families of elementary waves form wave curves that are used to construct solutions of Riemann problems. In Sec. IV we analyze the local structure, asymptotic behavior, and monotonicity properties of the Hugoniot locus, as they are related to conditions on the equation of state. The asymptotic behavior relates to the existence of solutions of Riemann problems, while monotonicity properties determine whether the solution is unique. Anomalous wave behavior that is associated with phase transitions is described in Sec. V. To obtain physical solutions, standard elementary waves that are unstable or inadmissible must be replaced by composite or split waves; then Riemann problems can be solved using wave curves in the same manner as for the standard case. In Sec. VI we discuss the relationship between shock instability and nonuniqueness of solutions of Riemann problems. One-dimensional solutions, when treated as multidimensional solutions with planar symmetry, may exhibit instabilities unless the equation of state satisfies an additional condition; this condition also results in uniqueness for Riemann solutions. In Sec. VII an example of an equation of state is presented to illustrate how seemingly reasonable models for real materials may exhibit unphysical behavior. Determining the range

of validity of an equation of state is important for numerical calculations. In Sec. VIII we conclude by summarizing our results and by mentioning several important open problems. Three appendixes are included: Appendix A summarizes the thermodynamic identities that are used in the discussion of the equation of state; Appendix B describes some properties of rarefaction and shock curves in the context of general conservation laws; and Appendix C contains supplementary material on viscous profiles for shock waves.

II. MATHEMATICAL FORMULATION AND PHYSICAL CONSTRAINTS

In this section we present the mathematical formulation for a continuum-mechanical description of a fluid material. There are two components in this description: the dynamical equations and the constitutive relations. The dynamical equations form a system of quasilinear hyperbolic partial differential equations that embody the conservation of mass, momentum, and energy. The constitutive relations, i.e., the EOS, defines the equilibrium thermodynamic properties of the material.

The qualitative character of the solutions of the conservation laws depends crucially on the thermodynamic properties of the material. Therefore we are careful to determine the constraints imposed on the EOS by the postulates of thermodynamics and to describe the physical motivation for further assumptions. The local properties of the EOS are specified by dimensionless derivatives of the energy function, while the global properties are determined by the asymptotic behavior of the energy.

Our model for fluid flow neglects such physical effects as viscosity, heat conduction, and radiation. As a result, the dynamics require only partial specification of the thermodynamics of the material, as contained in an incomplete EOS. In practice the incomplete EOS is rarely calculated from a complete, thermodynamically consistent EOS, and it is difficult to determine whether a given incomplete EOS arises from one. Whether an EOS correctly models a real material is, however, reflected in the solutions of the conservation laws; this motivates our study of wave structure in the Riemann problem.

A. Dynamical equations

In continuum mechanics the state of the material is characterized by several macroscopic variables. The principal ones are the mass density ρ , the specific internal energy E , and the particle velocity \mathbf{u} ; in addition, there may be internal state variables that describe the microscopic structure of the material, such as the relative concentrations of phases in multiphase flow. The evolution of the material is governed by the equations of conservation of mass, linear momentum, and energy:

$$\partial_t \rho + \nabla \cdot (\rho \mathbf{u}) = 0 , \quad (2.1)$$

$$\partial_t (\rho \mathbf{u}) + \nabla \cdot (\rho \mathbf{u} \mathbf{u}) + \nabla P = \nabla \cdot \Sigma , \quad (2.2)$$

$$\partial_t (\rho \mathcal{E}) + \nabla \cdot (\rho \mathcal{E} \mathbf{u}) + \nabla \cdot (P \mathbf{u}) = \nabla \cdot (\Sigma \cdot \mathbf{u}) - \nabla \cdot \mathbf{q} , \quad (2.3)$$

where $\mathcal{E} = \frac{1}{2} |\mathbf{u}|^2 + E$ is the total specific energy, P is the pressure, Σ is the extra stress tensor (containing, e.g., a Newtonian viscosity term), and \mathbf{q} is the heat flux. These equations are supplemented by dynamical evolution equations for the internal state variables (for instance, conservation of mass for each phase), and by constitutive equations relating P , Σ , and \mathbf{q} to ρ , E , \mathbf{u} , and the internal state variables.

For many applications the effects of viscosity, heat conduction, radiation, chemical reactions, relaxation, material strength, etc., either may be neglected or are not the focus of attention. In such situations it would seem appropriate to take P to be the equilibrium thermodynamic pressure and to make the approximations $\Sigma = 0$ and $\mathbf{q} = 0$. However, care must be exercised; the limiting equations admit solutions that do not resemble physical solutions, so the equation must be supplemented with conditions that exclude the unphysical solutions. These extra conditions should mimic the physical effects that are not fully modeled. In the standard theory of gas dynamics, simple rules such as the Lax (1957) characteristic criterion, or the requirement that entropy should not decrease, suffice to isolate physically reasonable solutions. In general, however, more intricate admissibility criteria are needed, such as requiring existence for viscous profiles (see Appendix C) or stability with respect to multidimensional perturbations (see Sec. VI). No general theory for defining appropriate conditions exists; this remains an important open problem. Having said this, we will restrict our attention to the inviscid flow equations that model equilibrium hydrodynamics:

$$\partial_t \rho + \nabla \cdot (\rho \mathbf{u}) = 0 , \quad (2.4)$$

$$\partial_t (\rho \mathbf{u}) + \nabla \cdot (\rho \mathbf{u} \mathbf{u}) + \nabla P = 0 , \quad (2.5)$$

$$\partial_t (\rho \mathcal{E}) + \nabla \cdot (\rho \mathcal{E} \mathbf{u}) + \nabla \cdot (P \mathbf{u}) = 0 , \quad (2.6)$$

where P is the equilibrium thermodynamic pressure. The pressure must be specified through a constitutive relation, the EOS, which characterizes the fluid material.

Remark. A major theme of this paper is the way the EOS affects flow dynamics. The dynamics are not solely determined by the form of Eqs. (2.4)–(2.6), but also by properties of P . For example, the equations for some models of viscoelastic fluids (Malkus *et al.*, 1988; Plohr, 1988b) take a form identical to Eqs. (2.4)–(2.6), but the domain of state space and the behavior of P are different from those of standard fluid dynamics. As a consequence, the dynamical behavior differs significantly from that of an ordinary fluid.

B. Equation of state

The thermodynamic properties of a material are embodied in the relation $E = E(V, S)$ expressing the specific internal energy E of an equilibrium state as a function of the specific entropy S and the specific volume $V = 1/\rho$.

Before formulating thermodynamic constraints on the domain of definition, smoothness, and asymptotic behavior of E , we introduce terminology for various derivatives of E in terms of which we will express the constraints.

The pressure $P = P(V, S)$ and the temperature $T = T(V, S)$ are given as first derivatives of E :

$$P(V, S) = -\frac{\partial E}{\partial V} \Big|_S \quad \text{and} \quad T(V, S) = \frac{\partial E}{\partial S} \Big|_V, \quad (2.7)$$

in accordance with the fundamental thermodynamic identity

$$dE = -P dV + T dS \quad (2.8)$$

(which combines the first and second laws of thermodynamics). Higher-order derivatives of E also play an important role in the fluid dynamics of the material. As described in Appendix A, any of the second derivatives of the thermodynamic potentials may be written in terms of quantities that are directly measurable, viz., the specific heats at constant volume and pressure,

$$C_V = T \frac{\partial S}{\partial T} \Big|_V \quad \text{and} \quad C_P = T \frac{\partial S}{\partial T} \Big|_P, \quad (2.9)$$

the isentropic and isothermal compressibilities,

$$K_S = -\frac{1}{V} \frac{\partial V}{\partial P} \Big|_S \quad \text{and} \quad K_T = -\frac{1}{V} \frac{\partial V}{\partial P} \Big|_T, \quad (2.10)$$

and the coefficient of thermal expansion,

$$\beta = \frac{1}{V} \frac{\partial V}{\partial T} \Big|_P. \quad (2.11)$$

Because two identities,

$$\frac{K_S}{K_T} = 1 - \frac{\beta^2 V T}{C_P K_T} = \frac{C_V}{C_P}, \quad (2.12)$$

relate these five measurable quantities, only three of them are independent.

We will find it convenient to work with the following dimensionless combinations of second derivatives (Davis, 1985):

$$\gamma = \frac{V}{P} \frac{\partial^2 E}{\partial V^2} \Big|_S = \frac{1}{PK_S}, \quad (2.13)$$

$$\Gamma = -\frac{V}{T} \frac{\partial^2 E}{\partial S \partial V} = \frac{\beta V}{C_V K_T}, \quad (2.14)$$

$$g = \frac{PV}{T^2} \frac{\partial^2 E}{\partial S^2} \Big|_V = \frac{PV}{C_V T}. \quad (2.15)$$

Here γ is called the adiabatic exponent, Γ is called the Grüneisen coefficient, and g is a dimensionless specific heat. A fourth dimensionless quantity that is important is the fundamental derivative

$$\mathcal{G} = -\frac{1}{2} V \frac{\partial^3 E / \partial V^3}{\partial^2 E / \partial V^2} \Big|_S, \quad (2.16)$$

which involves a third derivative of E .

These quantities may be interpreted as characterizing the behavior of isentropes.

(1) The adiabatic exponent

$$\gamma = -\frac{V}{P} \frac{\partial P}{\partial V} \Big|_S = -\frac{\partial \log P}{\partial \log V} \Big|_S \quad (2.17)$$

is the negative slope of the isentrope as drawn in the $\log P$ - $\log V$ plane. For V near V_0 , the isentrope through (V_0, P_0) is given approximately by

$$P \approx P_0 \left(\frac{V}{V_0} \right)^{-\gamma}, \quad (2.18)$$

where γ is evaluated at (V_0, P_0) ; whence the name adiabatic exponent. When γ is a constant, as for a polytropic gas, this relation holds exactly.

(2) The Grüneisen coefficient

$$\Gamma = -\frac{V}{T} \frac{\partial T}{\partial V} \Big|_S = -\frac{\partial \log T}{\partial \log V} \Big|_S \quad (2.19)$$

is the negative slope of the isentrope in the $\log T$ - $\log V$ plane. For V near V_0 , the isentrope through (V_0, T_0) is given approximately by

$$T \approx T_0 \left(\frac{V}{V_0} \right)^{-\Gamma}, \quad (2.20)$$

where Γ is evaluated at (V_0, T_0) , and this holds exactly when Γ is constant. Thermodynamic identities imply that the Grüneisen coefficient also measures the spacing of the isentropes in the $\log P$ - $\log V$ plane:

$$\Gamma = V \frac{\partial P}{\partial E} \Big|_V = \frac{V}{T} \frac{\partial P}{\partial S} \Big|_V = \frac{PV}{T} \frac{\partial \log P}{\partial S} \Big|_{\log V}. \quad (2.21)$$

(3) The dimensionless specific heat

$$g = \frac{PV}{T^2} \frac{\partial T}{\partial S} \Big|_V = \frac{PV}{T} \frac{\partial \log T}{\partial S} \Big|_{\log V} \quad (2.22)$$

measures the spacing of the isentropes in the $\log T$ - $\log V$ plane.

(4) The fundamental derivative

$$\mathcal{G} = -\frac{1}{2} V \frac{\partial^2 P / \partial V^2}{\partial P / \partial V} \Big|_S = \frac{1}{2} \frac{V^2}{\gamma P} \frac{\partial^2 P}{\partial V^2} \Big|_S \quad (2.23)$$

measures the convexity of the isentropes in the P - V plane (Thompson, 1972). In particular, if $\mathcal{G} > 0$, then the isentropes are convex. The fundamental derivative can be related also to convexity of the isentropes in other planes: using Eq. (2.17), one finds

$$\mathcal{G} = \frac{1}{2} \left[\gamma + 1 - \frac{V}{\gamma} \frac{\partial \gamma}{\partial V} \Big|_S \right]; \quad (2.24)$$

therefore the convexity of isentropes in the $\log P$ - $\log V$ plane, i.e., the sign of

$$\frac{\partial^2 \log P}{(\partial \log V)^2} \Big|_S = -\frac{\partial \gamma}{\partial \log V} \Big|_S , \quad (2.25)$$

is determined by the sign of $\mathcal{G} - \frac{1}{2}(\gamma + 1)$. Similarly,

$$\mathcal{G} = 1 + \frac{1}{2} \frac{1}{\gamma PV^2} \frac{\partial^2 P}{\partial \rho^2} \Big|_S , \quad (2.26)$$

so the convexity of isentropes in the P - ρ plane is determined by the sign of $\mathcal{G} - 1$.

Remark. In applications to fluid dynamics, γ and \mathcal{G} are most important. As will be shown in Sec. III, the adiabatic exponent γ is a dimensionless sound speed ($\gamma \equiv c^2/PV$), while the fundamental derivative \mathcal{G} determines how the sound speed varies across simple waves. When $\gamma > 0$, the fluid equations are strictly hyperbolic; when $\mathcal{G} > 0$, they are genuinely nonlinear. The Grüneisen coefficient Γ controls the mapping of isentropes into the P - V plane; when $\Gamma > 0$, isentropes do not cross each other in this plane. In Sec. IV we show that properties of shock waves and rarefaction waves are determined solely by γ , Γ , and \mathcal{G} ; the dimensionless specific heat g does not affect the dynamics when heat conduction is neglected.

Example. The polytropic gas provides a simple analytic example of an EOS. For an ideal gas, PV and E are independent of V at fixed T , according to the experiments of Boyle and of Joule-Thompson. It follows from the fundamental thermodynamic identity, Eq. (2.8), that $PV = RT$ for some constant R . Then, using thermodynamic identities, it can be shown that the measurable quantities are determined by the ratio of specific heats, $\gamma_0 = C_P/C_V$, which is generally a function of T :

$$\begin{aligned} C_V &= \frac{1}{\gamma_0 - 1} R, \quad C_P = \frac{\gamma_0}{\gamma_0 - 1} R , \\ K_S &= \frac{1}{\gamma_0 P}, \quad K_T = \frac{1}{P}, \quad \beta = \frac{1}{T} , \end{aligned} \quad (2.27)$$

so that

$$\gamma = \gamma_0, \quad \Gamma = \gamma_0 - 1, \quad \text{and} \quad g = \gamma_0 - 1 . \quad (2.28)$$

A polytropic gas is an ideal gas for which γ_0 is a constant. Thermodynamic stability, Eq. (2.32) below, requires that $\gamma_0 \geq 1$. In this case, $E = C_V T$ and $S = C_V \ln(TV^{\gamma_0-1}) + \text{const}$. Thus the equation of state of a polytropic gas is

$$E = E_0 \left(\frac{V}{V_0} \right)^{-(\gamma_0-1)} \exp \left[(\gamma_0 - 1) \frac{S}{R} \right] \quad (2.29)$$

for some constants γ_0 , R , E_0 , and V_0 . In addition, from Eq. (2.24) one finds that $\mathcal{G} = \frac{1}{2}(\gamma_0 + 1)$. In Sec. II.F, the incomplete form of the polytropic EOS,

$$P = (\gamma_0 - 1)E/V , \quad (2.30)$$

will be seen to be adequate for the dynamics of a polytropic gas.

Remark. It should be emphasized, however, that the

adiabatic exponent γ is not the ratio of specific heats γ_0 for a general EOS. In fact, Eq. (2.12) shows that $C_P/C_V = \gamma g / (\gamma g - \Gamma^2)$. As will be seen, the adiabatic exponent determines the speed of propagation of waves, while the ratio of the specific heats cannot be determined by measurements of fluid flows in which viscosity and heat conduction are negligible. For this reason, C_P/C_V is not appropriate for characterizing the dynamical response of a fluid, and we prefer, following Davis (1985), to make the above (arguably nonstandard) definition of adiabatic exponent.

C. Thermodynamic constraints

The equilibrium states of the system are parametrized by specific volume $V > 0$ and specific entropy $S \geq 0$. On this domain, the specific energy $E = E(V, S)$ is assumed to be continuously differentiable and piecewise twice continuously differentiable. The graph of E defines the two-dimensional manifold of equilibrium states. The pressure P and the temperature T are assumed to be non-negative; consequently, E is monotonic in V and S .

Remarks. (1) The justification for the assumed domain and smoothness for E is discussed in Sec. II.D. Although second derivatives of E may fail to exist at points along certain curves (saturation boundaries), they are, nevertheless, piecewise continuous; at worst they suffer jump discontinuities across these curves. Taking notice of this, one should interpret in the sense of distributions the various formulas that involve derivatives of E .

(2) The temperature can be negative in certain quantum spin systems and in steady-state nonequilibrium applications such as lasers, but not in the classical fluid systems that we consider.

(3) The assumption that $P \geq 0$ excludes the possibility that the material can support tension. This is appropriate in regimes where the material is fluid, i.e., material strength is negligible. When the material is solid, the hydrodynamic approximation may be inadequate. For instance, solids can support shear forces and tension and may not be isotropic because of crystal structure. In this case, the extra stress tensor Σ cannot be neglected, and extra internal variables (e.g., the strain) are needed. This requires a more elaborate continuum model, such as a viscoelastic or elastic-plastic model. Nevertheless, at sufficiently high pressures (far exceeding the yield strength), the hydrodynamic approximation may be adequate. This happens, for example, when metals are driven by high explosives.

Thermodynamic stability requires that E be jointly convex as a function of V and S . This implies that the Hessian matrix of second derivatives of E is non-negative:

$$\begin{aligned} \frac{\partial^2 E}{\partial S^2} \Big|_V &\geq 0, \quad \frac{\partial^2 E}{\partial V^2} \Big|_S \geq 0 , \\ \frac{\partial^2 E}{\partial S^2} \Big|_V \frac{\partial^2 E}{\partial V^2} \Big|_S &\geq \left(\frac{\partial^2 E}{\partial S \partial V} \right)^2 . \end{aligned} \quad (2.31)$$

This translates into the inequalities

$$g \geq 0, \quad \gamma \geq 0, \quad \text{and} \quad \gamma g \geq \Gamma^2 \quad (2.32)$$

or, equivalently,

$$C_V^{-1} \geq C_P^{-1} \geq 0 \quad \text{and} \quad K_S^{-1} \geq K_T^{-1} \geq 0. \quad (2.33)$$

In particular, P and T are monotonic in V and S , respectively.

Remarks. (1) Thermodynamic stability requires only that $\gamma \geq 0$, but for most materials (and for polytropic gases), $\gamma > 1$. In this case, E is strictly convex in $\log V$ along an isentrope.

(2) Thermodynamics places no constraint on the sign of Γ . The inequalities (2.33) imply that Γ has the same sign as β . Thus $\Gamma > 0$ when the material expands upon heating at constant pressure, which is true in most situations. But for some materials, Γ is negative in portions of state space. A notable example is water, which contracts upon heating near 0°C and 1 bar (Bethe, 1942).

(3) Thermodynamics places no constraint on the sign of \mathcal{G} . For many materials, away from phase transitions, $\gamma > 1$ and varies slowly along the isentrope ($|\partial \log \gamma / \partial \log V|_S | \ll 1$), so $\mathcal{G} > 1$, according to Eq. (2.24). In other words, isentropes are strictly convex in the P - ρ plane, and the sound speed increases with density along an isentrope. Moreover, some approximate Riemann problem solvers (Colella and Glaz, 1985) are based on these assumptions about γ . Near phase transitions, however, \mathcal{G} can be negative.

(4) Because the arithmetic mean bounds the geometric mean, the last inequality in (2.32) implies that $\frac{1}{2}(\gamma + g) \geq |\Gamma|$.

The third law of thermodynamics, as formulated by Planck, states that the $T=0$ isotherm and the $S=0$ isentrope coincide. This implies Nernst's theorem, that the entropy change in an isothermal process at $T=0$ is finite. It also implies that the energy and pressure on the cold curve (the $T=0$ isotherm) are $E_c(V) = \lim_{S \rightarrow 0} E(V, S)$ and $P_c(V) = \lim_{S \rightarrow 0} P(V, S)$, respectively. The temperature $T = \partial E / \partial S|_V$ is non-negative, so the energy is minimized on the cold curve, and we may write

$$E(V, S) \geq E_c(V) = E_{\min} + \int_V^\infty P_c(V') dV', \quad (2.34)$$

with $E_{\min} = \lim_{V \rightarrow \infty} E_c(V)$. The fact that the minimum energy E_{\min} is finite is known in physics as the "stability of matter" (see Lieb, 1976). Since only differences in energy are important for fluid dynamics, we choose the origin for energy such that $E_{\min} = 0$.

Remarks. (1) The value of E_{\min} is, in fact, significant when the system contains several materials and chemical reactions occur between them. In this case the value of E_{\min} for each material must be chosen to be consistent with the heat of formation of chemical compounds.

(2) When the $S=0$ isentrope coincides with the low-pressure boundary of the domain in the P - V plane, the inequality $P(V, S) \geq P_c(V)$ holds. This is usually a valid assumption.

(3) The coincidence of the $T=0$ isotherm and the $S=0$ isentrope implies that

$$-\gamma = \left. \frac{\partial \log P}{\partial \log V} \right|_S = \left. \frac{\partial \log P}{\partial \log V} \right|_T = -\gamma + \Gamma^2/g \quad (2.35)$$

at absolute zero. Hence $\Gamma^2/g = 0$ at $T=0$. Usually $C_V \rightarrow 0$ as $T \rightarrow 0$, so $g = \infty$ and Γ may be nonzero at absolute zero.

D. Domain of state space

The allowed states of V and S , as well as the properties of E , are conveniently characterized using Legendre transformations. More details about the following discussion are found in Appendix A [see also Wightman (1979)].

In principle, the equation of state is determined from (quantum) statistical mechanics. The starting point for practical calculations of equations of state (Zel'dovich and Raizer, 1966; More *et al.*, 1988) is usually the specific Helmholtz free energy, which is related to the specific energy through a partial Legendre transform:

$$F(V, T) = \inf_S \{E(V, S) - TS\}. \quad (2.36)$$

For simplicity, we imagine the constituent particles of the material (molecules, atoms, or ions and electrons) to be pointlike, with an interactive force that is strongly repulsive at short distances and weakly attractive elsewhere. (We only consider fluids in which constituent particles do not bind.) To construct the free energy, the partition function is calculated for a box with volume \mathcal{V} containing N particles with average mass m , and the thermodynamic limit is taken, i.e., $\mathcal{V} \rightarrow \infty$ and $N \rightarrow \infty$ with $\mathcal{V}/N = mV$. Our principal assumption, made primarily for convenience, is that this limit exists for all choices of $V > 0$ and $T \geq 0$. Since $C_V = T \partial S / \partial T|_V > 0$, S may be used in place of T as an independent variable. By the third law of thermodynamics, $T=0$ corresponds to $S=0$. At the other extreme, we assume that $S \rightarrow \infty$ as $T \rightarrow \infty$ with the volume fixed; this is reasonable because at high temperatures the thermal energy of the particles dominates their interaction potential energy, and the material behaves as an ideal gas. Consequently, the domain of definition for E comprises the quadrant $S \geq 0$ and $V > 0$.

Remarks. (1) For some physical applications the minimum attainable specific volume may be nonzero. One example is from astrophysics: a neutron star approximates "infinitely dense" matter for which $V \geq V_{\min} > 0$.

(2) At extremely high temperatures the thermal motion is limited by the speed of light and the material must be modeled by relativistic hydrodynamics. Furthermore, radiation transport becomes important.

(3) Even though we focus on the dynamics of material in a fluid state, we have set up the mathematical problem as if Eqs. (2.4)–(2.6) and the equilibrium EOS were ap-

propriate throughout state space, including regions where the material is not fluid. This allows the initial value problem to have a solution, for all time, and it simplifies the statement and proof of mathematical theorems on the wave structure. For the initial conditions corresponding to a given application, one can examine the solution *a posteriori* to decide whether the flow has remained in a regime in which the fluid equations and the EOS give an adequate model of the physical flow. For example, the solution does not model the physics well when the material is solid and material strength is important, or when the material is a rarefied gas (for which the time needed to attain thermal equilibrium is longer than the time scale of the flow problem). An alternative approach to the mathematical problem would limit state space to comprise only the vapor and liquid phases, but this would complicate all results because the solution might hit the boundary of state space. The approach we follow is in the spirit of other physical theories. For example, classical mechanics is a well-posed, consistent mathematical model that approximates physical reality well for a wide variety of problems, but it is known to break down at small distances because of quantum-mechanical effects and at large velocities because of relativistic effects.

A convex function defined on a convex domain corresponds naturally to a conjugate convex function, defined on a conjugate domain, through the Legendre transformation. Corresponding to the convex function E is the specific Gibbs free energy G , which is defined by

$$G(P, T) = \inf_{V, S} \{E(V, S) - TS + PV\} \quad (2.37)$$

whenever P and T are such that the infimum is finite. The energy may be recovered from the Gibbs function through the inverse relation

$$E(V, S) = \sup_{P, T} \{G(P, T) + TS - PV\}. \quad (2.38)$$

The geometry of the energy surface is intimately related to properties of G .

First of all, E is jointly convex if and only if G is jointly concave. Moreover, E is continuously differentiable if and only if G is strictly concave. A point in the P - T plane at which G is differentiable corresponds to unique values of V and S , since $V = \partial G / \partial P|_T$ and $S = -\partial G / \partial T|_P$, whereas a point at which G suffers jump discontinuities in its derivatives corresponds to a portion of the S - V plane throughout which E depends linearly on V and S . On most of its domain G is continuously differentiable, but along certain curves, called coexistence curves, G suffers jump discontinuities in its derivatives. Such singularities reflect the existence of phase transitions in the material. For simplicity we limit the discussion to a material that has three phases: solid, liquid, and vapor. A prototypical phase diagram in the P - T plane is shown in Fig. 1. (See, e.g., Reichl, 1980, Chap. 4.) The corresponding diagram in the S - V plane, constructed using the Legendre transformation, is shown in Fig. 2. The phase diagram in the P - V plane, shown in Fig. 3, is also

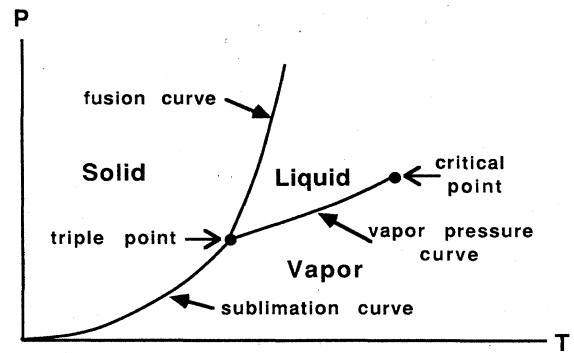


FIG. 1. Simplified phase diagram in the P - T plane.

useful.

Remark. Typical materials have many other phase transitions. Polymorphic phase transitions, in which the crystal structure of a solid phase changes, are most common. For instance, diamond and graphite are distinct crystal structures of carbon. Other kinds of phase transitions also occur, such as the superfluid transition in liquid helium.

A point at which G is differentiable corresponds to a pure equilibrium state; at a point on a coexistence curve, by contrast, the material is a mixture of the pure phases that border the point. End points of coexistence curves are called critical points, and intersections of coexistence curves are called triple points. Triple points, therefore, correspond to three-phase mixtures, while other points on the coexistence curve correspond to two-phase mixtures. A coexistence curve in the P - T plane expands to a multiphase or mixture region in the S - V plane. Bound-

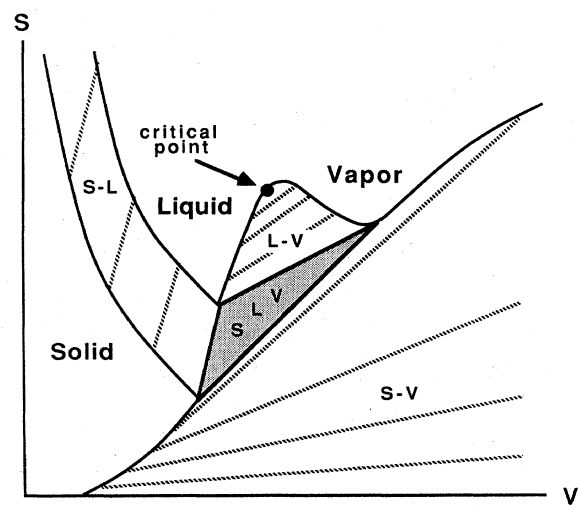


FIG. 2. Simplified phase diagram in the S - V plane. (Dotted lines correspond to points on the coexistence curves in the P - T plane; the shaded region corresponds to the triple point.)

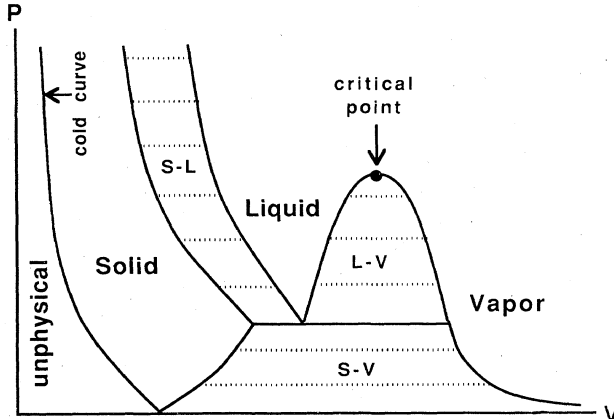


FIG. 3. Simplified phase diagram in the P - V plane. (Horizontal lines in the mixed-phase regions correspond to points on the coexistence curves in the P - T plane.)

boundaries between pure and mixed-phase regions are called saturated phase boundaries or, more simply, saturation boundaries. Triple points correspond to a triangular region; any other point on a coexistence curve corresponds to a line segment (indicated in Fig. 2 by a dashed line segment). The slope of this segment coincides with the slope of the tangent to the coexistence curve, according to the Clausius-Clapeyron equation:

$$\left. \frac{dP}{dT} \right|_{\text{coex}} = \frac{\Delta S}{\Delta V}. \quad (2.39)$$

States in the triangular three-phase region are convex combinations of the three pure states at the vertices of the triangle; two-phase states are convex combinations of the pure states at the end points of the line segment. We assume all mixture ratios to occur physically. The specific energy E depends linearly on V and S in three-phase triangles and along two-phase line segments. In a pure phase region the inequalities (2.32) are strict, whereas in a mixture region $\gamma g = \Gamma^2$. More precisely, $\gamma = \Gamma = g = 0$ in a three-phase region, while γ or g , but not both, may vanish in a two-phase region.

Remarks. (1) At sufficiently high temperatures all materials vaporize and behave as a gas, while at low temperatures the binding forces between constituent particles cause materials to solidify (except for ${}^4\text{He}$, which is a superfluid near absolute zero at low pressures).

(2) When heat conduction, viscosity, and surface tension are neglected, the dynamical equations do not distinguish between gases and liquids; we therefore speak of fluid dynamics. In fact, the distinction between the vapor phase and the liquid phase is only qualitative because the liquid-vapor coexistence curve ends at a critical point: a flow can continuously transform a material from the liquid to the vapor phase, or vice versa, without crossing a phase boundary.

(3) Because we are focusing on fluid dynamics and not

on the elastic-plastic properties of solids, we exclude the region of state space corresponding to material in tension. Thus the domain of state space is the quadrant $P \geq 0$ and $T \geq 0$. To be consistent, we assume that the solid-vapor coexistence curve ends at $P = T = 0$ with $dP/dT|_{\text{coex}} = 0$, and that the vapor saturation boundary extends to $V \rightarrow \infty$ as $P \rightarrow 0$, as indicated in Figs. 1–3.

(4) Phase transitions have important consequences for the wave structure of the dynamical equations, as discussed in Sec. V. A point on the coexistence curve at which $dP/dT|_{\text{coex}} = 0$ corresponds to a line segment in the S - V plane along which $\gamma = 0$, so the conservation laws are not strictly hyperbolic. Furthermore, $\gamma = 0$ throughout the three-phase regions corresponding to triple points, which are generic features of phase diagrams. However, this loss of strict hyperbolicity does not have the important consequences for the topology of wave curves in compressible fluid flow that it has for other non-strictly-hyperbolic systems. In a sense, phase transitions are removable singularities: G may be smoothed by convolution with a non-negative mollification function to obtain an approximation to the equation of state that exhibits no phase transitions. This contrasts with the situation for incompressible three-phase flow in petroleum reservoirs, where the singularity cannot be removed (Shearer, 1988).

E. Asymptotic conditions

The existence of solutions of the Riemann problem depends on the asymptotic properties of the EOS. We will not focus on this aspect of the problem as much as we will on the uniqueness of solutions of the Riemann problem, which depends on local properties of the EOS. Instead we will assume simple conditions that are physically motivated for classical hydrodynamics and sufficient to guarantee existence for the Riemann problem.

Since the space of equilibrium states contains the entire quadrant $V > 0$, $S \geq 0$, all isentropes extend toward the line $V = 0$ in the P - V plane. Because $\gamma \geq 0$, P is non-decreasing as $V \rightarrow 0$ along an isentrope. The first asymptotic condition assumes more strongly that

$$P(V, S) \rightarrow \infty \text{ as } V \rightarrow 0. \quad (2.40)$$

Physically, this results from repulsive forces between constituent nuclei and electrons at short distances. An important consequence follows from

Lemma 2.1. Suppose $P(V) \geq 0$ and $P'(V) \leq 0$. Let $E(V) = E_0 - \int_{V_0}^V P(V') dV'$, where $E_0 \geq 0$ and $V_0 > 0$. If $P(V) \rightarrow \infty$ as $V \rightarrow 0$, then

$$E/P \rightarrow 0 \text{ as } V \rightarrow 0. \quad (2.41)$$

Proof. By the monotonicity of P , $0 \leq E(V) \leq E_0 + P(V)(V_0 - V)$ when $V \leq V_0$. Therefore $0 \leq \limsup_{V \rightarrow 0} E(V)/P(V) \leq V_0$. Now let $V_0 \rightarrow 0$. \square

The second asymptotic condition supposes that all

isentropes extend to $P=0$:

$$P(V, S) \rightarrow 0 \text{ as } V \rightarrow \infty . \quad (2.42)$$

This can be justified by imagining the adiabatic expansion of the fluid to large specific volumes: as the constituents become farther apart, the forces between them become weaker, so the pressure falls to zero.

The last asymptotic condition is that

$$E(V, S) \rightarrow \infty \text{ and } P(V, S) \rightarrow \infty \text{ as } S \rightarrow \infty . \quad (2.43)$$

This would follow, for instance, from the assumption that $T(V, S) \rightarrow \infty$ as $S \rightarrow \infty$, provided Γ remains strictly positive in this limit. At high temperatures for fixed V , the thermal kinetic energy dominates the internal energy, which leads to dissociation of constituent molecules. Then the material behaves as an ideal gas, which exhibits the required asymptotic behavior.

Example. These asymptotic conditions are easily verified for a polytropic gas. Along an isentrope, $P/P_0 = (V_0/V)^\gamma$, so assumptions (2.40) and (2.42) hold. Furthermore, $E/E_0 = (V_0/V)^{\gamma-1}$, so $E/P = V/(\gamma-1) \rightarrow 0$ as $V \rightarrow 0$; also, $E/E_0 = P/P_0 = \exp[(\gamma-1)(S - S_0)/R]$ if V is fixed, so condition (2.43) is true.

F. Incomplete equation of state

The system of equations [Eqs. (2.4)–(2.6)] describing fluid flow must be supplemented by a constitutive relation. For this purpose only a relation of the form $P=P(V, E)$ is needed; such a relation is called an incomplete EOS. The complete EOS, $E=E(V, S)$, determines the incomplete EOS by solving for $S=S(V, E)$ (which is possible since $T=\partial E/\partial S|_V > 0$ unless $S=0$) and substituting for S in $P=P(V, S)$. But an incomplete EOS does not determine a corresponding complete EOS, as we now show.

The derivative along an isentrope,

$$\frac{\partial}{\partial V} \Bigg|_S = \frac{\partial}{\partial V} \Bigg|_E - P \frac{\partial}{\partial E} \Bigg|_V , \quad (2.44)$$

and the derivative

$$\frac{1}{T} \frac{\partial}{\partial S} \Bigg|_V = \frac{\partial}{\partial E} \Bigg|_V \quad (2.45)$$

are well defined by the incomplete EOS. Consequently,

$$\gamma = -\frac{V}{P} \left[\frac{\partial P}{\partial V} \Bigg|_E - P \frac{\partial}{\partial E} \Bigg|_V \right] , \quad (2.46)$$

$$\Gamma = V \frac{\partial P}{\partial E} \Bigg|_V , \quad (2.47)$$

and

$$\mathcal{G} = \frac{1}{2} \left[\gamma + 1 - \frac{V}{\gamma} \left[\frac{\partial \gamma}{\partial V} \Bigg|_E - P \frac{\partial \gamma}{\partial E} \Bigg|_V \right] \right] . \quad (2.48)$$

may be calculated. We require that the incomplete EOS define a non-negative adiabatic exponent γ , in accordance with thermodynamic stability. Moreover, the incomplete EOS determines the differential $T dS = dE + P dV$, so that an entropy function may be obtained by finding an integrating factor $1/T$ for the differential $dE + P dV$. Such an integrating factor is not unique, however, so there may be more than one complete EOS corresponding to the given incomplete EOS. In other words, an incomplete EOS determines the isentropes (curves along which S is constant) through the differential equation $dE = -P dV$, but it does not determine the values of S that label the isentropes. On the other hand, the complete EOS must be thermodynamically consistent, i.e., it must conform to the thermodynamic constraints of Sec. II.C, and it may happen that no choice of integrating factor yields such an EOS. To check thermodynamic consistency, one must verify that $T \geq 0$, that $S=0$ when $T=0$, and that $S=S(V, E)$ is concave.

Suppose one choice for the temperature and entropy, T and S , has been found to satisfy $T dS = dE + P dV$. Alternative choices for the entropy and temperature are given by $\tilde{S}=f(S)$ and $\tilde{T}=T/f'(S)$ for an arbitrary function f . For thermodynamic consistency we require that $\tilde{T}=T/f'(S) \geq 0$, the $\tilde{T}=0$ isotherm and $\tilde{S}=0$ isentrope are identical, and $\tilde{g} \geq \Gamma^2/\gamma$, so $\tilde{S}=\tilde{S}(V, E)$ is concave. In particular, $f(S)$ must not decrease with S if the original choice of temperature is non-negative. Furthermore, the formula

$$\tilde{g} = g - \frac{PV}{T} \frac{f''(S)}{f'(S)} \quad (2.49)$$

shows that concavity of $\tilde{S}=\tilde{S}(V, E)$ is equivalent to

$$\frac{f''(S)}{f'(S)} \leq \min_V \left\{ (\gamma g - \Gamma^2) \frac{T}{\gamma PV} \right\} . \quad (2.50)$$

A choice for the function f that satisfies these conditions, i.e., one that yields a thermodynamically consistent EOS, may not exist or may not be unique.

Example. The nonuniqueness in determining T and S can be illustrated with a polytropic gas EOS, defined by the incomplete equation of state $P=(\gamma_0-1)E/V$ for some constant $\gamma_0 > 1$. Equations (2.46)–(2.48) may be used to calculate that γ_0 coincides with the adiabatic exponent γ , and that $\Gamma=\gamma_0-1$ and $\mathcal{G}=\frac{1}{2}(\gamma_0+1)$. One choice for the entropy and temperature corresponds to an ideal gas with constant specific heat $C_V=R/(\gamma_0-1)$:

$$T = (\gamma_0-1)E/R , \quad (2.51)$$

$$S = \frac{R}{\gamma_0-1} \ln \left[\frac{E}{E_0} \left(\frac{V}{V_0} \right)^{\gamma_0-1} \right] . \quad (2.52)$$

This choice, however, does not satisfy the third law of thermodynamics. A complete EOS for a polytropic gas that does satisfy this law can be found by choosing the entropy to be, for example,

$$\tilde{S} = f(S) = \frac{1}{2}[S + (S^2 + S_0^2)^{1/2}] . \quad (2.53)$$

In this case the specific heat \tilde{C}_V tends to the constant $R/(\gamma_0 - 1)$ at high temperatures and to zero at low temperatures. The transition is determined by the choice of S_0 . The requirement $\tilde{g} \geq \Gamma^2/\gamma$ leads to the constraint $S_0 \geq (\sqrt{3}/4)R\gamma_0/(\gamma_0 - 1)$.

For an inviscid, non-heat-conducting, nonradiating fluid, only those quantities that are determined by the incomplete EOS are relevant (Davis, 1985). For instance, the temperature T , the entropy S , and the specific heat C_V do not appear in the fluid equations in isolation. In this light, the flow dynamics are independent of the temperature and entropy-related properties of the material embodied in the specific heat g . It is important to notice, however, that an incomplete EOS must derive from some thermodynamically consistent EOS in order to be a physical constitutive relation. In the subsequent sections we will implicitly assume that the incomplete EOS has been obtained from a complete EOS that satisfies the thermodynamic constraints.

As will be seen, the dimensionless quantities γ , Γ , and \mathcal{G} determine the structure of solutions of the Riemann problem. The standard analysis of the Riemann problem in gas dynamics by Weyl (1949; see also Courant and Friedrichs, 1948) assumes that $\Gamma > 0$ and $\mathcal{G} > 0$. The same conclusions were obtained by Bethe (1942) under the weaker conditions that $\Gamma > -2$ and $\mathcal{G} > 0$. Wendroff (1972) and Liu (1975) studied the Riemann problem when \mathcal{G} may become negative, assuming that $\gamma > \Gamma > 0$ and that \mathcal{G} is smooth with isolated zeros along isentropes. In the presence of phase transitions, all of these assumptions may break down. We explain in the subsequent sections how this affects the wave structure.

II. ONE-DIMENSIONAL SCALE-INVARIANT FLOWS

In this section we study the structure of one-dimensional flows. These flows idealize three-dimensional flow with planar symmetry. With the symmetry plane perpendicular to the x axis, the only nonzero component of velocity is the x component u , and all variables are independent of y and z . Therefore the governing equations [Eqs. (2.4)–(2.6)] reduce to

$$\rho_t + (\rho u)_x = 0 , \quad (3.1)$$

$$(\rho u)_t + (\rho u^2 + P)_x = 0 , \quad (3.2)$$

$$(\frac{1}{2}\rho u^2 + \rho E)_t + [u(\frac{1}{2}\rho u^2 + \rho E + P)]_x = 0 . \quad (3.3)$$

We will be concerned primarily with scale-invariant solutions, since they form the components of the solution of the Riemann problem. The scale invariance reduces the partial differential equations to ordinary differential equations for smooth solutions and to algebraic equations for discontinuous solutions. First we describe alternate forms of the flow equations that are satisfied by smooth solutions (rarefaction waves). Next we examine discontinuous solutions (shock waves and contact discontinui-

ties). Combinations of smooth and discontinuous solutions are then constructed (composite waves). Finally, we define wave curves and explain their use in solving the Riemann problem.

Remark. Other one-dimensional flows of physical interest are obtained by imposing different symmetries or further approximations; these include spherically symmetric flow and flow in a duct with variable area. We will not consider these flows because the conservation laws governing them have source terms, so that scale-invariant solutions do not exist. [For special initial conditions, however, they do admit other types of similarity solutions, such as the Guderley (1942) solution for converging spherical shock waves.] Nevertheless, scale-invariant solutions approximate the flow for short durations even when source terms are present. They are useful, therefore, in numerical algorithms.

A. Rarefaction waves

At a point where the solution is differentiable, Eqs. (3.1)–(3.3) are equivalent to the Lagrangian equations

$$\rho \dot{V} - u_x = 0 , \quad (3.4)$$

$$\rho \dot{u} + P_x = 0 , \quad (3.5)$$

$$\rho(\frac{1}{2}u^2 + E) + (uP)_x = 0 . \quad (3.6)$$

Here a dot denotes the convective derivative $\partial_t + u \partial_x$, which differentiates along the paths of particles in the flow. These equations follow by using Eq. (3.1) in Eqs. (3.2) and (3.3). By using Eq. (3.5) in Eq. (3.6), the latter becomes $\rho \dot{E} + P u_x = 0$, and therefore, by Eq. (3.4), $\dot{E} + P \dot{V} = 0$. According to the fundamental thermodynamic identity, it follows that $T \dot{S} = 0$, so entropy is constant along particle paths in smooth flow. In addition, we may evaluate

$$\dot{P} = \left. \frac{\partial P}{\partial V} \right|_E \dot{V} + \left. \frac{\partial P}{\partial E} \right|_V \dot{E} = -\frac{\gamma P}{V} \dot{V} , \quad (3.7)$$

where γ is the adiabatic exponent given by Eq. (2.46). If we now define the sound speed c as

$$c = \sqrt{\gamma PV} , \quad (3.8)$$

then $\dot{P} = -\rho^2 c^2 \dot{V}$. Therefore Eqs. (3.4)–(3.6) may be combined into the equivalent characteristic form

$$\dot{P} + cP_x + \rho c(\dot{u} + cu_x) = 0 , \quad (3.9)$$

$$\dot{P} - cP_x - \rho c(\dot{u} - cu_x) = 0 , \quad (3.10)$$

$$\dot{E} + P \dot{V} = 0 . \quad (3.11)$$

Equations (3.9)–(3.11) involve the derivatives $\partial_t + (u \pm c) \partial_x$ and $\partial_t + u \partial_x$, respectively, so that signals propagate at the characteristic velocities $u \pm c$, corresponding to right-facing (left-facing) sound waves, and u , corresponding to particle paths.

The adiabatic exponent γ is now seen to be a dimen-

sionless measure of the sound speed c . The sound speed is real because $\gamma \geq 0$, as required by thermodynamic stability. Moreover, sound speed is strictly positive, except where $\gamma = 0$, which can happen only in three-phase regions (i.e., triple points) and at special points in two-phase regions. Away from such points, Eqs. (3.1)–(3.3) form a hyperbolic system with distinct characteristic velocities; thus the system of conservation laws is strictly hyperbolic. Regions where $\gamma = 0$ are called umbilic regions. The occurrence of umbilic points in models of three-phase flow in petroleum reservoirs has led to several striking phenomena (Shearer *et al.*, 1987; Isaacson, Marchesin, and Plohr, 1988a; Isaacson, Marchesin, Plohr, and Temple, 1988; Isaacson and Temple, 1988a, 1988b).

We now restrict attention to scale-invariant, or self-similar, solutions of Eqs. (3.9)–(3.11). Such solutions depend on x and t only through the velocity variable $\xi = x/t$ when $t > 0$, i.e., they are constant along rays through the origin in space-time. In this case, $t\partial_t = -\xi\partial_\xi$ and $t\partial_x = \partial_\xi$, so Eqs. (3.9)–(3.11) require that

$$(u + c - \xi)(P_\xi + \rho c u_\xi) = 0, \quad (3.12)$$

$$(u - c - \xi)(P_\xi - \rho c u_\xi) = 0, \quad (3.13)$$

$$(u - \xi)(E_\xi + PV_\xi) = 0. \quad (3.14)$$

These equations are satisfied if one imposes that

$$\mp \rho c = \rho(u - \xi), \quad (3.15)$$

$$\mp \rho c du + dP = 0, \quad (3.16)$$

$$dE + P dV = 0, \quad (3.17)$$

with

$$\rho c = \left[-\frac{\partial P}{\partial V} \Big|_S \right]^{1/2}. \quad (3.18)$$

Such solutions correspond to right-facing and left-facing rarefaction waves, according to the choice of sign. The quantity ρc is the acoustic impedance; it plays the role of the signal propagation speed in Lagrangian coordinates when x is replaced by the mass coordinate \tilde{x} satisfying $d\tilde{x} = \rho dx$.

Equations (3.16)–(3.18) are ordinary differential equations whose orbits in V - E - u space are called rarefaction curves. The states in a rarefaction wave lie along a rarefaction curve, with their dependence on ξ determined by Eq. (3.15): $\xi = u \pm c$. According to Eq. (3.17) and the fundamental thermodynamic identity, the entropy S is constant along rarefaction curves. Moreover, the Riemann invariant

$$r_\mp = u \pm \int^V \rho c dV \Big|_{S=\text{const}} \quad (3.19)$$

is constant along right-facing (left-facing) rarefaction curves, since along these curves $dr_\mp = du \pm \rho c dV = du \mp dP/\rho c = 0$. This gives a procedure for calculating the rarefaction curve through an initial state (V_0, E_0, u_0) : first

determine the isentrope $S = S_0$ through the initial state using Eq. (3.17), and then calculate the particle velocity

$$u = u_0 \pm \int_{P_0}^P \frac{dP}{\rho c} \Big|_{S=S_0} \quad (3.20)$$

by integrating along this isentrope, where ρc is given by Eq. (3.18). Notice that the particle velocity varies monotonically across a rarefaction wave.

Example. For a polytropic gas, the Riemann invariants are $r_\mp = u \mp [2/(\gamma-1)]c$. More generally, when $\mathcal{G} > 1$, the sound speed c varies monotonically along an isentrope, and Eq. (3.19) together with Eq. (3.22) below gives

$$r_\mp = u \pm \int^c \frac{dc}{\mathcal{G}-1} \Big|_{S=\text{const}}. \quad (3.21)$$

Of course, such a rarefaction solution is realizable in space-time only if $\xi = u \pm c$ varies monotonically across the wave. The variation of the sound speed along an isentrope is related to the fundamental derivative \mathcal{G} :

$$\begin{aligned} \frac{\partial c}{\partial V} \Big|_S &= \frac{1}{2} \rho c \frac{\partial}{\partial \log V} \Big|_S \log(\gamma PV) \\ &= -\frac{1}{2} \rho c \left[\gamma - 1 - \frac{V}{\gamma} \frac{\partial \gamma}{\partial V} \Big|_S \right] \\ &= -\rho c (\mathcal{G} - 1). \end{aligned} \quad (3.22)$$

Combining this with $du = \pm dP/\rho c = \mp \rho c dV$ shows that

$$d\xi = d(u \pm c) = \mp \rho c \mathcal{G} dV = \pm \mathcal{G} dP/\rho c \quad (3.23)$$

along a rarefaction curve.

This important relation implies that \mathcal{G} never vanishes inside a rarefaction wave. In the language of conservation laws, the sound-wave modes of Eq. (3.1)–(3.3) are genuinely nonlinear if and only if \mathcal{G} is of one sign throughout state space. As mentioned in Sec. II, the condition $\mathcal{G} > 0$ is equivalent to convexity of isentropes in the P - V plane. When $\mathcal{G} > 0$, the Eulerian wave speed $u + c$ decreases monotonically with increasing specific volume across a right-facing rarefaction wave. The Lagrangian wave speed ρc varies in the same way, since Eq. (3.22) may be manipulated to read

$$\mathcal{G} = \frac{1}{c} \frac{\partial \rho c}{\partial \rho} \Big|_S. \quad (3.24)$$

In the case $\mathcal{G} > 0$, Eq. (3.23) dictates that an element of fluid is rarefied (i.e., its specific volume increases and its pressure decreases) as it is overtaken by a rarefaction wave. In the opposite case, $\mathcal{G} < 0$, the fluid element is compressed by a rarefaction wave (the name “rarefaction” notwithstanding).

The monotonicity of the wave speed is also reflected in the convexity of rarefaction curves in the P - u plane. Indeed, differentiating $dP/du = \pm \rho c$ with respect to u and using $dV/du = \pm 1/\rho c$ and Eq. (3.24) shows that $d^2P/du^2 = \rho \mathcal{G}$ along a rarefaction curve. Thus rarefac-

tion curves are convex in the P - u plane when $\mathcal{G} > 0$.

Remarks. (1) We notice that the sound speed c , by itself, decreases monotonically only if the stronger condition $\mathcal{G} > 1$ holds, according to Eq. (3.22). The condition $\mathcal{G} > 1$ is equivalent to convexity of isentropes in the P - ρ plane.

(2) The pressure P is constant, so the sound speed is zero, along a portion of an isentrope that lies in a three-phase region. This portion therefore coincides with a critical isotherm in the P - V plane. The fundamental derivative \mathcal{G} is undefined in a three-phase region.

(3) If the limit of \mathcal{G} as $V \rightarrow \infty$ along an isentrope exists, then the limit is greater than or equal to 1, since otherwise Eq. (3.22) could be integrated twice to show that $E \rightarrow -\infty$ logarithmically as $V \rightarrow \infty$. Suppose that in fact $\mathcal{G} \geq 1 + \epsilon > 1$ when V is large. Then Eq. (3.22) implies that $c \rightarrow 0$ as $V \rightarrow \infty$, and Eq. (3.21) shows that particle velocity at the back edge of a rarefaction wave remains finite in this limit. Thus there is maximum velocity, the escape velocity, that is attained as $V \rightarrow \infty$ and $P \rightarrow 0$. For example, a rarefaction wave is formed when a piston is withdrawn from a tube filled with gas; if the piston velocity exceeds the escape velocity, cavitation will result. The escape velocity is $u = u_0 \mp [2/(\gamma - 1)]c_0$ for a polytropic gas. This limit on the velocity attained in a rarefaction wave implies that two wave curves of opposite families might not intersect in the P - u plane. To solve the Riemann problem it is necessary, in general, to admit solutions that contain a region of vacuum.

(4) Let us suppose that a rarefaction wave bounds a region of vacuum. Then the boundary is a particle trajectory as well as a characteristic, so that the sound speed must be zero. Therefore the vacuum is characterized by the coincidence of all wave speeds. We notice that $P = 0$ corresponds to the vacuum only because of the asymptotic assumptions on the EOS. For some useful equations of state (such as a stiffened gas; see Sec. VII), $P = 0$ does not imply that $c = 0$. If the pressure is arbitrarily cut off at zero for such an EOS, the equations of motion may drive the flow out of the domain. In this instance, numerical calculations may exhibit instabilities.

(5) The equations for two-dimensional steady supersonic flow are hyperbolic (see, e.g., Courant and Friedrichs, 1948; Whitham, 1974). For this system of conservation laws, the simple waves (i.e., the analogs of rarefaction waves) are Prandtl-Meyer fans. The condition $\mathcal{G} > 0$ also implies that this system of equations is genuinely nonlinear (Thompson, 1971).

B. Shock waves and contact discontinuities

At a point where the solution has a jump discontinuity propagating with velocity σ , the Rankine-Hugoniot jump conditions

$$-\sigma\Delta\rho + \Delta(\rho u) = 0, \quad (3.25)$$

$$-\sigma\Delta(\rho u) + \Delta(\rho u^2 + P) = 0, \quad (3.26)$$

$$-\sigma\Delta(\frac{1}{2}\rho u^2 + \rho E) + \Delta[u(\frac{1}{2}\rho u^2 + \rho E + P)] = 0, \quad (3.27)$$

corresponding to Eqs. (3.1)–(3.3) must hold; these jump conditions reflect conservation of mass, momentum, and energy through the discontinuity. Here the jump ΔA in a quantity A is defined by $\Delta A = A_+ - A_-$, where A_\pm is the limiting value of A on the right (left) of the discontinuity. In addition, let \bar{A} denote the average $\bar{A} = \frac{1}{2}(A_+ + A_-)$ of A across the discontinuity.

Using the Leibniz rule $\Delta(AB) = \bar{A} \cdot \Delta B + \Delta A \cdot \bar{B}$, one finds Eqs. (3.25)–(3.27) to be equivalent to the Lagrangian jump conditions

$$\mp m \Delta V - \Delta u = 0, \quad (3.28)$$

$$\mp m \Delta u + \Delta P = 0, \quad (3.29)$$

$$\mp m \Delta(\frac{1}{2}u^2 + E) + \Delta(uP) = 0, \quad (3.30)$$

where $m = \mp \sqrt{\rho(u - \sigma)} \geq 0$ is the mass flux across the discontinuity. The mass flux m is the shock propagation speed in Lagrangian coordinates.

There are two types of (nontrivial) solutions of the jump conditions.

(1) In case $m = 0$,

$$\Delta u = 0 \text{ and } \Delta P = 0, \quad (3.31)$$

but V jumps arbitrarily; this solution corresponds to a contact discontinuity.

(2) In case $m > 0$,

$$\rho_-(u_- - \sigma) = \mp m = \rho_+(u_+ - \sigma), \quad (3.32)$$

$$\mp m \Delta u + \Delta P = 0, \quad (3.33)$$

$$\Delta E + \bar{P} \Delta V = 0, \quad (3.34)$$

with

$$m = \left[-\frac{\Delta P}{\Delta V} \right]^{1/2}; \quad (3.35)$$

this solution corresponds to a right-facing (left-facing) shock wave. Because the mass flux m is real, $-\Delta P \Delta V > 0$ for such a solution (i.e., the pressure must increase across a compressive shock wave and decrease across an expansive shock wave). Equation (3.34) is called the Hugoniot relation. The equations above should be compared with Eqs. (3.15)–(3.18).

Given an initial state (V_0, E_0, u_0) , Eqs. (3.33)–(3.35) are algebraic equations for the locus of final states (V, E, u) connected to the initial state by a shock wave. This locus is called the shock curve. The shock curve may be calculated using a procedure similar to that used for rarefaction curves: first determine the relationship between thermodynamic variables along the shock curve using Eq. (3.34), and then calculate the particle velocity from

$$u = u_0 \pm \frac{P - P_0}{m}, \quad (3.36)$$

where m is given by Eq. (3.35). It is also useful to note that Eqs. (3.32)–(3.35) may be manipulated to obtain the relations

$$\begin{aligned}\frac{1}{2}(u-u_0)^2 &= E - E_0 + P_0(V - V_0) \\ &= \frac{1}{2}(P - P_0)(V_0 - V),\end{aligned}\quad (3.37)$$

$$\sigma = (\rho u - \rho_0 u_0) / (\rho - \rho_0), \quad (3.38)$$

$$P - P_0 = \rho_0(\sigma - u_0)(u - u_0), \quad (3.39)$$

$$\frac{1}{2}(\sigma - u)^2 + H = \frac{1}{2}(\sigma - u_0)^2 + H_0, \quad (3.40)$$

where $H = E + PV$ is the specific enthalpy. The last equation states that Bernoulli's law holds across a shock wave in the rest frame of the shock front.

Remarks. (1) Because there is no mass flow through a contact discontinuity, it also may represent the interface between materials with different equations of state.

(2) The jump conditions have useful geometric interpretations in the P - V plane (see Cowan, 1958; Zel'dovich and Raizer, 1966). In particular, $-m^2$ is the slope of the chord line drawn from (V_0, P_0) to (V, P) , which is called the Rayleigh line; $(u - u_0)^2$ is the area of the rectangle with opposite corners (V_0, P_0) and (V, P) ; and $E - E_0$ is the (signed) area of the trapezoid with corner points $(V_0, 0)$, (V_0, P_0) , (V, P) , and $(V, 0)$.

Not all solutions of Eqs. (3.32)–(3.35) represent physically realizable solutions. For instance, certain solutions will be seen to violate the second law of thermodynamics, which requires that entropy not decrease. The selection of physically admissible discontinuous solutions is a delicate matter. Ultimately it is determined by physical processes obscured in the passage from Eqs. (2.1)–(2.3) to Eqs. (3.1)–(3.3). In the standard theory of shock waves, it suffices to rely on the second law of thermodynamics to define admissible shock waves; however, this principle is inadequate in general. A more stringent criterion is that realizable shock solutions should admit viscous profiles, as described in Appendix C. However, even this criterion seems to fall short because, for some equations of state, certain initial value problems have multiple solutions. This situation will be discussed in Sec. VI.

For now we consider the implications of the second law of thermodynamics for solutions of Eqs. (3.1)–(3.3). Smooth solutions conserve entropy in the sense that

$$(\rho S)_t + (\rho u S)_x = 0; \quad (3.41)$$

this follows from Eq. (3.11) combined with Eq. (3.1). Entropy is not conserved, however, across discontinuous waves. In fact, an element of fluid undergoes the change in entropy

$$S_{\text{behind}} - S_{\text{ahead}} = \mp \Delta S \quad (3.42)$$

when it is overtaken by a right-facing (left-facing) shock wave. Therefore the second law of thermodynamics requires that

$$-\sigma \Delta(\rho S) + \Delta(\rho u S) = m(S_{\text{behind}} - S_{\text{ahead}}) \geq 0 \quad (3.43)$$

for a physically realizable shock wave.

For weak shock waves, i.e., when ΔS is small, the Hugoniot relation (3.34) approximates the equation for

an isentrope, so the entropy change is small. More precisely, Bethe (1942) has shown (by repeatedly differentiating the Hugoniot relation) that the entropy change is

$$\Delta S = -\frac{1}{6} \mathcal{G} \frac{c^2}{T} (\Delta V/V)^3 [1 + O(\Delta V/V)]. \quad (3.44)$$

Weak shock waves therefore are compressive when $\mathcal{G}_0 > 0$. In this case, only the compression branch of the shock curve contains admissible weak shock waves; the complementary branch is disallowed. At the same time, only the expansion branch of rarefaction waves may be realized physically. Thus, when $\mathcal{G}_0 > 0$, a weak elementary wave must be a shock wave if it is compressive and a rarefaction wave if it is expansive.

As will be seen in Sec. IV, an admissible weak shock wave has the property that the flow ahead of it is supersonic relative to the shock front, and the flow behind it is subsonic. Geometrically this means that the characteristics of the same family as the shock wave impinge on the discontinuity on both sides, while the characteristics of the opposite family pass through the wave. Lax (1957) introduced this geometric criterion as an admissibility requirement for discontinuous solutions of general systems of conservation laws. The Lax characteristic criterion is necessary for linear stability of shock waves (see Sec. VI), so we will require that our solutions satisfy it. This criterion, however, does not suffice to resolve nonuniqueness of solutions of the Riemann problem when the fluid is governed by an arbitrary equation of state.

C. Composite and split waves

Having described the basic scale-invariant solutions of the fluid equations, we now consider general scale-invariant solutions. Such solutions may contain several elementary waves, i.e., rarefaction waves, shock waves, and contact discontinuities. A scale-invariant solution may be decomposed into groups of elementary waves that belong to the same characteristic family, since waves corresponding to the distinct characteristic speeds $u - c$, u , and $u + c$ move apart from each other as time progresses. Groups of waves of a given family generalize the classical simple waves, since the appropriate Riemann invariant is piecewise constant across the group. Any scale-invariant solution consists of left-facing waves separated from right-facing waves by a contact discontinuity.

The simplest wave group consists of a single rarefaction or shock wave, but more generally it may be formed from many elementary waves. Although rarefaction and shock waves are the only possibilities when isentropes are convex and smooth, as in the standard theory, other configurations of waves can occur if isentropes are not convex. When several elementary waves propagate as a single entity, they form what is called a composite wave; if they move apart from each other, the wave is said to be split.

Two elementary waves of the same family may appear

together in a scale-invariant solution only if their propagation speeds are compatible: they may not approach each other. The outer edges of a rarefaction wave propagate with the characteristic speeds of the corresponding states, and shock wave propagate with the speed of the discontinuity; these speeds must be ordered monotonically across the wave. This principle extends the rule that the characteristic speed must vary monotonically across a rarefaction wave. To enumerate the possible composite and split waves, we must determine the conditions under which two elementary waves may be adjacent to each other in the solution.

Let us suppose that two rarefaction waves appear next to each other. Consider the fluid state between them. If the isentrope through this state is smooth when drawn in the P - V plane, then the sound speed, and hence the characteristic speed, is uniquely defined for this state. Therefore the neighboring edges of the two rarefaction waves propagate at the same speed, with the result that the waves are contiguous, and we regard the two waves as forming a single rarefaction wave. On the other hand, the isentrope may have a kink (a discontinuity in slope) at this point, as happens when it passes through a saturation boundary (see Sec. V). In this case the sound speed is discontinuous and the neighboring edges of the two rarefaction waves propagate at distinct speeds. The discontinuity in sound speed must be such that the waves move apart, so the solution is split into separate rarefaction waves.

Two adjacent shock waves are compatible only if they split. (If they move at the same speed they may be combined into a single discontinuity.) Suppose the state that lies between them has a well-defined sound speed. The characteristic for this state cannot impinge on both shock waves, so one of them violates the Lax admissibility criterion. This and other admissibility criteria, such as stability, imply that such a configuration of two shock waves cannot occur physically. When the sound speed is discontinuous at the middle state, however, it is possible for both shock waves to be physical. Solutions consisting of two shock waves that move apart exist if the kink in the isentrope is sufficiently large. This is the phenomenon of shock splitting, which is discussed in Sec. V.

Remark. In multidimensional flow, the subsonic/supersonic admissibility criterion does not imply that two shock waves of the same family must collide; steady-state flows with several shock waves of the same family are possible. This is because the flow in the directions tangent to the shock fronts may cause the particle trajectories to converge and diverge, resulting in transonic flow, just as in a nozzle. This occurs when a supersonic gas jet is injected into a medium with lower ambient pressure (see, e.g., Adamson and Nicholls, 1959).

The same considerations imply that a shock wave may be contiguous to a rarefaction wave only if the shock wave propagates at the same speed as the rarefaction edge. Such a shock wave is said to be sonic, since it moves at the speed of sound relative to the fluid on one

side. We refer to a wave configuration combining a sonic shock wave with a rarefaction wave as a simple composite wave. A rarefaction wave and a shock wave also may be split from each other if the state between them lies on a saturation boundary.

As will be seen, sonic shock waves cannot occur if isentropes are convex. The possibility of composite and split waves therefore requires anomalous behavior of the isentropes: loss of convexity or kinks. In the standard theory, when isentropes are convex and smooth, only individual rarefaction and shock waves may arise. When phase transitions are present, however, composite and split waves are important features of the fluid flow.

In solving the Riemann problem it is advantageous to construct one-parameter families of scale-invariant waves. The shock curve based on a given initial state is a locus of shock waves; similarly, a rarefaction curve is a family of rarefaction waves, each corresponding to a segment of the curve. Shock curves and rarefaction curves also determine families of split shock and rarefaction waves. To construct a locus of simple composite waves, we combine the differential equations for a rarefaction curve with the Rankine-Hugoniot jump conditions, as follows.

A simple composite wave consists of a rarefaction wave adjoining a sonic shock wave. To establish notation, let the rarefaction wave correspond to states along the rarefaction curve between (V_*, E_*, u_*) and (V_0, E_0, u_0) , and let (V, E, u) be the state on the opposite side of the shock wave from (V_0, E_0, u_0) . Families of composite waves may be constructed by allowing either (V_*, E_*, u_*) or (V, E, u) to vary: either the shock wave is fixed and the rarefaction wave is changed, or vice versa. In the first case, (V_*, E_*, u_*) is varied along a rarefaction curve, so this type of composite locus involves the same equations as for rarefaction curves. When (V, E, u) varies, however, (V_0, E_0, u_0) must also vary, since the shock wave joining these states is required to be sonic. The state (V_0, E_0, u_0) follows the rarefaction curve, so we may parametrize the composite locus by V_0 : we set

$$E_0 = E(V_0, S_*) \quad (3.45)$$

and

$$u_0 = u_* \mp \int_{V_*}^{V_0} \rho c \, dV \Big|_{S=S_*}, \quad (3.46)$$

where $S_* = S(V_*, E_*)$, and then solve Eqs. (3.34)–(3.36) together with the sonic condition

$$m = \rho_0 c_0 \quad (3.47)$$

to determine the state (V, E, u) . (A geometrical interpretation of the sonic condition is given in Sec. IV.C.) As V_0 is varied, this procedure defines a one-parameter family of simple composite waves.

In addition to simple composite waves, it is possible for multiple rarefaction and sonic shock waves to propagate together as a single entity. Such complex composite waves arise when isentropes alternate from convexity to

concavity many times. In general, therefore, a scale-invariant wave of a given family may be split into several waves, each being a complex composite wave. The importance of composite and split waves for fluid dynamics is discussed at length in Sec. V.

Remark. Analogously, composite waves may arise in two-dimensional steady supersonic flow. Such a wave consists of an oblique shock wave followed by a compressive Prandtl-Meyer fan.

D. Wave curves and the Riemann problem

The Riemann problem is the initial value problem with scale-invariant initial data. In one dimension, the initial data consist of distinct constant states on the left and right of a jump discontinuity. Because the equations are scale invariant and the initial data are scale invariant, the solution is expected to be scale invariant. (Otherwise the scale invariance would be a "broken-symmetry," in the parlance of physics.) In fact, the Riemann problem may be solved by piecing together the elementary scale-invariant solutions (rarefaction waves, shock waves, and contact discontinuities) that were constructed in Secs. III.A and III.B. In solving the Riemann problem, wave curves play a central role; such a wave curve consists of states connected to a given initial state by a scale-invariant solution. Here we describe wave curves for the standard theory, $\mathcal{G} > 0$, and outline the modifications needed for arbitrary equations of state. The results are proved in Secs. IV and V.

The solution of the Riemann problem consists of a left-facing wave separated from a right-facing wave by a contact discontinuity. Given the left and right states in the initial data, a contact discontinuity must be constructed such that the states on its two sides are connected to the left and right initial states by left- and right-facing waves. Because the jump conditions satisfied across a contact discontinuity are $\Delta u = 0$ and $\Delta P = 0$, the states on the two sides project to the same point in the $P-u$ plane. This fact considerably simplifies the solution of the Riemann problem. Define the right wave curve for a fixed initial state to comprise states that are connected to it by a right-facing wave, with the initial state lying on the right side of the wave; define the left wave curve in the symmetric manner. Then the solution of the Riemann problem may be found by constructing the left and right wave curves starting at the left and right initial states, projecting them onto the $P-u$ plane, and finding their intersections. An intersection point determines two states, corresponding to left- and right-facing waves, that lie on the respective wave curves and have the same pressure and particle velocity, thus forming a contact discontinuity. In essence, the Riemann problem is reduced to constructing wave curves.

Remarks. (1) The system of three conservation laws for one-dimensional fluid dynamics behaves as if it were a system of only two equations because the characteristic speed for contact discontinuities is linearly degenerate.

(2) This procedure for solving the Riemann problem also works when the left and right initial states correspond to materials with different equations of state. We emphasize that a wave curve depends on the EOS as well as the initial state.

Because of Galilean and parity invariance of the fluid equations, wave curves have some symmetry properties: the wave curves for two initial states with the same thermodynamic state but different particle velocities are related by incrementing the velocities, and the left wave curve is the reflection of the right wave curve through the plane $u = u_0$. Therefore we may restrict attention to right-facing waves for initial states with $u_0 = 0$.

In the standard case, $\mathcal{G} > 0$, wave curves are particularly simple, as will be proved in Sec. IV. The Bethe-Weyl theorem shows that a point on the shock curve satisfies the thermodynamic admissibility requirement $S > S_0$ precisely when the wave is compressive, i.e., the state behind the wave has higher pressure. At the same time, the characteristic speed decreases monotonically across the rarefaction wave if and only if it is expansive. The key properties of the elementary waves are as follows: (1) The flow ahead of a shock wave is supersonic relative to the shock front, and the flow behind is subsonic. (2) Rarefaction waves move with the characteristic velocity. As a result, two waves of the same family must overtake each other, so wave splitting and composite waves do not occur. Therefore wave curves consist of shock waves on the compressive branch and rarefaction waves on the expansive branch when $\mathcal{G} > 0$.

The asymptotic behavior of the EOS implies that $|u| \rightarrow \infty$ and $P \rightarrow \infty$ along the compressive branch of the shock curve, and that the expansive branch of the rarefaction curve extends to $P=0$. In general, though, u tends to a finite limit, the escape velocity, as $P \rightarrow 0$ along an isentrope. Therefore wave curves are continuous and semi-infinite. As a result, there are five possibilities for the solution of the Riemann problem, as illustrated in Fig. 4. When the wave curves for the left and right initial states intersect, the left- and right-facing waves may be either shock waves or rarefaction waves. If the wave curves do not intersect, the solution is slightly different from the usual form: it contains two rarefaction waves that reach to the state $P=0$, separated by a region throughout which $P=0$, $V=\infty$, and u is undefined. Such a solution corresponds physically to the opening of a void, or a vacuum, in the material. (For fluids this process is called cavitation, while a solid is said to spall.) Provided one allows for the formation of voids, the solution of the Riemann problem always exists when $\mathcal{G} > 0$, as a result of the asymptotic properties of the EOS.

The uniqueness of the solution to the Riemann problem is related to the monotonicity of wave curves in the $P-u$ plane. When the wave curves are strictly monotonic, $dP/du > 0$ for the right wave curve and $dP/du < 0$ for the left wave curve, they can intersect only at one point and the solution to the Riemann problem is unique. If the wave curves are not monotonic, more than one intersection is possible for some initial conditions and the

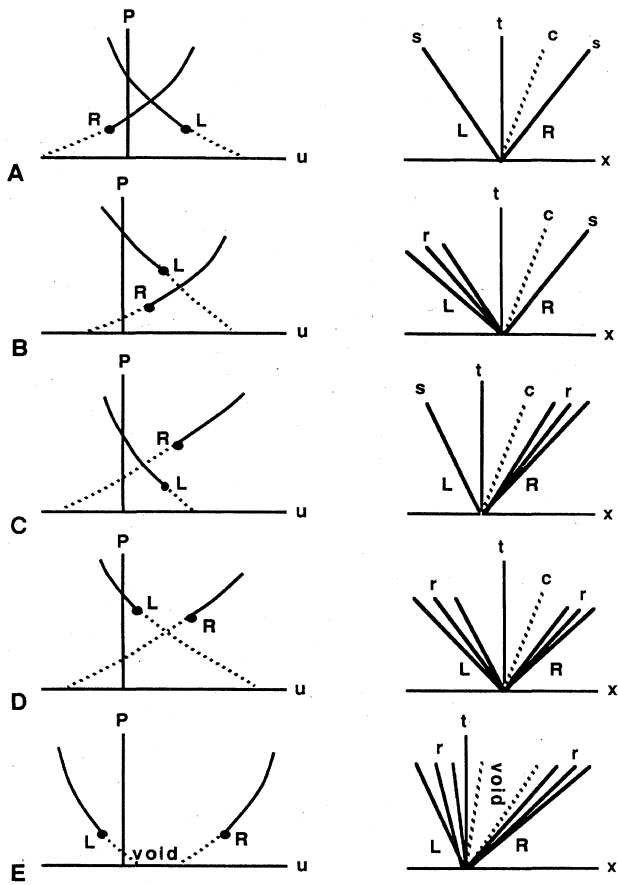


FIG. 4. Possible solutions of Riemann problems.

solution to the Riemann problem is not unique. Such a situation is depicted in Fig. 5. The asymptotic behavior of wave curves implies that there must be an odd number of solutions. Rarefaction curves are always monotonic, since $dP/du = \pm pc$, but shock curves need not be so. Even when $\mathcal{G} > 0$ and $\Gamma > 0$, additional conditions (described in Sec. IV) must be satisfied by the EOS in order that the solution of the Riemann problem be unique.

When a general EOS, not satisfying $\mathcal{G} > 0$, is considered, the Riemann problem may be solved in the same manner by employing wave curves that allow for split

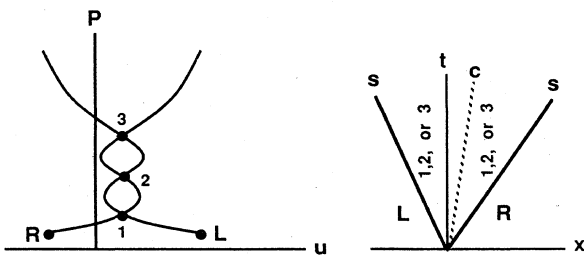


FIG. 5. Nonuniqueness of solutions of a Riemann problem when the wave curve is not monotonic in the $P-u$ plane.

waves and composite waves. Here we outline the results presented in Sec. V. Near its initial state, a wave curve still consists of a branch of shock waves on one side and rarefaction waves on the other. The rarefaction branch must end, however, at the first place that \mathcal{G} vanishes; the wave curve is then continued by a locus of composite waves. Similarly, the shock branch ends if the shock wave becomes sonic, and this branch is followed by a locus of composite or split waves. Further transitions to different types of waves may occur along a wave curve. These transitions correspond to points where the propagation speed of the last wave in the composite, i.e., the characteristic speed for rarefaction waves and the propagation speed for shock waves, reaches a minimum or maximum, respectively. This is because the characteristic speed must vary monotonically across rarefaction waves, and because the monotonicity of shock speed is related to the existence of viscous profiles for shock waves. With the incorporation of these new types of waves, wave curves are again continuous and semi-infinite, and a solution to the Riemann problem always exists. As before, the uniqueness of the solution to the Riemann problem depends on the monotonicity of wave curves.

To summarize, the solution of the Riemann problem may be reduced to constructing wave curves whose asymptotic properties are related to existence of solutions and whose monotonicity is related to uniqueness of solutions. The assumptions made about the asymptotic behavior of the EOS imply that a solution of the Riemann problem always exists, but additional conditions must be satisfied by the EOS in order for the solution to be unique. Without these additional conditions, it is an open problem as to how the nonuniqueness of the Riemann problem is resolved. The resolution of nonuniqueness must incorporate additional physics that is not contained in the simplified equations used to model the dynamics of the system.

IV. PROPERTIES OF SHOCK CURVES

The structure of wave curves, and therefore the solution of the Riemann problem, depends on the geometry of rarefaction and shock curves. In the standard case when $\mathcal{G} > 0$, as will be proved in Sec. IV.B, all states on the expansion branch of the rarefaction curve correspond to physically realizable rarefaction waves, and all states on the compression branch of the shock curve correspond to physical shock waves; these two branches constitute the wave curve. In this case, the questions of existence and uniqueness for the Riemann problem may be answered by establishing some geometrical properties of shock curves.

More generally, a wave curve is the locus of states (V, S, u) that are joined to a fixed initial state (V_0, S_0, u_0) by scale-invariant solutions corresponding to a given wave family. A wave curve comprises rarefaction, shock, and composite waves, as described in Sec. III.D. Portions of it coincide with shock and rarefaction curves,

and the properties of these curves largely determine the structure of the wave curve. In the present section we will concentrate on the properties of shock curves.

After establishing some local and asymptotic properties of shock curves, we study the structure of wave curves when $\mathcal{G} > 0$. The main result is the Bethe-Weyl theorem, generalized to allow arbitrary values of Γ . Then we systematically derive monotonicity properties of shock curves. These properties are used to establish criteria for the equation of state that guarantee uniqueness of solutions of the Riemann problem, following ideas of Smith (1979). We will also use the geometrical properties of shock curves in the next section when we study wave curves in the general case when $\mathcal{G} > 0$ is not assumed.

A. Local structure

A shock curve comprises states satisfying the Rankine-Hugoniot conditions. Because of Galilean and reflection covariance of the fluid equations, we may restrict our analysis to shock curves of right-facing waves for which the initial state lies on the right side of the wave, so that (V_0, S_0, u_0) is the state ahead of the wave and (V, S, u) is the state behind. (The left shock curve for an initial state is simply the reflection, through the plane $u = u_0$, of the corresponding right shock curve.) The state ahead of the shock wave is regarded as being fixed, so the notation used in Sec. III will be modified slightly: the jump ΔA in a quantity A is defined to be $\Delta A = A - A_0$, and the average is $\bar{A} = \frac{1}{2}(A + A_0)$.

The key to analyzing the shock curve is first solving the Hugoniot relation

$$\Delta E + \bar{P}\Delta V = 0, \quad (4.1)$$

since other quantities of interest may be determined afterward:

$$m = (-\Delta P / \Delta V)^{1/2}, \quad (4.2)$$

$$u = u_0 + \Delta P / m, \quad (4.3)$$

$$\sigma = u_0 + V_0 m = u + V m. \quad (4.4)$$

The Hugoniot locus is the set of solutions of the Hugoniot relation, i.e., the projection of the shock curve onto the thermodynamic variables. For a fixed initial state (V_0, S_0) , we define the Hugoniot function by

$$h(V, S) = E(V, S) - E_0 + \frac{1}{2}[P(V, S) + P_0](V - V_0), \quad (4.5)$$

where $E_0 = E(V_0, S_0)$ and $P_0 = P(V_0, S_0)$. The Hugoniot locus is then the solution set of the equation $h(V, S) = 0$.

Remark. On occasion it will be useful to consider the state (V, S) to be fixed and to allow (V_0, S_0) to vary. This locus of initial states that are connected by a shock wave to the given final state is called the backward Hugoniot locus.

In addition to studying the Hugoniot locus in the S - V

plane, we will find it convenient to map the locus onto other thermodynamic planes. The most important is the P - V plane, even though we do not require that $\Gamma > 0$ and thus allow the energy to be multivalued as a function of P and V . It follows from Eq. (4.1) that the Hugoniot locus lies in the quadrant $-\Delta E \Delta V \geq 0$, and equality holds only if $V = V_0$ and $S = S_0$. Furthermore, convexity of E implies that $-P\Delta V + T\Delta S \geq \Delta E \geq -P_0\Delta V + T_0\Delta S$, which when combined with the Hugoniot relation yields the inequality $-\Delta P\Delta V \geq 2 \max\{-T\Delta S, T_0\Delta S\}$. Thus the Hugoniot locus lies in the quadrant $-\Delta P\Delta V \geq 0$, where again equality only holds for the trivial solution (except in the rare circumstance that the initial state lies in a mixture region where $\gamma = 0$). In particular, the mass flux defined by Eq. (4.2) is real all along the Hugoniot locus. Consequently there is a one-to-one correspondence between solutions of the Hugoniot relation and solutions of the Rankine-Hugoniot jump conditions, Eqs. (3.25)-(3.27).

Suppose (V, S) is on the Hugoniot locus, so that $h(V, S) = 0$. Suppose, too, for the moment, that P is continuously differentiable at (V, S) . By the implicit function theorem, the Hugoniot locus is a one-dimensional manifold (i.e., a curve) in a neighborhood of (V, S) , provided that the derivative of h is not zero; otherwise the Hugoniot bifurcates at (V, S) . According to the fundamental thermodynamic identity and the relation $V dP = -\gamma P dV + \Gamma T dS$, the differential of h is

$$dh = \left[1 + \frac{1}{2}\Gamma \frac{\Delta V}{V} \right] T dS - \frac{1}{2} \left[\gamma \frac{\Delta V}{V} + \frac{\Delta P}{P} \right] P dV. \quad (4.6)$$

Therefore bifurcation occurs at a point on the Hugoniot locus if and only if

$$1 + \frac{1}{2}\Gamma \frac{\Delta V}{V} = 0 \quad \text{and} \quad \gamma \frac{\Delta V}{V} + \frac{\Delta P}{P} = 0, \quad (4.7)$$

or equivalently

$$-\frac{V}{P} \frac{\Delta P}{\Delta V} = \gamma = \frac{1}{2}\Gamma \frac{\Delta P}{P}. \quad (4.8)$$

In particular, the Rayleigh line must be tangent to an isentrope, by the first equality. Thus bifurcation occurs only when $m = pc$, or equivalently $\sigma = u + c$, so that the shock wave is sonic.

If (V, S) lies on a saturation boundary, the usual formulation of the implicit function theorem does not apply. However, the energy surface corresponding to the pure phase can be extended across the saturation boundary as a twice continuously differentiable function (physically corresponding to a supersaturated metastable phase), and the arguments above then give the branch of the Hugoniot locus in the pure phase. The branch in the mixed phase is constructed similarly, and the branches join to form a piecewise continuously differentiable curve. Bifurcation may occur only if Eq. (4.8) is satisfied in the limit as the saturation boundary is approached from one side or the other, or if one of the branches is tangent to the saturation boundary. (The behavior of Hugoniot loci

near saturation boundaries is treated in more detail in Sec. V.A.)

Near a bifurcation point, the Hugoniot locus is determined by the Hessian matrix h'' of second derivatives of h , assuming it to be nondegenerate (i.e., to have no zero eigenvalues). It is reasonable to assume that bifurcations occur only at isolated points where the Hessian matrix is nondegenerate (so that h is a Morse function); this is because if h were degenerate, a small perturbation of the EOS would make it nondegenerate. If the signs of the eigenvalues of h'' are the same, the bifurcation point is an isolated solution of the Hugoniot relation, while, if the signs are opposite, the Hugoniot locus crosses itself transversally at the bifurcation point, with tangent directions determined by the eigenvectors of h'' .

Bifurcation does not seem to occur for physically realistic equations of state, although it does play a role in other types of fluid flow, such as immiscible three-phase flow (Shearer *et al.*, 1987). There are several situations in which bifurcation is not possible. For instance, in the standard case when $\mathcal{G} > 0$, the Bethe-Weyl theorem (see below) precludes any shock wave from being sonic. Another sufficient condition that excludes bifurcation is $2\gamma > \Gamma \geq 0$, according to Eq. (4.8); the first inequality, called the weak condition in Sec. IV.C, is expected to hold for most real materials. A bifurcation point on the Hugoniot does occur, however, in the model EOS discussed in Sec. VII; this is an unphysical aspect of that model. In this paper we will presume that bifurcations do not occur.

The Hugoniot curve nearly coincides with an isentrope in the vicinity of the initial state: Eq. (3.44) shows that it has second-order contact with the isentrope $S = S_0$. Therefore the Hugoniot locus near the initial state may be parametrized by specific volume V . It follows from Eq. (4.2) that m has the limit $m_0 = \rho_0 c_0$ as $S \rightarrow S_0$ along the Hugoniot. Moreover, twice differentiating the relation $\Delta u = -m \Delta V$ with respect to V and using $du = -pc dV$ shows that

$$2 \frac{dm}{dV} \Big|_h = - \frac{d^2u}{dV^2} \Big|_h = - \frac{d^2u}{dV^2} \Big|_S = \frac{dpc}{dV} \Big|_S = -\rho_0^2 c_0 \mathcal{G}_0$$

at (V_0, S_0) . (4.9)

In particular, $m \approx m_0 + \frac{1}{2}(pc - \rho_0 c_0) = \frac{1}{2}(\rho_0 c_0 + pc)$ for weak shock waves. When $\mathcal{G}_0 > 0$ the Hugoniot locus is convex in the P - V plane near the initial state; so since $-m^2$ is the slope of the Rayleigh line, the inequalities $\rho_0 c_0 < m < pc$ hold on the compression side, where $V < V_0$ and $S > S_0$. By Eq. (4.4), Lax's characteristic criterion (Lax, 1957),

$$u_0 + c_0 < \sigma \quad \text{and} \quad u < \sigma < u + c , \quad (4.10)$$

for the admissibility of shock waves is satisfied on the compression branch when $\mathcal{G}_0 > 0$; similarly, this criterion and the entropy condition $S \geq S_0$ are satisfied on the expansion branch $V > V_0$ when $\mathcal{G}_0 < 0$. Lax's criterion implies that, relative to the shock front, the flow ahead of

the wave is supersonic ($|u_0 - c_0| < c_0$) and the flow behind it is subsonic ($|u - \sigma| > c$). Geometrically, both characteristics impinge on the shock front from ahead, while one characteristic enters and one leaves the shock front from behind. These conditions, which have been shown to hold for weak waves, are necessary, but not sufficient, for the stability of the shock waves of arbitrary strength, as will be discussed further in Sec. VI.

B. Asymptotic properties

A fundamental result concerning the structure of Hugoniot loci is the following characterization:

Theorem 4.1 (Bethe, 1942; Weyl, 1949). *The Hugoniot locus through an initial state (V_0, S_0) intersects each isentrope at least once. Moreover, if $\mathcal{G} > 0$ along an isentrope, then the Hugoniot locus intersects it exactly once; in this case, $V < V_0$ and $|u - \sigma| < c$ if $S > S_0$, while the opposite inequalities hold if $S < S_0$.*

Proof. Let h_S be the Hugoniot function restricted to the isentrope with entropy S :

$$h_S(V) = E(V, S) - E_0 + \frac{1}{2}[P(V, S) + P_0](V - V_0) . \quad (4.11)$$

From the asymptotic properties (2.40) and (2.41) it follows that $h_S(V) \rightarrow -\infty$ as $V \rightarrow 0$; and since $h_V(S) > -E_0 + \frac{1}{2}P_0(V - V_0)$ when $V > V_0$, $h_S(V) \rightarrow +\infty$ as $V \rightarrow \infty$. By continuity, therefore, h_S has at least one root, so that the Hugoniot locus intersects the isentrope at least once.

Assume now that $\mathcal{G} > 0$. Notice that h_S may be written

$$h_S(V) = E(V_0, S) - \int_{V_0}^V P(V', S) dV' - E_0 + \frac{1}{2}[P(V, S) + P_0](V - V_0) . \quad (4.12)$$

Since $\mathcal{G} > 0$, isentropes are strictly convex in the P - V plane; consequently,

$$\frac{1}{2}[P(V, S) + P_0](V - V_0) > \int_{V_0}^V P(V', S) dV' \quad (4.13)$$

when $V > V_0$. In addition, $E(V_0, S) - E(V_0, S_0) \geq 0$ when $S \geq S_0$, since $T > 0$. As a result, $h_S(V) > 0$ when $V > V_0$ and $S \geq S_0$. Similarly, $h_S(V) < 0$ when $V < V_0$ and $S \leq S_0$. Therefore the roots of h_S occur with $V < V_0$ when $S > S_0$, and with $V > V_0$ when $S < S_0$.

Differentiating Eq. (4.11) yields

$$h'_S(V) = -\frac{1}{2} \left[P - P_0 - \frac{\partial P}{\partial V} \Big|_S (V - V_0) \right] \quad (4.14)$$

and

$$h''_S(V) = \frac{1}{2}(V - V_0) \frac{\partial^2 P}{\partial V^2} \Big|_S . \quad (4.15)$$

Because of the convexity of the isentrope, h_S is strictly concave when $V < V_0$ and strictly convex when $V > V_0$. This implies the uniqueness of the root of h_S .

Furthermore, $h'_S(V) > 0$ at the point where $h_S(V) = 0$.

Equation (4.14), combined with Eqs. (3.34), (3.31), and (3.18), shows that

$$h'_S(V) = -\frac{1}{2}\rho^2(V-V_0)[c^2-(u-\sigma)^2] > 0. \quad (4.16)$$

Therefore $|u-\sigma| < c$ when $V < V_0$, and $|u-\sigma| > c$ when $V > V_0$. \square

Remarks. (1) The original proofs of this theorem involved different arguments. The proof by Bethe (1942) is valid for $\Gamma > -2$, and the proof by Weyl (1949) is valid for $\Gamma > 0$. Our proof makes no assumptions about Γ . Anomalies that occur when Γ changes sign are discussed in Sec. V.C.

(2) The proof of the theorem may be extended to show what happens when \mathcal{G} is allowed to change sign. In this instance, the number of times the Hugoniot locus intersects an isentrope is no more than 1 plus the number of sign changes of \mathcal{G} along that isentrope. Moreover, intersections of the Hugoniot with an isentrope $S > S_0$ may occur with $V > V_0$. Such an intersection corresponds to a shock wave that rarefies the fluid even though it increases entropy; this type of wave will be discussed in more detail in Sec. V.B. Furthermore, the possibility arises that the Hugoniot locus has a disconnected branch or loop. The weak condition, which is discussed below, excludes this from occurring. Thus when the weak condition holds, the Hugoniot locus is a single curve connected to the initial state, but it might not be parametrized by entropy.

(3) This theorem has a geometric interpretation: the isentropes foliate state space, and the Hugoniot curve is a continuous cross section of this foliation when $\mathcal{G} > 0$.

(4) Notice that the Hugoniot locus intersects the $S=0$ isentrope, i.e., the cold curve, at a finite specific volume V_∞ , which depends on (V_0, S_0) and satisfies

$$E_c(V_\infty) - E_0 + \frac{1}{2}[P_c(V_\infty) + P_0](V_\infty - V_0) = 0. \quad (4.17)$$

Thus $E \rightarrow E_c(V_\infty)$ and $P \rightarrow P_c(V_\infty)$ as $S \rightarrow 0$ along the Hugoniot curve.

For real materials, the condition $\mathcal{G} > 0$ is satisfied only in restricted regions of state space, so the second half of the Bethe-Weyl theorem might seem to have limited applicability. Nevertheless, its proof has important consequences for most materials. Consider strong, compressive shock waves, viz., those with large entropy S and with $V < V_0$. Typically $T(V, S) > T(V_0, S) \rightarrow \infty$ and $P(V, S) > P(V_0, S) \rightarrow \infty$ as $S \rightarrow \infty$, so that states with large S and $V < V_0$ have uniformly high temperatures and pressures. Most materials vaporize and behave as an ideal gas under these conditions. (This is discussed in Sec. IV.C.) When S is large, therefore, an isentrope is expected to be convex for all $V < V_0$. The proof of the Bethe-Weyl theorem then shows the compressive branch of the Hugoniot locus intersects an isentrope with large entropy exactly once, and that $|u-\sigma| < c$ for the corresponding shock wave.

We now draw some conclusions from the Bethe-Weyl theorem under the assumption that $\mathcal{G} > 0$ throughout state space. First of all, the Hugoniot locus does not bi-

furcate because shock waves cannot be sonic. Thus the Hugoniot locus is a continuous curve consisting of a single connected branch, which may be parametrized by S , $0 \leq S < \infty$. Because the entropy must not decrease across a physical shock wave, i.e., $S \geq S_0$, only the compression branch ($V < V_0$) of the Hugoniot corresponds to physical shock waves. On the other hand, only the expansion branch ($V \geq V_0$) of the isentrope $S = S_0$ corresponds to realizable rarefaction waves, as follows from Eq. (3.23) with $\mathcal{G} > 0$; this branch may be parametrized by $V \geq V_0$. The union of these two branches is the wave curve.

As described in Sec. III.D, the asymptotic behavior of wave curves determines whether solutions of the Riemann problem exist. By the asymptotic property (2.43) of the EOS, $P \rightarrow \infty$ and $E \rightarrow \infty$ as $S \rightarrow \infty$ along the shock branch of a wave curve. Therefore Eqs. (3.37) and (3.38) show that $|u| \rightarrow \infty$ and $|\sigma| \rightarrow \infty$ as $S \rightarrow \infty$. Moreover, the asymptotic condition (2.42) shows that $P \rightarrow 0$ as $V \rightarrow \infty$ along the rarefaction branch of a wave curve. (As mentioned in Sec. III.A, however, $|u|$ may remain bounded as $V \rightarrow \infty$ along the rarefaction branch.) These asymptotic properties of wave curves, which hold when $\mathcal{G} > 0$, guarantee that any Riemann problem has at least one solution. This solution consists of left- and right-facing waves, which are either compressive shock waves or expansive rarefaction waves, separated by a contact discontinuity or a vacuum region.

Remarks. (1) When $\mathcal{G} > 0$ does not hold, the structure of the wave curve is more complicated. Nevertheless, the arguments just given usually extend to the general case. As discussed above, strong compressive waves are shock waves. Therefore the compressive branch of a general wave curve eventually coincides with the Hugoniot locus and has the same asymptotic behavior as when $\mathcal{G} > 0$. Moreover, the expansive branch usually extends to $P=0$. We conclude that a solution of any Riemann problem exists and has the standard structure, except that the left- and right-facing waves also may be composite or split waves.

(2) Equations (3.37)–(3.39) show that

$$E \rightarrow \frac{1}{2}u^2, \quad P \rightarrow \rho_0 u \sigma, \quad \text{and } u \rightarrow (1 - \rho_0/\rho)\sigma \quad (4.18)$$

in the limit of strong shock waves, $S \rightarrow \infty$. (More precisely, the ratios of the sides approach unity.)

When $\mathcal{G} > 0$, the Hugoniot locus is parametrized by the mass flux m , and hence the shock speed $\sigma = u_0 + V_0 m$, as well as by the entropy S : differentiating Eq. (4.1) and using the fundamental thermodynamic identity shows that

$$\begin{aligned} T dS &= \frac{1}{2} \Delta P dV - \frac{1}{2} \Delta V dP \\ &= \frac{1}{2} (\Delta V)^2 d \left[-\frac{\Delta P}{\Delta V} \right] = (\Delta V)^2 m dm. \end{aligned} \quad (4.19)$$

Thus the shock speed σ and the negative slope m^2 of the Rayleigh line both increase as the shock strength increases. In particular, $m^2 > m_0^2 = \rho_0^2 c_0^2$. Equivalently, $\sigma > u_0 + c_0$, i.e., $|u_0 - \sigma| > c_0$, when $S > S_0$. In the Galilean frame in which the shock wave is stationary,

therefore, the flow is supersonic ahead of the wave and subsonic behind the wave. Consequently, the Lax admissibility conditions (4.10) are equivalent to the entropy criterion $S > S_0$ for arbitrarily strong shock waves, provided that $\mathcal{G} > 0$.

Remark. The Galilean frame in which $u_0 = 0$ is especially convenient for experimental work with shock waves. Shock Hugoniot data is often presented in plots of the shock speed $U_s = \sigma$ versus the particle speed $U_p = u$, as measured in this frame (Marsh, 1980). The intercept of this curve at $U_p = 0$ is $U_s = c_0$. As seen from the asymptotic relations (4.18), U_s is proportional to U_p in the strong shock regime, $U_p \rightarrow \infty$, with proportionality constant determined by the limiting compression ratio. (In fact, for many materials the $U_s - U_p$ relation is very nearly linear for pressures up to several megabars. However, the slope of the curve in this range is not the asymptotic slope.) The Lax conditions require that $c_0 < U_s$ and $U_p < U_s < U_p + c$. In general, however, there are no inequalities relating c to U_p or U_s . For a polytropic gas in the strong shock limit,

$$\frac{U_p}{c} \rightarrow \left[\frac{2}{\gamma(\gamma-1)} \right]^{1/2},$$

$$\frac{U_s}{c} \rightarrow \frac{\gamma+1}{[2\gamma(\gamma-1)]^{1/2}}. \quad (4.20)$$

Therefore $c < U_p$ when $1 < \gamma < 2$, whereas $c > U_p$ when $\gamma > 2$; $c < U_s$ when $1 < \gamma < 2 + \sqrt{5}$, whereas $c > U_s$ when $\gamma > 2 + \sqrt{5}$. Furthermore, $c > U_s$ occurs for weak shock waves in the model described in Sec. VII. The results of these examples may be stated another way. For a right-facing wave, the subsonic/supersonic condition implies that the speed of the fast characteristic relative to the shock front increases across the wave: $u + c - \sigma > 0 > u_0 + c_0 - \sigma$. However, the speed of the slow characteristic relative to the shock front, $u - c - \sigma$, may either increase or decrease.

C. Monotonicity properties

Uniqueness of solutions of the Riemann problem depends on the local geometry of Hugoniot loci. To understand this geometry, we establish criteria under which various quantities parametrize the Hugoniot locus. Throughout this section, points where the Hugoniot locus intersects a saturation boundary, as well as bifurcation points, will be excluded from consideration. Behavior near saturation boundaries is studied in Sec. V.A, where results similar to those of the present section are proved.

At points where the pressure is continuously differentiable (i.e., away from saturation boundaries), the Hugoniot locus may be parametrized smoothly by a single variable, which we regard as measuring shock strength. A convenient choice of the shock strength parameter α is given by requiring that

$$dV = - \left[1 + \frac{1}{2} \Gamma \frac{\Delta V}{V} \right] V d\alpha \quad (4.21)$$

along the Hugoniot locus. For weak shock waves, then, specific volume decreases with increasing shock strength, as is consistent with the standard theory. Once this choice has been made, the variation of other quantities with shock strength is determined. First of all, by equating dh in Eq. (4.6) to zero, one finds that

$$T dS = -\frac{1}{2} \frac{\Delta V}{V} \left[\gamma + \frac{V}{P} \frac{\Delta P}{\Delta V} \right] PV d\alpha$$

$$= -\frac{1}{2} \frac{\Delta V}{V} [c^2 - (u - \sigma)^2] d\alpha. \quad (4.22)$$

[To be precise, α is defined by Eq. (4.22) when the quantity in large parentheses in Eq. (4.21) vanishes.] Thus S increases with shock strength along the compression branch if and only if $c > |u - \sigma|$; i.e., the flow is subsonic behind the shock. Furthermore, the identity $V dP = -\gamma P dV + \Gamma T dS$ shows that

$$dP = \left[\gamma - \frac{1}{2} \Gamma \frac{\Delta P}{P} \right] P d\alpha. \quad (4.23)$$

Similar relations for dE and dT follow from the fundamental thermodynamic identity and the relation $(PV/T)dT = -\Gamma P dV + gT dS$:

$$dE = \left[\frac{\bar{P}}{P} - \frac{1}{2} (\gamma - \Gamma) \frac{\Delta V}{V} \right] PV d\alpha \quad (4.24)$$

and

$$dT = \left[\Gamma - \frac{1}{2} g \frac{\Delta P}{P} - \frac{1}{2} (\gamma g - \Gamma^2) \frac{\Delta V}{V} \right] T d\alpha. \quad (4.25)$$

The mass flux m , the particle velocity u , and the shock speed σ are defined along the Hugoniot locus through Eqs. (4.2). A simple calculation using Eqs. (4.21) and (4.23) yields

$$dm = \rho_0 d\sigma = \frac{1}{2} \frac{P}{\Delta P} \left[\gamma + \frac{V}{P} \frac{\Delta P}{\Delta V} \right] m d\alpha \quad (4.26)$$

and

$$du = \frac{1}{2} \left[\gamma - \Gamma \frac{\Delta P}{P} - \frac{V}{P} \frac{\Delta P}{\Delta V} \right] \frac{P}{m} d\alpha. \quad (4.27)$$

These formulas lead to some interesting relations. For example, Eqs. (4.21) and (4.23) show that

$$-\frac{V}{P} \frac{dP}{dV} \Big|_h = \frac{\gamma - \frac{1}{2} \Gamma \Delta P / P}{1 + \frac{1}{2} \Gamma \Delta V / V}, \quad (4.28)$$

which implies that Γ may be determined along a Hugoniot locus from measurements of the slope of the Hugoniot and the sound speed. Equation (4.28) may be rewritten as

$$-\frac{dP}{dV} \Big|_h + \frac{\Delta P}{\Delta V} = \left[\frac{\gamma P}{V} + \frac{\Delta P}{\Delta V} \right] \Big/ \left[1 + \frac{1}{2} \Gamma \frac{\Delta V}{V} \right], \quad (4.29)$$

which relates the slopes of the Hugoniot, Rayleigh line, and isentrope. Similarly, Eqs. (4.23) and (4.27) combine to give a formula for $dP/du|_h$. For later purposes it is convenient to express this quantity in terms of $dP/dV|_h$:

$$\frac{dP}{du} \Big|_h = 2m \left[1 - \frac{m^2}{dP/dV|_h} \right]^{-1}. \quad (4.30)$$

As another example, combining Eqs. (4.22) and (4.26) demonstrates that

$$T dS = (\Delta V)^2 m dm \quad (4.31)$$

along the Hugoniot locus. An important consequence is the following.

Theorem 4.2. *At a point on a shock curve where it is smooth, the following conditions are equivalent: (a) the entropy S is an extremum; (b) the mass flux m is an extremum; (c) the shock speed σ is an extremum; (d) the slope of the Rayleigh line is an extremum; (e) the Rayleigh line is tangent to the Hugoniot locus; (f) the Rayleigh line is tangent to an isentrope; (g) $|u - \sigma| = c$ (i.e., the shock wave is sonic). When these conditions hold, the Hugoniot locus is tangent to an isentrope. Conversely, conditions (a)–(g) are true if the Hugoniot is tangent to an isentrope and $\Gamma \neq 0$ at this point.*

Proof. Conditions (a) and (b) are equivalent by Eq. (4.31). Conditions (b) and (c) are equivalent because $\sigma = u_0 + V_0 m$, and (b) and (d) are equivalent because $-m^2$ is the slope of the Rayleigh line. Since the Rayleigh line is a chord on the graph of the Hugoniot, the equivalence of (d) and (e) is a geometrical fact; analytically it follows from differentiating the difference quotient. Conditions (d) and (f) are equivalent by Eq. (4.26). Finally, conditions (f) and (g) are equivalent because $-\partial P/\partial V|_S = \rho^2 c^2$ and $-\Delta P/\Delta V = m^2 = \rho^2(u - \sigma)^2$.

Conditions (e) and (f) imply that Hugoniot is tangent to an isentrope. Conversely, the identity $\Gamma T dS = V dP + \gamma P dV$ shows that the entropy along any curve in the P - V plane is an extremum at a point of tangency with an isentrope, provided that $\Gamma \neq 0$. \square

Remark. A variant of this theorem that holds even when the Hugoniot intersects a saturation boundary is proved in Sec. V.A.

Several conditions on the EOS were introduced by Smith (1979) in analyzing the uniqueness of the Riemann problem. They are also important for discussing monotonicity of thermodynamic and hydrodynamic quantities along the Hugoniot locus. The conditions are

$$\Gamma \leq PV/E \quad (\text{strong condition}),$$

$$\Gamma \leq \gamma + \frac{1}{2}PV/E \quad (\text{medium condition}),$$

$$\Gamma \leq 2\gamma \quad (\text{weak condition}).$$

Under the assumption that $\mathcal{G} > 0$, these conditions are related in the manner suggested by their names; this relationship is a consequence of the following result.

Lemma 4.3 (Smith, 1979). *If $\mathcal{G} > 0$, then*

$$\gamma > \frac{1}{2}PV/E. \quad (4.32)$$

Proof. Notice that $\lim_{V \rightarrow \infty} E(V, S) \geq E_{\min} = 0$, so

$$E(V, S) \geq \int_V^\infty P(V', S) dV'. \quad (4.33)$$

Since isentropes are strictly convex when $\mathcal{G} > 0$, the integral may be bounded below by the area of the inscribed triangle with hypotenuse tangent to the isentrope at (V, P) ; thus

$$\int_V^\infty P(V', S) dV' > \frac{1}{2}P(V, S) \frac{P(V, S)}{-\partial P/\partial V|_S} = \frac{1}{2}PV/\gamma, \quad (4.34)$$

so $E(V, S) > \frac{1}{2}PV/\gamma$. \square

Corollary 4.4. *If $\mathcal{G} > 0$, then the strong condition implies the medium condition, and the medium condition implies the weak condition.*

Remarks. (1) We emphasize that Eq. (4.32) and the preceding corollary may not be true if $\mathcal{G} > 0$ is violated.

(2) Smith defined his strong condition to be $\Gamma < \gamma$. In contrast to the conditions above, it is not directly related to monotonicity of a variable along the Hugoniot, so we prefer the definition above. Although Smith's strong condition neither implies, nor is implied by, our strong condition, it does imply the medium condition. The equivalent condition $\partial P/\partial V|_E < 0$ was first employed by Bethe (1942), who showed it to be sufficient to obtain uniqueness of the Riemann problem, assuming $\mathcal{G} > 0$ and $\Gamma > -2$. Wendroff (1972) and Liu (1975) also used this condition in studying the Riemann problem when \mathcal{G} may be negative.

Smith's conditions are local conditions on the EOS. Their importance derives from their relation to the monotonicity of quantities along the Hugoniot locus. Smith (1979) recognized the relationship between uniqueness of solutions of the Riemann problem, which is essentially a question of monotonicity of u and P along wave curves, and the medium and weak conditions. More generally we have the following.

Theorem 4.5. *At a point on the compression branch of the Hugoniot, in the direction of increasing shock strength, (a) V decreases monotonically if the strong condition holds; (b) E and u increase monotonically if the medium condition holds; (c) P increases monotonically if the weak condition holds.*

Proof. According to Eq. (4.21), V decreases monotonically with α if $1 + \frac{1}{2}\Gamma\Delta V/V > 0$. Since $-\Delta V = \Delta E/\bar{P} > 0$ on the compression branch, the strong condition implies that

$$1 + \frac{1}{2}\Gamma \frac{\Delta V}{V} = 1 - \frac{\Gamma}{V} \frac{E - E_0}{P + P_0} \geq 1 - \frac{P}{E} \frac{E - E_0}{P + P_0} > 0; \quad (4.35)$$

this establishes (a). Results (b) and (c) are proved by analogous arguments. \square

Remark. In Sec. V.A it is shown that this result remains true at points where the Hugoniot locus intersects the saturation boundary.

Other monotonicity results may be derived.

(1) The Bethe-Weyl theorem implies that S and σ increase monotonically along the Hugoniot, provided $\mathcal{G} > 0$.

(2) The temperature T increases monotonically along the compression branch of the Hugoniot if the condition $\Gamma \geq \frac{1}{2}\mathcal{G}$ holds, as is seen from Eq. (4.25). This condition also implies the weak condition, since $\gamma\mathcal{G} \geq \Gamma^2$. Alternatively, the identity

$$(\gamma PV/T)dT = \Gamma V dP + (\gamma\mathcal{G} - \Gamma^2)T dS \quad (4.36)$$

shows that T increases monotonically if $\mathcal{G} > 0$, $\Gamma \geq 0$, and the weak condition holds.

(3) The specific enthalpy $H = E + PV$ satisfies the identity $dH = T dS + V dP$. Therefore it increases with shock strength if $\mathcal{G} > 0$ and the weak condition holds.

(4) The behavior of the sound speed c along the Hugoniot is determined by the dimensionless third derivative

$$\mathcal{H} = \frac{V^2}{2\gamma T} \frac{\partial^3 E}{\partial S \partial V^2} = \frac{1}{2} \left[\Gamma + \frac{PV}{\gamma} \frac{\partial \gamma}{\partial E} \Big|_V \right], \quad (4.37)$$

which may be calculated knowing only the incomplete EOS. Since \mathcal{H} may be written

$$\mathcal{H} = \frac{1}{2\gamma} \frac{\partial c^2}{\partial E} \Big|_V = \frac{1}{2\gamma T} \frac{\partial c^2}{\partial S} \Big|_V = \frac{\mathcal{G}}{2\gamma} \frac{T}{PV} \frac{\partial c^2}{\partial T} \Big|_V, \quad (4.38)$$

$\mathcal{H} > 0$ if and only if c increases with temperature. The coefficient \mathcal{H} enters the thermodynamic identities

$$(1/2\gamma)dc^2 = \mathcal{H}T dS - (\mathcal{G} - 1)P dV, \quad (4.39)$$

$$\frac{1}{2}dc^2 = [\gamma\mathcal{H} - \Gamma(\mathcal{G} - 1)]T dS + (\mathcal{G} - 1)V dP, \quad (4.40)$$

$$(\Gamma/2\gamma)dc^2 = [\gamma\mathcal{H} - \Gamma(\mathcal{G} - 1)]P dV + \mathcal{H}V dP. \quad (4.41)$$

In order that c should increase monotonically along the Hugoniot, it is necessary to assume that $\mathcal{G} > 1$, because $dc/d\alpha \rightarrow -dc/\partial V|_S = (\mathcal{G} - 1)c$ in the limit of weak shock waves. According to Eq. (4.39), one sufficient set of conditions for c to increase with shock strength is that $\mathcal{G} > 1$, $\mathcal{H} \geq 0$, and the strong condition holds. For example, these conditions hold for a polytropic gas. By Eq. (4.40), another set of sufficient conditions is that $\mathcal{G} > 1$, $\gamma\mathcal{H} \geq \Gamma(\mathcal{G} - 1)$, and the weak condition holds. To understand these conditions better, observe that the definition $c^2 = \gamma PV$ and Eq. (4.41) show that

$$-\frac{\partial \log P}{\partial \log V} \Big|_c = 1 + \frac{V}{\gamma} \frac{\partial \gamma}{\partial V} \Big|_c = \gamma - \Gamma(\mathcal{G} - 1)/\mathcal{H}. \quad (4.42)$$

When $\Gamma > 0$, $\mathcal{G} > 1$, and $\mathcal{H} > 0$, we have the upper bound

$-\partial \log P / \partial \log V|_c < \gamma$, so isentropes in the P - V plane cross curves of constant c with greater negative slope. The lower bound $0 \leq -\partial \log P / \partial \log V|_c$ is equivalent to the condition $\gamma\mathcal{H} \geq \Gamma(\mathcal{G} - 1)$ used above, provided $\mathcal{H} > 0$. For a polytropic gas, $\mathcal{H} = \mathcal{G} - 1$ and $\Gamma = \gamma - 1$, so that $-\partial \log P / \partial \log V|_c = 1$. For most real materials, away from phase transitions, $\Gamma > 0$, $\gamma > 1$, and γ varies slowly. In this case, Eqs. (2.24), (4.37), and (4.42) imply that $\mathcal{G} > 1$, $\mathcal{H} > 0$, and $-\partial \log P / \partial \log V|_c > 0$. Therefore we expect c to be monotonically increasing with shock strength for most real materials in their pure phases when the weak condition holds.

The sound speed does not always vary monotonically, however. For instance, if there is a sonic point on the Hugoniot locus (which requires that $\mathcal{G} < 0$ somewhere), then c must lose monotonicity; this is described in more detail in Sec. V.C. Another exception (see Sec. V.D) occurs when isentropes cross (which requires that $\Gamma < 0$). In addition, there is a region in which c decreases with shock strength in the model EOS analyzed in Sec. VII.

Remarks. (1) The variation of γ is given by

$$\begin{aligned} \frac{1}{2}PV d\gamma &= [\gamma\mathcal{H} - \Gamma(\mathcal{G} - \frac{1}{2})]T dS \\ &\quad + [\mathcal{G} - \frac{1}{2}(\gamma + 1)]V dP. \end{aligned} \quad (4.43)$$

Comparing this with Eq. (4.40), we see that γ need not vary monotonically along the Hugoniot locus even if c^2 does. In fact, γ decreases with shock strength when a strong shock wave causes gas molecules to ionize and dissociate.

(2) The variation of Γ with V along an isentrope is related to \mathcal{H} just as the variation of γ with V is related to \mathcal{G} :

$$-V \frac{\partial \gamma}{\partial V} \Big|_S = 2\gamma\mathcal{G} - \gamma(\gamma + 1), \quad (4.44a)$$

$$-V \frac{\partial \Gamma}{\partial V} \Big|_S = 2\gamma\mathcal{H} - \Gamma(\Gamma + 1). \quad (4.44b)$$

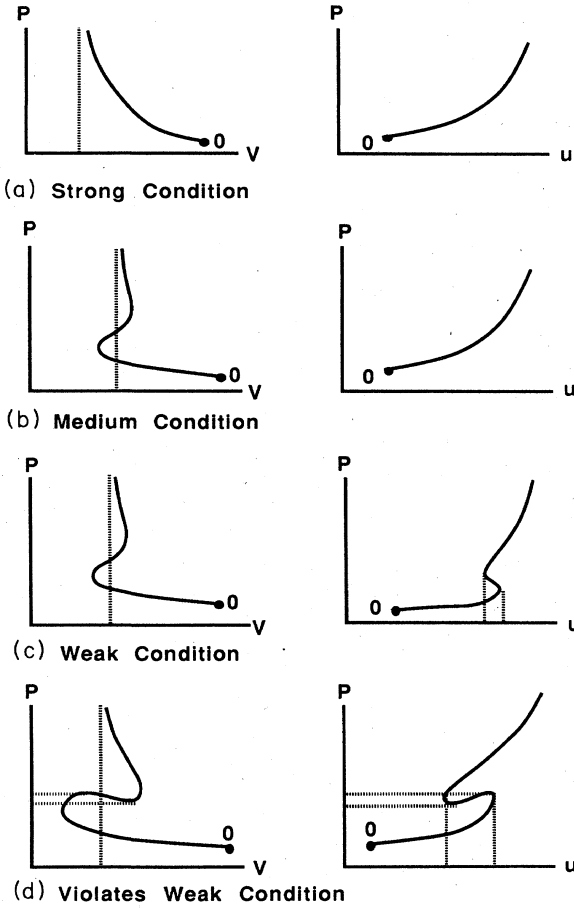
In addition, notice that $\Gamma = -(V/T)\partial T/\partial V|_S$ and that

$$\mathcal{H} = \frac{V^2}{2\gamma T} \frac{\partial^2 T}{\partial V^2} \Big|_S. \quad (4.45)$$

Consequently, T is decreasing and convex as a function of V along an isentrope when $\Gamma > 0$ and $\mathcal{H} > 0$. This is the analog of having P decreasing and convex as a function of V along an isentrope when $\gamma > 0$ and $\mathcal{G} > 0$. Conversely, if $\Gamma < 0$ in some bounded region, but Γ becomes positive asymptotically as $V \rightarrow 0$ and $V \rightarrow \infty$ along an isentrope, then $\mathcal{H} > 0$ is violated.

(3) Besides \mathcal{G} and \mathcal{H} , there are two other third derivatives of E . One is related to $\partial \Gamma / \partial S|_V$, and the other to $\partial \mathcal{G} / \partial S|_V$. For our purposes these additional derivatives are not important.

Examples of Hugoniot loci corresponding to the Smith conditions are sketched in Fig. 6. In these examples we have assumed that $\mathcal{G} > 0$. The strong condition [Fig. 6(a)]

FIG. 6. Hugoniot locus in the P - V and P - u planes.

is satisfied by polytropic gases, for which $\Gamma = PV/E$. In addition, the strong condition typically holds in the limit of strong shock waves, as we now argue. Because of the high temperatures behind strong shock waves, the material behaves as an ideal gas. More precisely, the thermal kinetic energy dominates the internal energy of the constituents at large temperatures for fixed V , so that the material behaves as a gas of weakly interacting particles with strongly repulsive cores. In this case, arguments similar to those leading to the van der Waals approximation show that the EOS is given by

$$P[V - V_*(E)] = (\gamma_0 - 1)E \quad (4.46)$$

to leading order in the virial expansion, where V_* is the effective excluded core volume and γ_0 is a constant. Furthermore, as $E \rightarrow \infty$ the constituents may approach each other more closely, so $V_*(E)$ decreases as E increases. It follows that

$$\frac{PV}{E} - \Gamma = -\frac{1}{\gamma_0 - 1} \frac{P^2 V}{E} \frac{dV_*}{dE} \geq 0. \quad (4.47)$$

Thus the strong condition holds in the strong shock limit. Equation (4.47) also implies that

$$(\gamma - 1) - \Gamma = -\frac{V}{P} \frac{\partial P}{\partial V} \Big|_E - 1 = \frac{V_*}{V - V_*} \geq 0, \quad (4.48)$$

so that $\Gamma \rightarrow \gamma - 1$ as $T \rightarrow \infty$ at fixed V . (In Sec. VI we will see that this is required for stability of strong shock waves in more than one dimension.) Moreover, PV/T for an ideal gas remains bounded in this limit, so the first equality in Eq. (4.22) implies that $\alpha \rightarrow \infty$ as $S \rightarrow \infty$ along the Hugoniot locus. In the limit of infinitely strong shock waves, therefore, V decreases to its limiting value, and all thermodynamic variables have the same asymptotic behavior as for an ideal gas. Observe that this result requires rather special assumptions on the EOS.

Remark. To be precise, the discussion above requires more careful consideration of the physics. At very high temperatures atoms are completely ionized, so that the material is a plasma of electrons and ions. The dominant interaction is the Coulomb force, which has a long range of influence. However, because of Debye-Hückel screening, the interaction is effectively short range (Landau and Lifshitz, 1958). Therefore the argument above, which assumes weakly interacting particles, is essentially correct.

For moderately strong shock waves, however, real gases typically violate the strong condition, even away from phase transitions. This is because the temperature behind a shock wave may be higher enough to cause dissociation and ionization of the molecules in the gas. Below the dissociation (ionization) threshold, energy is absorbed by vibrational (electron excitation) modes; so a large increase in the internal energy corresponds to only a small increase in the pressure. Thus $-\Delta V = \Delta E/\bar{P}$ grows quickly and the material is "soft," i.e., has a low sound speed. When the threshold has been surpassed, the dissociation or ionization leads to more constituent particles, and a large increase in pressure behind the shock yields only a small increase in the internal energy. Therefore $-\Delta V = \Delta E/\bar{P}$ decreases, and local extrema in the specific volume result. Multiple extrema may occur, each corresponding to a different internal mode.

The medium condition [Fig. 6(b)] is important because it implies uniqueness of the solution of the Riemann problem when $\mathcal{G} > 0$, as discussed in Sec. III.D. We will see in Sec. VI, however, that the medium condition does not guarantee stability of shock waves in more than one dimension. When the medium condition is violated but the weak condition holds [Fig. 6(c)], there are multiple solutions for certain Riemann initial data. The weak condition does exclude secondary bifurcations, as mentioned in Sec. IV.A. It also excludes the Hugoniot locus from having loops and disconnected branches. All real materials known to us satisfy the medium condition, with one possible exception: there is experimental evidence that shock waves in liquids with large heat capacities are unstable (as three-dimensional fronts) near the liquid-vapor phase transitions (Thompson *et al.*, 1986); these materials may satisfy the medium condition but violate the stability condition (Sec. VI), or they may only satisfy the weak condition. We know of no evidence that the weak condition is ever violated [Fig. 6(d)].

Remarks. (1) Smith (1979) has given examples of equations of state for which each condition is violated. However, his examples do not necessarily satisfy the thermodynamic stability requirements $g > 0$ and $g > \Gamma^2/\gamma$. He did not take specific heat into account because it does not affect the dynamics.

(2) If $dV/d\alpha \leq 0$ and $\Gamma > -2$, then $V/V_0 \geq \Gamma/(\Gamma+2)$. The maximum compression ratio is therefore given in terms of the limiting value of Γ . In the limit of strong shock waves, $\Gamma \rightarrow \gamma - 1$, and the limiting compression ratio takes the same form as for polytropic gases: $V_0/V \rightarrow (\gamma + 1)/(\gamma - 1)$. From Eq. (3.32) it follows that $|u - \sigma| > |u_0 - \sigma| \Gamma/(\Gamma+2)$. In particular, $c > |u_0 - \sigma| \Gamma/(\Gamma+2) > \frac{1}{2} \Gamma |u - u_0|$ when the state behind the shock wave is subsonic and $\Gamma > 0$. Similarly, $(1 + \frac{1}{2} \Gamma) |u - u_0| > |\sigma - u_0| > |u - u_0|$ whenever $dV/d\alpha > 0$ and $\Gamma > -2$.

The previous theorem states that the Smith conditions are sufficient for monotonicity of variables along the Hugoniot locus. In a sense, these conditions are also necessary, as we now describe. The key idea, due to Smith (1979), is to study the limit of strong shock waves. Suppose, for instance, that the strong condition is violated at some point (V, S) : $\Gamma > PV/E$. Fixing this state, we consider its backward Hugoniot, i.e., initial states (V_0, S_0) , $V_0 > V$, whose Hugoniot loci contain (V, S) . In the limit of strong shock waves, $S_0 \rightarrow 0$, the specific volume tends to a limit V_∞ that depends on (V, S) ; also, $P_0 \rightarrow P_\infty = P_c(V_\infty)$ and $E_0 \rightarrow E_\infty = E_c(V_\infty)$. We assume, for the moment, that $P_\infty = 0$ and $E_\infty = 0$. Then

$$1 + \frac{1}{2} \Gamma \frac{\Delta V}{V} = 1 - \frac{\Gamma}{V} \frac{E - E_0}{P + P_0} < 1 - \frac{P}{E} \frac{E - E_0}{P + P_0}, \quad (4.49)$$

and the last expression can be made arbitrarily small by taking S_0 close to zero. Thus there are initial states (V_0, S_0) for which $1 + \frac{1}{2} \Gamma \Delta V/V$ is negative near (V, S) ; since this quantity is positive for weak shock waves, the specific volume cannot be monotonic all along the Hugoniot through (V_0, S_0) , according to Eq. (4.21). When $P_\infty \neq 0$ or $E_\infty \neq 0$, Γ must violate the strong condition to a more extreme degree, $\Gamma > (P + P_\infty)V/(E - E_\infty)$, in order for this argument to work. For simplicity we state the following theorem; it is proved using arguments similar to those just given.

Theorem 4.6. Suppose that $P_0 \rightarrow 0$ and $E_0 \rightarrow 0$ as $S_0 \rightarrow 0$ along the backward Hugoniot of a state (V, S) . Then there exists an initial state (V_0, S_0) such that monotonicity along the Hugoniot is violated at (V, S) for these variables: (a) V when the strong condition is violated; (b) u and E when the medium condition is violated; (c) P when the weak condition is violated.

Remarks. (1) We emphasize that violating a monotonicity condition at a point does not mean that all Hugoniot loci that contain this point are nonmonotone. For instance, a Hugoniot locus whose initial state (V_0, S_0) is close to (V, S) is monotone near (V, S) . The theorem only shows that the Hugoniot for some initial state loses

monotonicity.

(2) One may ask whether the condition $\Gamma \leq (P + P_\infty)V/(E - E_\infty)$, which is weaker than $\Gamma \leq PV/E$, is sufficient for monotonicity of V along the Hugoniot locus. In this case, Eq. (4.35) is replaced by

$$\begin{aligned} 1 + \frac{1}{2} \Gamma \frac{\Delta V}{V} &= 1 - \frac{\Gamma}{V} \frac{E - E_0}{P + P_0} \geq 1 - \frac{P + P_\infty}{E - E_\infty} \frac{E - E_0}{P + P_0} \\ &= \frac{V_\infty - V_0}{V_\infty - V}. \end{aligned} \quad (4.50)$$

Thus the proof is as before so long as $V_0 < V_\infty$ for V_0 along the backward Hugoniot of the state (V, S) . This extra condition is satisfied provided V_0 increases monotonically along the backward Hugoniot, which is true if, for example, $\Gamma \geq 0$ everywhere (since then $1 + \frac{1}{2} \Gamma \Delta V/V > 0$ when $\Delta V > 0$). Similar statements hold in regard to the monotonicity of other variables.

(3) When the entropy increases along the Hugoniot curve (e.g., $\mathcal{G} > 0$) and $\Gamma > 0$, the thermodynamic identity $\Gamma T dS = \gamma P dV + V dP$ shows that $dP/d\alpha < 0$ and $dV/d\alpha < 0$ are incompatible. It follows, then, that monotonicity along the Hugoniot is lost first in V , then in u and E , and finally in P . Similar results were obtained by Hayes (1958).

(4) As a consequence of the asymptotics of the wave curve in the $P-u$ plane, i.e., $P \rightarrow \infty$ as $|u| \rightarrow \infty$, the Riemann problem must have an odd number of solutions. When the medium condition is violated, so that monotonicity in u is lost, the Riemann problem for certain initial data has three solutions. When the weak condition is violated, so that monotonicity is lost first in u and then in P , the Riemann problem for certain initial data has five solutions.

Finally, we observe that Eqs. (4.21)–(4.28) may be used to obtain geometric interpretations for local extremum of the hydrodynamic quantities along the Hugoniot locus. This is based on some simple geometric relations: Consider a curve in the $x-y$ plane; then (1) $f = \Delta y/\Delta x$ has an extremum if and only if $dy/dx = \Delta y/\Delta x$; (2) $g = \Delta x \Delta y$ has an extremum if and only if $dy/dx = -\Delta y/\Delta x$; (3) $h = (\Delta x)^2/\Delta y$ has an extremum if and only if $dy/dx = 2\Delta y/\Delta x$. These relations are obtained by differentiating the definitions of f , g , and h .

Proposition 4.7. Consider a point where the Hugoniot locus is smooth. (a) In the $P-V$ plane, $dm = 0$ if and only if $\partial P/\partial V|_h = \Delta P/\Delta V$; $du = 0$ if and only if $\partial P/\partial V|_h = -\Delta P/\Delta V$. (b) In the $P-u$ plane, $dm = 0$ if and only if $\partial P/\partial u|_h = \Delta P/\Delta u$; $dV = 0$ if and only if $\partial P/\partial u|_h = 2\Delta P/\Delta u$. (c) In the $V-u$ plane, $dm = 0$ if and only if $\partial u/\partial V|_h = \Delta u/\Delta V$; $dP = 0$ if and only if $\partial u/\partial V|_h = 2\Delta u/\Delta V$.

Proof. The results follow from Rankine-Hugoniot formulas. For (a) use $m^2 = -\Delta P/\Delta V$ and $(\Delta u)^2 = -\Delta P \Delta V$; for (b) use $m = \Delta P/\Delta u$ and $\Delta V = -(\Delta u)^2/\Delta P$; for (c) use $m = -\Delta u/\Delta V$ and $\Delta P = -(\Delta u)^2/\Delta V$. \square

For a general EOS, the Hugoniot locus is not known analytically, as it is for a polytropic gas. Computing

solutions of the Rankine-Hugoniot conditions usually requires an iterative method to determine the solution of nonlinear equations. Typically the state of the fluid behind the shock is to be calculated once the value of one quantity behind the shock, together with the state ahead of the shock, has been specified. The iteration algorithm is much simpler if this quantity varies monotonically along the Hugoniot locus; in fact, some algorithms require convexity of this quantity as a function along the Hugoniot. As we have seen, however, some variables, such as V , need not be monotonic, let alone convex. Thus the monotonicity conditions are important in designing numerical algorithms, as well as for uniqueness of solutions of the Riemann problem.

V. ANOMALOUS WAVE STRUCTURE CAUSED BY PHASE TRANSITION

The behavior of the isentropes and the Hugoniot loci in the P - V plane is the key to determining the structure of scale-invariant waves. In the case of an isentrope, this is because its negative slope $-\partial P/\partial V|_S$ in this plane is the square of the acoustic impedance, $(\rho c)^2$, which governs the propagation of waves. In particular, the variation of the characteristic speed along a rarefaction curve is proportional to $\partial^2 P/\partial V^2|_S$. Changes in the convexity of an isentrope thus result in the formation of composite or split waves. Furthermore, the behavior of isentropes is reflected in the behavior of Hugoniot loci. Sufficiently large changes in convexity of isentropes lead to sonic points on Hugoniot loci, which give rise to composite waves or split shock waves. Generally speaking, anomalous wave structure is associated with loss of convexity.

One consequence is that wave curves may have multiple branches, which leads to nonuniqueness of solutions of Riemann problems. The nonuniqueness is a result of using idealized evolution equations that neglect certain physical effects, such as viscosity and heat conduction. In the standard theory, nonuniqueness of the wave curve is resolved rather easily by the entropy condition or the Lax characteristic criterion. The nonuniqueness in anomalous cases must be resolved by accounting for additional physics effects that become important, such as by requiring the existence and stability of viscous profiles for shock waves. This is also important for computations: a numerical algorithm, e.g., a finite difference scheme, is deterministic and leads to a definitive result, but not necessarily the correct answer if subgrid effects are important but are modeled inadequately.

Phase transitions in the fluid are a principal cause of nonconvexity, since the sound speed in a mixed-phase region is smaller than in the pure phase. This phenomenon is the object of study in the present section. We must emphasize, however, that we have made an assumption that generally is inappropriate when the fluid undergoes a phase change: the pressure appearing in the dynamical equations is the equilibrium pressure. The use of the

equilibrium pressure is tantamount to assuming instantaneous transitions. In actuality, the transition from one phase to another does not take place instantaneously, and the fluid is out of equilibrium during the transition. If the time for transition between phases is short relative to the time scale of the flow, an equilibrium model may be adequate. (Even in this case, though, the flow may be profoundly affected by the dynamics of the transition.) When the transition time is not short, account must be made for nonequilibrium phenomena. We regard the present paper, in which the fluid is assumed to be always in thermodynamic equilibrium, as a step towards constructing and analyzing models that account for non-equilibrium effects.

Let us mention some qualitative phenomena caused by phase transitions. If a shock wave initiates a phase change, it cannot be regarded as a simple jump discontinuity. Immediately behind the wave the fluid is in a metastable state; farther downstream the fluid relaxes to an equilibrium state. For example, in a transition from a vapor to a liquid, the vapor is supersaturated initially and then condenses as the shock wave passes. Thus a discontinuity is followed by a relaxation wave (see, e.g., Zel'dovich and Raizer, 1966) in which the fluid returns to equilibrium. The further the fluid is out of equilibrium, the faster is the relaxation. There are several situations in which such internal structure for shock waves is crucial.

(1) Shock waves in supersonic flow through nozzles, such as wind tunnels and jet engines, may cause condensation of a supersaturated vapor (e.g., water vapor). These waves are called condensation shock waves.

(2) A detonation wave is a shock wave followed by a narrow zone in which chemical reactions occur (Hayes, 1958; Fickett and Davis, 1979). The reaction may be regarded as a relaxation process starting from a metastable unreacted state to a fully reacted equilibrium state. The precise manner in which the chemical reaction proceeds has important consequences for the dynamics of the wave; thus the reaction zone may not be ignored even if it is thin. For instance, both the reaction rate (Fickett and Davis, 1979) and the propagation speed of a detonation wave (Bdzil and Stewart, 1986; Jones, 1987, 1989; Bukiet, 1989) are affected by the curvature of the wave front (in contrast to ordinary shock waves). The steady portion of the reaction zone may end at a sonic point in which the fluid is only partially reacted; in this case, determination of the state behind a detonation wave requires more information than simply the equilibrium EOS for the reaction products.

(3) The van der Waals EOS provides a standard analytical EOS that exhibits a phase transition. In portions of state space, however, the van der waals EOS does not conform to the requirements of thermodynamic stability. Unless the Maxwell equal-area rule is applied to modify the EOS, van der Waals loops cause the sound speed to be imaginary and the fluid equations to be of mixed hyperbolic/elliptic type. If the van der Waals equation of state is adopted, then the pressure that appears in the

system of conservation laws is not the equilibrium pressure. However, one may regard the van der Waals EOS as providing a dynamical model for nonequilibrium phenomena. Admissibility conditions for shock waves in a van der Waals fluid were analyzed by Shearer (1983) and Slemrod (1983). All of these cases are excluded in this paper by assuming an equilibrium EOS.

Near a phase transition, the standard assumption about the equation of state, viz., convexity and nonoverlap of isentropes, may be violated. In this section, we first determine the behavior of isentropes and Hugoniot loci in the neighborhood of phase transitions. In particular, the results in Sec. IV.C about monotonicity are generalized to account for kinks in the Hugoniot loci at saturation boundaries. Then these results are applied to determine the structure of wave curves in three situations: (1) when the wave curve crosses the saturation boundary and has kinks; (2) when the wave curve passes near the saturation boundary and loses convexity; and (3) when Γ may vanish, so that the entropy is multivalued in the P - V plane. Finally we summarize these results.

A. Behavior of isentropes and Hugoniot loci at saturation boundaries

The nonanalytic behavior of the equation of state caused by phase transitions is a principal source for loss of convexity. This is illustrated in Fig. 7, in which an isotherm (T), an isentrope (S), and a Hugoniot locus (H) are drawn passing through a saturation boundary in the P - V plane. The qualitative features of this diagram are justified by the following considerations.

A single point on the coexistence curve in the P - T plane (Fig. 1) corresponds to a line segment of mixed states in other thermodynamic planes. Thus isotherms and isobars coincide in the mixed phase; in particular,

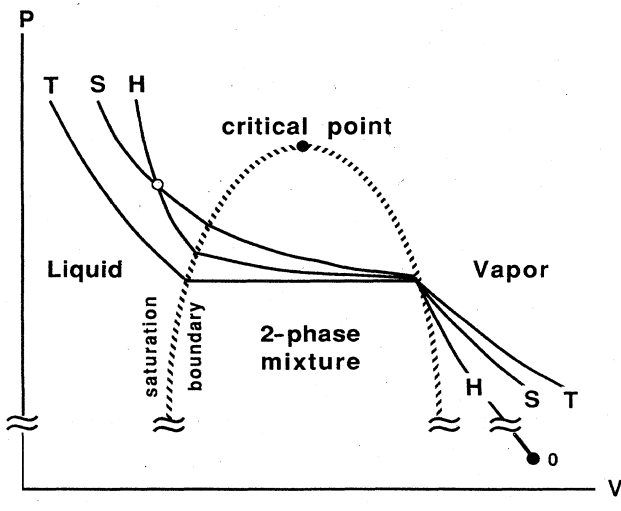


FIG. 7. Isotherm (T), isentrope (S), and Hugoniot locus (H) in the P - V plane near a phase transition. It is possible for the intersection of H and S to lie inside mixed-phase region.

isotherms are horizontal in the P - V plane (Fig. 3). An isotherm drawn in this plane therefore has a kink (a discontinuity in slope) at a saturation boundary, as indicated in Fig. 7. Correspondingly, an isentrope also has a kink, which may be expressed as a jump in the sound speed c and in the adiabatic exponent $\gamma = -(V/P)dP/dV|_S$:

$$\frac{c^2 - c_m^2}{c_m^2} = \frac{\gamma - \gamma_m}{\gamma_m} = (\gamma g - \Gamma^2) \left[\frac{T}{V} \frac{dS}{dP} \Big|_{\text{sat}} \right]^2 \geq 0, \quad (5.1)$$

where the subscript m indicates that the quantity is evaluated in the mixed phase, and all other quantities are evaluated in the pure phase. (We refer to Appendix A for derivations of this and other thermodynamic results used in this section.) This important relation shows that the sound speed is always smaller on the mixed-phase side of the saturation boundary. (It is an example of Le Chatelier's principle.) In Fig. 7 the isentrope has a shallower slope in the mixed phase, in conformity with this discontinuous drop in sound speed. According to Eq. (2.24), the jump in γ entails a δ -function singularity in the fundamental derivative \mathcal{G} . The coefficient of the δ function is non-negative if and only if the isentrope is convex at the saturation boundary.

It also may be shown that Γ is discontinuous at a saturation boundary:

$$\frac{\xi - \gamma}{\Gamma} = \frac{\xi - \gamma_m}{\Gamma_m}, \quad (5.2)$$

where $\xi = -(V/P)dP/dV|_{\text{sat}}$ measures the slope of the saturation boundary in the P - V plane. Assuming that Γ and Γ_m are nonzero, either the isentrope is tangent to the boundary on both sides ($\gamma = \xi = \gamma_m$), or it crosses transversally through the boundary ($\gamma \neq \xi$ and $\gamma_m \neq \xi$). In the latter case, noting that the isentrope may be parametrized by V , geometrical considerations show that $\xi - \gamma$ and $\xi - \gamma_m$ must have the same sign, so that Γ and Γ_m have the same sign. Furthermore, since $\gamma \geq \gamma_m$, either $\xi > \gamma$ and $|\Gamma_m| \geq |\Gamma|$, or $\xi < \gamma_m$ and $|\Gamma_m| \leq |\Gamma|$.

It is useful to classify a point on a saturation boundary as being normal if the isentrope through it is strictly convex there, and as being retrograde otherwise. Equivalently, a point is normal if the isentrope passing through it crosses from the mixed to the pure phase, so that the sound speed increases as the density increases. In Fig. 7 the saturated vapor boundary is shown as being retrograde, while the saturated liquid boundary is normal. According to this definition, retrograde behavior of saturation boundaries (usually) leads to anomalous wave structure. In studies of liquid-vapor phase transitions (Thompson *et al.*, 1986), the dimensionless quantity

$$r = \frac{\partial T}{\partial V} \Big|_P \frac{dS}{dP} \Big|_{\text{sat}}, \quad (5.3)$$

called the retrogradicity, is introduced. To see how r relates to the behavior of the saturation boundary, we express r as

$$r = \frac{\gamma - \gamma_m}{\gamma_m} \frac{\xi}{\xi - \gamma} \quad (5.4)$$

by using thermodynamic identities and Eq. (5.3). Suppose that at a point on the saturation boundary the mixed phase has higher density than the pure phase at the same pressure, as is true along the saturated vapor boundary of the liquid-vapor transition (Fig. 3). Then the geometry implies that the point is normal if and only if $0 \leq \xi < \gamma$; by Eqs. (5.4) and (5.1), this is equivalent to $r \leq 0$. Similarly, a point is normal when $r \geq 0$, provided that the pure phase is the higher-density phase, as along the saturated liquid boundary. The saturation boundaries for the liquid-vapor transition are usually normal, but in fluids with high heat capacity, a portion of the saturated vapor boundary may be retrograde (Thompson *et al.*, 1986). Such a situation is indicated in Fig. 2 by the portion along which $dS/dV|_{\text{sat}} < 0$. Furthermore, saturation boundaries for liquid-solid transitions and for polymorphic transitions are often retrograde.

We now consider the behavior of a Hugoniot locus as it passes through a saturation boundary. The results of Sec. IV.C were proved under the assumption that the pressure was continuously differentiable. When the pressure has a jump discontinuity in its derivative, we require a slight generalization of the implicit function theorem.

Lemma 5.1. Suppose that f is continuous on a neighborhood of a point (x_0, y_0) for which $f(x_0, y_0) = 0$. Suppose also that for each x , $(\partial f / \partial y)(x, y)$ exists for almost every y , and that there are constants c and C such that $0 < c \leq \partial f / \partial y \leq C$. Then there are piecewise continuously differentiable functions \hat{x} and \hat{y} such that $\hat{x}(0) = x_0$, $\hat{y}(0) = y_0$, and $f(\hat{x}(\alpha), \hat{y}(\alpha)) = 0$ for sufficiently small α . Moreover, the parametrization may be chosen such that $d\hat{x}/d\alpha = \partial f / \partial y$ and $d\hat{y}/d\alpha = -\partial f / \partial x$ wherever the derivatives exist.

Proof. In the standard proof of the implicit function theorem, an auxiliary function ϕ_x , defined by

$$\phi_x(y) = y - \left[\frac{\partial f}{\partial y}(x_0, y_0) \right]^{-1} f(x, y),$$

is shown to be a contraction mapping, so that it has a unique fixed point $y = \bar{y}(x)$ for x close to x_0 . The same proof works in the present case if ϕ_x is defined instead by $\phi_x(y) = y - C^{-1}f(x, y)$; we omit the details. Since $\partial f / \partial y$ is bounded away from zero, we can solve the differential equation $d\hat{a}/dx = (\partial f / \partial y)^{-1}$ subject to $\hat{a}(x_0) = 0$. Invert the relation $\alpha = \hat{a}(x)$ to obtain $x = \hat{x}(\alpha)$, and let $y = \hat{y}(\alpha) = \bar{y}(\hat{x}(\alpha))$. Then $d\hat{x}/d\alpha = \partial f / \partial y$, and $d\hat{y}/d\alpha = -\partial f / \partial x$ follows from $df/d\alpha = 0$. \square

Proposition 5.2. Consider a point where the Hugoniot locus intersects a saturation boundary. Assume that on each side of the saturation boundary the bifurcation condition Eq. (4.8) is violated and the Hugoniot locus is not tangent to the boundary. Then the Hugoniot locus may be parametrized by shock strength α , satisfying Eqs. (4.21) and (4.22), in a neighborhood of the intersection point.

Proof. The normals dh and $(dh)_m$ are not opposite in

direction (since the Hugoniot locus is not tangent to the boundary), so there is a coordinate direction dy such that $\partial h / \partial y$ is positive on both sides of the saturation boundary. If a complementary coordinate direction dx is chosen such that the Jacobian determinant of the map from (x, y) to (V, S) is $-V/T$, the parametrization by α in the lemma is equivalent to Eqs. (4.21) and (4.22), as seen from Eq. (4.6). \square

By utilizing this result in the arguments of Sec. IV.C, the monotonicity results are seen to hold even at saturation boundaries. In particular, if the weak condition $\Gamma \leq 2\gamma$ holds, pressure increases with shock strength along the Hugoniot locus. Such a situation is shown in Fig. 7.

In analogy with ξ and γ , let us define

$$\xi = -\left. \frac{V}{P} \frac{dP}{dV} \right|_h = \frac{\gamma - \frac{1}{2}\Gamma\Delta P/P}{1 + \frac{1}{2}\Gamma\Delta V/V} \quad (5.5)$$

to measure the slope of the Hugoniot locus in the P - V plane. Combining this with Eq. (5.2) implies that

$$\frac{\xi - \xi}{\Gamma} \left[1 + \frac{1}{2}\Gamma \frac{\Delta V}{V} \right] = \frac{\xi - \xi_m}{\Gamma_m} \left[1 + \frac{1}{2}\Gamma_m \frac{\Delta V}{V} \right]. \quad (5.6)$$

Notice that $1 + \frac{1}{2}\Gamma V/V \neq 0$ if and only if ξ is finite (i.e., the Hugoniot locus is not vertical); this follows from Eq. (5.5) because bifurcations are excluded. Assuming, then, that ξ and ξ_m are finite and that Γ and Γ_m are nonzero, the Hugoniot locus must either be tangent to the boundary ($\xi = \xi = \xi_m$) or cross transversally through the boundary ($\xi \neq \xi$ and $\xi_m \neq \xi$), just as in the case of isentropes. (We have not precluded the possibility that the Hugoniot locus is vertical on one side and tangent on the other.)

The manner in which the Hugoniot locus suffers a kink at a saturation boundary may be determined using Eq. (5.6). For example, we have the following.

Proposition 5.3. Suppose that the volume decreases with shock strength along the Hugoniot locus near a point on the saturation boundary, and suppose that $dP/dV|_{\text{sat}} - dP/dV|_h$ has the same sign as $dP/dV|_{\text{sat}} - \partial P / \partial V|_S$ on each side of the saturation boundary. Then the Hugoniot locus kinks in the same direction as does the isentrope; i.e., $-dP/dV|_h$ is larger in the pure phase.

Proof. Because the Hugoniot locus is parametrized by V , $1 + \frac{1}{2}\Gamma\Delta V/V > 0$ on both sides of the saturation boundary, and simple geometrical considerations imply that $\xi - \xi$ and $\xi - \xi_m$ have the same sign. By hypothesis, $\xi - \gamma$ and $\xi - \xi$ have the same sign, and so do $\xi - \gamma_m$ and $\xi - \xi_m$. In the case when $\xi > \gamma$, therefore, $|\Gamma_m| \geq |\Gamma|$ with Γ and Γ_m having the same sign; consequently, Eq. (5.6) implies that $\xi - \xi_m > \xi - \xi > 0$. Similarly, $\xi - \xi > \xi_m - \xi > 0$ in the alternative case $\xi < \gamma_m$. In both cases $\xi > \xi_m$. \square

The following variant of Theorem 4.2 is true even at points where the Hugoniot locus intersects the saturation boundary.

Theorem 5.4. Suppose that the weak condition holds at a point on the compression branch of a shock curve. Then the following conditions are equivalent: (a) the entropy S increases with shock strength; (b) the mass flux m increases with shock strength; (c) the shock speed σ increases with shock strength; (d) the negative slope of the Rayleigh line increases with shock strength; (e) $-dP/dV|_h < 0$ or $-\Delta P/\Delta V < -dP/dV|_h$; (f) $-\Delta P/\Delta V < -dP/dV|_S$; (g) $|u - \sigma| < c$ (i.e., the flow behind the shock wave is subsonic).

Proof. The proof is based on the same relations invoked in the proof in Sec. IV.C. In proving the equivalence of (d) and (e), notice that Eq. (5.5) may be used to show that

$$\begin{aligned} \frac{dm^2}{d\alpha} &= \frac{d}{d\alpha} \left(-\frac{\Delta P}{\Delta V} \right) \\ &= -\frac{P}{\Delta V} \left[\gamma - \frac{1}{2} \Gamma \frac{\Delta P}{P} \right] \left[1 - \left(\frac{dP}{dV} \Big|_h \right)^{-1} \frac{\Delta P}{\Delta V} \right]. \end{aligned} \quad (5.7)$$

The weak condition implies that $\gamma - \frac{1}{2} \Gamma \Delta P/P > 0$ on the compression branch, so that $dm^2/d\alpha > 0$ is equivalent to having the bracketed quantity positive, which is equivalent to condition (e). \square

There is an important consequence of this theorem. Suppose that the Hugoniot locus intersects the saturation boundary and that the isentrope through this point has a kink such that it lies below the Rayleigh line on both sides of the boundary; then the wave speed has a local maximum along the Hugoniot curve at the saturation boundary. When this occurs, anomalous wave structure results. This result is a form of the Bethe-Wendroff theorem described below.

The situation just described occurs in Fig. 7 at the saturated vapor boundary. [See also Fig. 8(b) below for a more detailed picture.] Because the isentrope in the mixed phase lies below the Rayleigh line, the entropy decreases along the Hugoniot locus after reaching a max-

imum at the saturation boundary. Therefore the Hugoniot locus lies below the isentrope in the mixed phase near its intersection with the boundary. Eventually the Hugoniot locus crosses above the isentrope as the shock strength increases; here we have shown the crossing to occur outside of the mixed-phase region, but it could have occurred inside the vapor dome.

B. Anomalous wave structure caused by kinks

Kinks in isentropes and Hugoniot loci have consequences for wave curves. To illustrate this, we consider a material with a liquid-vapor phase transition and assume that a portion of the saturated vapor boundary is retrograde. We also assume, for simplicity, that both Γ and \mathcal{G} are positive away from the saturation boundary. (Of course, \mathcal{G} has a δ -function singularity with a negative coefficient along the retrograde portion of the saturation boundary.)

First consider the compression branch H_0 of a Hugoniot locus through an initial state 0. Normally the locus appears as in Fig. 8(a): the Rayleigh line R_1 through a state 1 on H_0 lies above the isentrope S_1 and below the Hugoniot locus H_1 that form the wave curve starting at state 1; this follows from part (f) of Theorem 5.4. If the shock wave from state 0 to state 1 were followed by a shock wave from state 1 to another state on the compression branch of H_1 , the second shock would have a steeper Rayleigh line and hence a faster wave speed; therefore it would overtake the first shock wave. In this sense, shock waves in the standard case are stable against splitting.

If, however, H_0 intersects the retrograde portion of the saturated vapor boundary at state 1, the situation may be different, as can be seen geometrically in Fig. 8. Suppose that the kink in the isentrope through state 1 is severe enough that it lies below the Rayleigh line R_1 in the mixed phase. Then the compression branch H_1 of the Hugoniot locus through state 1, being tangent to this portion of the isentrope, lies below R_1 , as shown in Fig. 8(b). Furthermore, H_1 lies above the continuation of H_0 through the saturation boundary because the entropy maximizes at state 1 along H_0 . The entropy continues to decrease along H_0 until a state 3 is reached at which H_0 is tangent to the Rayleigh line R_3 , whereupon the entropy increases again.

Consider the state 2 at which the extension of the Rayleigh line R_1 intersects H_1 . (This intersection must exist because of our assumptions about the asymptotic behavior of the equation of state.) The state 2 also lies on H_0 , as follows from

Proposition 5.5 (Triple Shock Rule). Consider a system of conservation laws $u_t + f(u)_x = 0$. Suppose that the state u_1 is connected to the state u_2 by a shock with speed s , and that u_2 is connected to the state u_3 by a shock with the same speed s . Then u_1 is connected to u_3 by a shock with speed s .

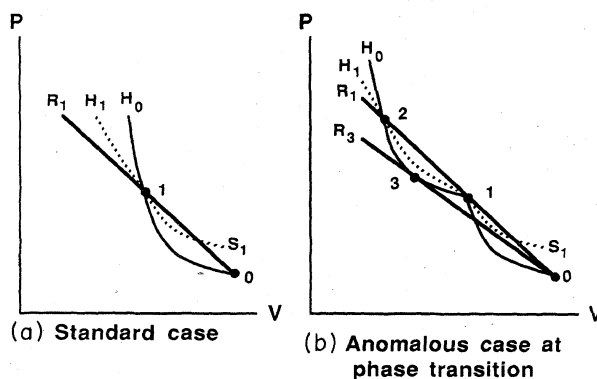


FIG. 8. Hugoniot loci, Rayleigh lines, and isentropes for the standard and anomalous cases at a phase transition.

Proof. Add the Rankine-Hugoniot equations $-s(u_2 - u_1) + f(u_2) - f(u_1) = 0$ and $-s(u_3 - u_2) + f(u_3) - f(u_2) = 0$. \square

In contrast to the standard case [Fig. 8(a)], the anomalous case [Fig. 8(b)] allows for splitting of shock waves (Rice *et al.*, 1958; Zel'dovich and Raizer, 1966). A state b along H_1 between states 1 and 2 corresponds to a shock wave that propagates more slowly than does the shock wave joining states 0 and 1, so that the two waves may coexist in a scale-invariant solution. In this limited range, therefore, split shock waves are possible. For states above state 2, though, shock splitting is disallowed, just as in the standard case.

Remarks. (1) The lead shock wave, joining states 0 and 1 in the vapor phase, is called the precursor, in analogy with the elastic precursor that occurs in an elastic-plastic material that is shocked beyond its elastic limit. The second shock wave carries the fluid from pure vapor (state 1) to a mixed liquid/vapor or a pure liquid state (state b). The transition between the different phases does not occur instantly, so that the second shock wave is smeared more than the precursor when relaxation effects are taken into account.

(2) When the time scale for achieving thermodynamic equilibrium is long, the flow may carry material past the saturation boundary along a metastable isentrope for the pure phase. For example, the metastable fluid may be a superheated liquid or supercooled vapor. When a shock wave causes a nonequilibrium state to occur, shock splitting does not occur at the saturation boundary (Chaves *et al.*, 1985; Meier and Thompson, 1985). In addition, the latent heat or volume change at a phase transition may lead to a self-sustaining wave similar to a weak detonation (Rabie *et al.*, 1979).

(3) Experiments measure the shock speed $U_s = \sigma$ and the particle speed $U_p = u$ (in the Galilean frame where $u_0 = 0$) as the driving pressure is increased. When the shock wave splits, only the precursor is measured. As plotted in the U_s - U_p plane, the data consist of two disconnected portions, the first corresponding to shock waves between states 0 and 1 and the second to shock waves above state 2; split shock waves between states 1 and 2 are measured as the precursor shock wave from state 0 to state 1. Therefore a phase transition stands out as a discontinuous jump in the particle speed in such a plot (Marsh, 1980).

(4) An interesting question is whether state 2, where the Hugoniot loci H_0 and H_1 intersect, lies inside or outside the mixed-phase region.

The possibility of shock splitting leads to branching of the wave curve and nonuniqueness for solutions of the Riemann problem. Indeed, the compression branch of the wave curve through state 0, which starts as the Hugoniot locus H_0 , may be continued past state 1 in two ways. The first way is to continue along H_0 . Notice that even though the entropy decreases between states 1 and 3, the entropy change across the corresponding shock waves is still positive (at least near state 1), so that the en-

tropy inequality (3.32) required by thermodynamics is satisfied. The second way to continue the wave curve is to follow H_1 until state 2 is reached, and then to switch back to following H_0 . States along the portion of H_1 between states 1 and 2 correspond to shock waves that split at state 1. These waves, too, satisfy the entropy inequality, since the entropy change results from the second shock wave in addition to the lead shock wave from state 0 to state 1; thus the entropy of the final state increases monotonically along this alternative continuation of the wave curve.

This branching of the wave curve causes nonuniqueness for the Riemann problem. For example, consider a state a along H_0 between states 1 and 2, as shown in Fig. 9. The Riemann problem with state a on the left and state 0 on the right has a solution consisting of the direct shock wave connecting these states. This same Riemann problem, however, has an alternative solution consisting of a (relatively weak) left-facing shock wave, a contact discontinuity, and a split pair of right-facing shock waves. To see this, we look in the P - u plane.

The qualitative behavior of the relevant curves is shown in Fig. 9. In particular, the shock curve H_0 lies below H_1 in the P - u plane: at state 1 in the P - V plane, $\xi_0 < \xi_1 = \gamma_m$; combining this with Eq. (4.30) implies that $dP/du|_{H_0} < \rho_1 c_m = dP/du|_{H_1}$. Therefore the curve H_a of left-facing shock waves (which is the reflection of the curve of right-facing waves) intersects H_1 at some point b . This point corresponds to two states, b and b' , that are connected by a contact discontinuity. Thus the direct shock wave from state 0 to state a may split into two right-facing shock waves (from state 0 to state 1 and from state 1 to state b), a left-facing shock wave (from state a to state b'), and a contact discontinuity (joining states b and b').

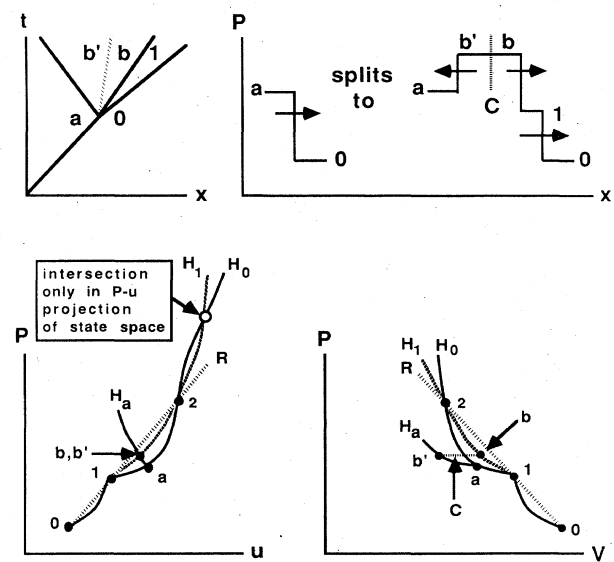


FIG. 9. Shock splitting at a phase transition caused by a kink in the Hugoniot locus.

Another feature of Fig. 9 warrants explanation: in the $P-u$ plane, but not in the $P-V$ plane, the Hugoniot locus H_1 eventually crosses above H_0 again. In the limit of strong shock waves, $P \rightarrow \rho_0(1-\rho_0/\rho)^{-1}u^2$ according to Eq. (4.18), and the compression ratio ρ/ρ_0 approaches a limiting value $(\Gamma+2)/\Gamma$ that is independent of the initial state, as argued in Sec. IV.C. Since $\rho_1 > \rho_0$, therefore, the pressure grows faster along H_1 than along H_0 , as a function of u ; thus H_1 crosses H_0 again in the $P-u$ plane. Notice, however, that having H_0 and H_1 cross in either the $P-u$ or $P-V$ plane need not imply that they cross in the other plane, unless the point of crossing corresponds to a shock with the same speed as the shock wave from state 0 to state 1.

Remark. This asymptotic behavior has an interesting consequence. When one shock wave overtakes another, the result is a shock wave and a reflected wave. In general the reflected wave may be either a rarefaction or a shock wave, depending on whether the state behind the overtaking shock wave lies above or below the Hugoniot of the lead shock wave, as drawn in the $P-u$ plane. When the overtaking shock wave is strong, however, the asymptotic behavior implies that the reflected wave must be a rarefaction wave.

The nonuniqueness of solutions of the Riemann problem may be resolved in several ways. First of all, notice that the entropy is decreasing along H_0 between states 1 and 3, so that by Theorem 5.4 the flow behind a shock wave on this portion of the curve is supersonic. Shock waves in this range therefore violate Lax's characteristic criterion. Physically, such shock waves are unstable with respect to small perturbations of the initial data, as will be shown in Sec. VI. For instance, if the discontinuity in the initial data is smoothed, the dynamics causes the profile to steepen into the configuration of shock waves predicted by solving the Riemann problem using split shock waves. However, this argument does not resolve the nonuniqueness for shock waves between states 3 and 2.

Another way to resolve the nonuniqueness is to consider physical effects that become important at the shock front but which have been neglected by modeling the dynamics using Eqs. (2.4)–(2.6). For example, viscosity and heat conduction terms involve two spatial derivatives and therefore are dominant near the discontinuity; they act to smear the front. Physically realizable solutions should arise as limits of solutions of the more complete equations as the viscosity and heat conduction coefficients vanish. When the solution consists of a single shock wave, one expects it to arise as the limit of traveling-wave solutions of the system of equations with viscosity and heat conduction. A traveling-wave solution approaches two asymptotic states as $x \rightarrow \pm\infty$, and these states must satisfy the Rankine-Hugoniot conditions with the speed being the propagation speed of the traveling wave. If two states satisfying the Rankine-Hugoniot condition are the asymptotic states for some traveling wave, then the shock wave is said to admit a viscous profile. Only these shock

waves are physically admissible.

The construction of traveling waves leads to a system of ordinary differential equations that can be studied by generalizing the phase-plane analysis of Weyl (1949). (See Appendix C for a review of this subject.) Intersections of the Hugoniot locus and the Rayleigh line are critical points of the ordinary differential equation and, therefore, the only possible asymptotic states for traveling waves. A critical point has a stable (unstable) manifold for each characteristic speed smaller (larger) than the shock speed. For instance, if a right-facing shock wave obeys the Lax criterion, the state behind the shock wave is a critical point with one stable and one unstable manifold (since the flow is subsonic), while the state ahead is a critical point with two stable manifolds (since the flow is supersonic).

When the speed of the traveling wave corresponds to a state a along H_0 between states 3 and 2, the Rayleigh line intersects the Hugoniot locus at four points, which correspond to two saddle points and two attracting nodes. We show in Appendix C that there is no orbit for the ordinary differential equations that connects state 0 to state a ; rather, state 0 is connected to the critical point between states 0 and 1. Consequently, shock waves to states on H_0 between states 3 and 2 do not admit viscous profiles and are not physical. On the other hand, shock waves from state 1 to states on H_1 do admit profiles, as does the shock wave from state 0 to state 1. Therefore the physical wave curve between states 1 and 2 comprises split shock waves along H_1 and excludes points along H_0 . By invoking physical admissibility criteria, then, the wave curve no longer branches, and solutions of the Riemann problem are unique (in this case).

An analogous wave structure occurs along the expansion portion of the wave curve. (See Zel'dovich and Raizer, 1966, Chap. XI, Sec. 20.) Suppose that the isentrope through an initial state 0 in the liquid phase intersects the saturated liquid boundary at state 1 and then the retrograde portion of the saturated vapor boundary at state 2. At state 1 the isentrope has a kink but remains convex, so that the sound speed decreases, although discontinuously. Therefore the wave curve continues past state 1 by following the isentrope, but a point a between states 1 and 2 corresponds to a pair of rarefaction waves that split at state 1. The characteristic velocity at the end of the first rarefaction, which connects state 0 to state 1, is larger than the characteristic velocity at the beginning of the second rarefaction, which connects state 1 to state a . The constant state 1 on the saturation boundary separates the two rarefaction waves.

At state 2, however, the sound speed increases discontinuously, so that the wave curve cannot continue along the isentrope past state 2. Instead the wave curve is continued using composite waves that are based on the rarefaction waves already constructed. At first the composite waves comprise a split rarefaction wave, such as that corresponding to state a , followed by a shock wave to a state b in the vapor phase. This shock wave is sonic at state a ,

and it acts to rarefy the fluid. (If state a is near to state 2, the proof of Theorem 5.4 may be used to show that a sonic shock exists and that entropy increases across it; the construction may be continued by moving state a back along the rarefaction.) The sonic condition implies that the Rayleigh line for the shock wave is tangent to the isentrope at state a and guarantees that the shock wave propagates together with the second rarefaction wave as a single entity. In contrast with the standard case, the entropy is increased by waves on the expansive branch, since they cross a retrograde saturation boundary.

As the pressure of the final state b is lowered, the intermediate state a moves back along the isentrope. This continues until either the shock wave becomes sonic at state b or state a reaches state 1. In the former case, the wave curve continues by following the isentrope through state b . The wave structure is as follows: a rarefaction wave connecting states 0 and 1, a constant state 1, a rarefaction wave connecting states 1 and a , a shock wave from state a to state b that is sonic at both of these states, and a rarefaction wave connecting state b with another state c . Because the flow is sonic both ahead and behind the shock wave, the last three waves in the composite propagate together. The presence of the shock wave in the composite wave causes the entropy of the isentrope at state b to be higher than the entropy of state 0. In the later case, the wave structure consists of the rarefaction wave between states 0 and 1 separated by the constant state 1 from a shock wave from state 1 to state b , since the second rarefaction wave has disappeared. As the pressure of state b is lowered still further, either the shock wave becomes sonic at state b , in which case the wave curve is continued in the manner just described, or the shock speed increases to coincide with the characteristic speed at the end of the first rarefaction; i.e., the shock wave is sonic at state 1. In this last case the wave curve continues with simple composite waves: a rarefaction wave connecting state 0 to a state in the liquid phase, followed by a sonic shock wave that vaporizes the fluid. In addition, the initial rarefaction wave may disappear as the pressure of the final state is lowered, whereupon the wave curve follows the Hugoniot through state 0. Eventually, though, the shock speed must stop decreasing; the wave curve then follows an isentrope.

Thus even in the presence of phase transitions a wave curve along which the entropy is nondecreasing can be defined by using composites as elementary waves. Because the resulting wave curve is continuous, the graphical analysis of the Riemann problem proceeds in the usual manner.

C. Anomalous wave structure caused by smooth loss of convexity

Even if an isentrope does not cross a saturation boundary, it may be distorted if it passes near a phase transition. This may cause the standard assumption on the EOS, $\mathcal{G} > 0$, to break down within a pure-phase region, as illustrated in Fig. 10. For example, the van der Waals

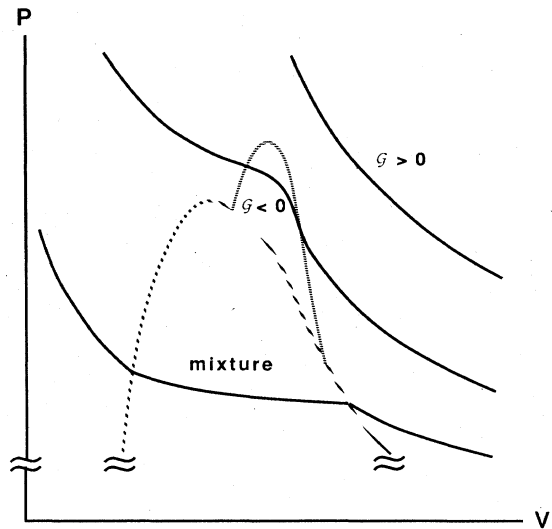


FIG. 10. Nonconvex isentropes.

EOS exhibits a region around the vapor dome in which $\mathcal{G} < 0$ (see Cramer and Sen, 1987). When this occurs the wave speed need not be monotonic along Hugoniot loci and isentropes, and the construction of the wave curve must be modified. Just as in Sec. V.B, additional wave types are possible and wave curves may branch. The wave structure when the isentropes are not convex was studied by Cowperthwaite (1968) and Wendroff (1972). Here we discuss the properties important for the Riemann problem when $\Gamma > 0$ but $\mathcal{G} > 0$ is violated.

A typical Hugoniot locus for this case is sketched in Fig. 11. The following are the important features. Let H_0 be the Hugoniot locus through the initial state 0. Following along H_0 in the direction of increasing P and decreasing V , there is a state 1 at which the Hugoniot

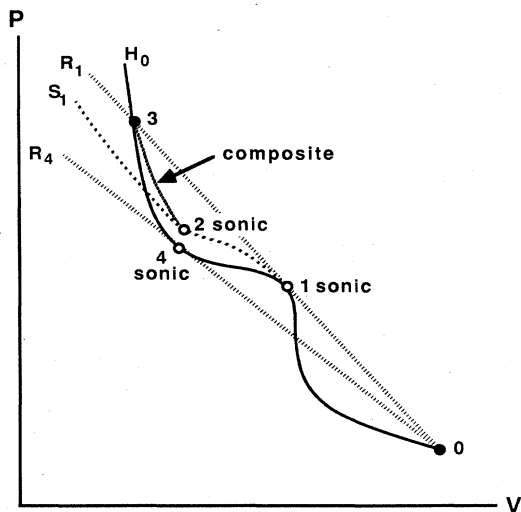


FIG. 11. Hugoniot loci for an anomalous equation of state ($\mathcal{G} > 0$ is violated).

H_0 , the isentrope S_1 , and the Rayleigh line R_1 are all tangent. According to Theorem 4.2, this is a sonic point and a local maximum in entropy. As the shock strength is increased further, the wave speed and entropy decrease until a state 4 is reached, where another Rayleigh line R_4 is tangent to H_0 . This is also a sonic point, but now at a local minimum in entropy. [The entropy at state 4 may be greater than the entropy of the initial state 0, however; in this case these shock waves would be admissible according to the entropy condition (3.43).] Also of interest is the state 3 where R_1 intersects H_0 a second time: the propagation speeds for the shock waves to states 1 and 3 are equal. The characteristic velocity, the shock velocity, and the entropy, as plotted along H_0 , are sketched in Fig. 12 in accordance with the following result.

Theorem 5.6 [Bethe-Wendroff (Bethe, 1942; Wendroff, 1972, Isaacson, Marchesin, and Plohr, 1988b)]. Consider the Hugoniot locus through a state u_0 . Let σ and λ denote shock and characteristic speeds along this curve, and let an overdot denote differentiation with respect to shock strength. Assuming that the locus does not bifurcate at a point u , then the following are equivalent: (a) $\dot{\sigma} = 0$; (b) $\lambda = \sigma$; (c) $\dot{S} = 0$. In this instance, $\lambda - \sigma$, $\dot{\sigma}$, and \dot{S} all vanish to the same order, and the locus is tangent to a rarefaction curve.

Proof. See Appendix B. \square

At a sonic point, the Hugoniot locus is tangent to an isentrope; therefore $dS = 0$ and Eq. (3.23) holds:

$$d(u + c) = -\rho c \mathcal{G} dV. \quad (5.8)$$

It follows from this equation, the Bethe-Wendroff theorem, and Fig. 12 that $\mathcal{G} < 0$ at the first sonic point, because locally λ and V are decreasing. The same result can be obtained by noting that

$$T \frac{d^2S}{dV^2} \Big|_h = \frac{1}{2}(V_0 - V) \frac{d^2P}{dV^2} \Big|_S = \frac{\gamma P}{V} \frac{V_0 - V}{V} \mathcal{G} \quad (5.9)$$

at a sonic point, as follows from differentiating Eq. (3.34) twice. Because sonic points are local extrema in entropy,

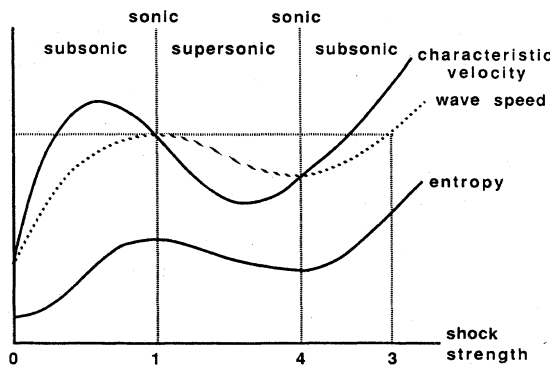


FIG. 12. Entropy, wave speed, and characteristic velocity along a Hugoniot locus for an anomalous equation of state ($\mathcal{G} > 0$ is violated).

the sign of \mathcal{G} alternates at successive sonic points; and since the Rayleigh line is tangent to the Hugoniot locus at a sonic point, the curvatures of the Hugoniot locus and the isentrope have the same sign in the P - V plane at a sonic point (assuming that the weak condition holds). In the degenerate case when $\mathcal{G} = 0$ at a sonic point, the entropy has an inflection point instead of a local extremum, as illustrated in Fig. 13.

When the weak condition holds, V decreases with shock strength at all sonic points, since $-dP/dV|_h = -\Delta P/\Delta V > 0$. It follows from the relation $(\Delta u)^2 = -\Delta P \Delta V$ that the particle velocity increases monotonically along H_0 , as seen from Fig. 11. In order for $\lambda = u + c$ to coincide with σ at state 1, therefore, the sound speed must decrease with shock strength as state 1 is approached. [Another way of seeing this is from Eq. (4.39): c must decrease at the sonic point because $\mathcal{G} < 1$.] This confirms the remark made in Sec. IV that neither λ nor c need vary monotonically along the portion of the wave curve corresponding to shock waves. In addition, $d^2P/du^2|_h < 0$ near the sonic point at state 1, since the Rayleigh line is also tangent to the Hugoniot locus in the P - u plane; therefore the Hugoniot locus may lose convexity in this plane, too. This may cause difficulty for numerical algorithms that solve the Riemann problem using iterative methods to find intersections of wave curves.

As in the case when the isentrope loses convexity because of a kink, the wave curve between state 1 and state 3 is branched. The resulting nonuniqueness of solutions of the Riemann problem is resolved by considering the existence of viscous shock profiles, just as in Sec. V.B. The wave curve is formed by following a segment of shock waves along H_0 up to the sonic point at state 1, and then following a segment of composite waves until a state 2 at which $\mathcal{G} = 0$. Each composite wave consists of the sonic shock wave to state 1 adjoined by a smooth compressive wave that lies along the isentrope S_1 . Because $\mathcal{G} < 0$ along the isentrope from state 1 to state 2, the compressive wave does not steepen to form a shock wave. Beyond state 2 a second sonic shock wave is formed. Composite waves are then of the form sonic shock/compressive wave/sonic shock; this is sketched in Fig. 14(a). Both ends of the compressive wave are sonic

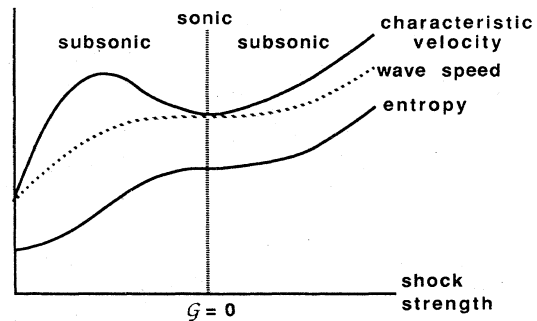


FIG. 13. Entropy, wave speed, and characteristic velocity along a Hugoniot locus for an anomalous equation of state ($\mathcal{G} = 0$ at a sonic point).

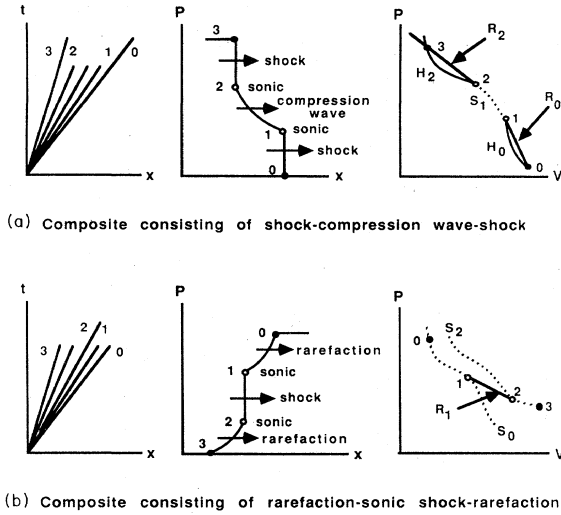


FIG. 14. Composite wave.

relative to the adjacent shock waves and so move with the corresponding shock velocities. Thus the composite wave propagates as a single entity. As the pressure along the wave curve is increased, the second shock wave becomes stronger and the compressive wave weaker. When the compressive wave vanishes, the two shock waves move at the same speed; this occurs at state 3. The wave is analogous to the double-shock structure that occurs when the Hugoniot locus has a kink [Fig. 8(b)]. The wave curve then continues with a branch of shock waves along H_0 . If there were additional oscillations in \mathcal{G} about zero, then the pattern of composite waves would repeat: shock, compression wave, shock, compression wave, etc. Notice that the entropy increases monotonically along the wave curve just constructed.

Remarks. (1) The smooth compression waves are simple waves across which one of the Riemann invariants is constant. Analogously, one of the Riemann invariants is piecewise constant across a composite wave, with the jumps occurring at the sonic shock waves.

(2) In a numerical calculation, a composite wave consisting of a shock/compression wave may not be distinguishable from a shock wave that has been smeared out by lack of grid resolution and artificial viscosity.

A connection may be drawn between the present situation and that in Sec. V.B by considering \mathcal{G} to become more negative over smaller regions, i.e., to develop a δ -function singularity. Then the isentrope develops a kink and the compression wave shrinks to zero strength. To distinguish between these cases experimentally, it is necessary to measure the pressure profile to detect the compression wave. In practice this is difficult to accomplish: most experiments only observe the first shock front.

An analogous wave structure occurs along the expansion portion of the wave curve, as illustrated in Fig. 14(b). The wave curve follows an isentrope until $\mathcal{G}=0$.

Loss of genuine nonlinearity then causes composite waves to be formed, each consisting of a rarefaction wave followed by a sonic shock wave that rarefies the fluid further. Thus the Rayleigh line for the shock wave is tangent to the isentrope at its initial state, the end of the preceding rarefaction. Such a shock wave increases the entropy because $\mathcal{G}<0$, according to Eq. (3.44). Since the flow behind the shock wave is subsonic, the wave curve continues with a segment of composite waves by weakening the rarefaction wave and strengthening the shock wave until the flow behind the shock wave is sonic; at this point the Rayleigh line of the shock wave is tangent to the isentropes at both the initial and the final state. The wave curve then continues with a composite of the form rarefaction/sonic shock/rarefaction. As in the previous section, the shock wave jumps over the region with $\mathcal{G}<0$, and the second rarefaction wave in the composite wave lies on an isentrope with higher entropy than does the first rarefaction wave.

Remarks. (1) Composite waves also occur in the mathematical theory for a scalar quasilinear hyperbolic partial differential equation (Gelfand, 1959). The sonic condition is replaced with the condition that the chord line is tangent to the flux function. For scalar conservation laws, therefore, the flux function plays the role of the isentropes. An entropy condition that guarantees uniqueness for solutions of the Cauchy problem has been given by Oleinik (1959). The wave curve that obeys the entropy condition is constructed from convex hulls of the flux function.

(2) Under the additional assumptions that $\gamma > \Gamma > 0$, Liu (1975) has shown that the construction we outlined with composites leads to a smooth wave curve, and that there exists a unique solution to the Riemann problem. The construction to obtain a single-branched wave curve utilizes an extension of the Oleinik entropy condition: the slope of the Rayleigh line varies monotonically along the Hugoniot locus for any shock wave occurring on the wave curve. In addition, Liu (1976) has shown that only those shock waves that satisfy the Liu-Oleinik criterion have a viscous profile. The existence of shock profiles associated with viscosity and heat conduction is the basis of an extended entropy condition, as discussed in Appendix C. An alternative proof of the uniqueness of solutions of the Riemann problem, under different assumptions, has been given by Sidorenko (1982).

We have been assuming that $\mathcal{G}>0$ at the initial point for the wave curve. In this case the wave curve starts with shock waves for $V < V_0$ and rarefaction waves for $V > V_0$, according to the local theory of Lax (1957). If $\mathcal{G}<0$ at the initial point, then the wave curve starts with smooth compressive waves for $V < V_0$ and shock waves that rarefy the fluid for $V > V_0$; this is a consequence of Eq. (3.44). When $\mathcal{G}=0$ at the initial point,

$$\Delta S = - \frac{V^4}{4!T} \frac{d^3 P}{dV^2} \Big|_S (\Delta V/V)^4 \{1 + O(\Delta V/V)\}, \quad (5.10)$$

as can be shown by repeatedly differentiating Eq. (3.34)

and using the fundamental thermodynamic identity. Consequently, the wave curve either starts with shock waves in both directions or rarefaction waves in both directions, according to the sign of $d^3P/dV^3|_S$.

As we have seen, waves can be combined to form a single-branched, continuous wave curve even when $\mathcal{G} > 0$ is violated. The graphical analysis of the Riemann problem using wave curves is as before.

D. Overlap of isentropes in the P - V plane

Near a phase transition, the coefficient of thermal expansion β , or equivalently the Grüneisen coefficient $\Gamma = \beta V/(C_V K_T)$, may be negative. A notable example is water near freezing. We have shown in Sec. IV.B that the Bethe-Weyl theorem does not require Γ to be positive. Here we discuss some unusual behavior that does occur if $\Gamma > 0$ is violated.

When $\Gamma = (V/T)\partial P/\partial S|_V$ changes sign, S is multivalued if considered to be a function of P and V . To understand this geometrically, consider the equation of state to be a surface in P - V - S space defined by the single-valued function $P = P(V, S)$, as illustrated in Fig. 15. An isentrope is the projection onto the P - V plane of the intersection of this surface with a plane $S = \text{const}$. Changes of sign in Γ lead to folds in this surface, which cause the isentropes to overlap in the manner of Fig. 16. (The projection has the topology of a fold catastrophe. See, e.g., Gilmore, 1981.) The set $\Gamma = 0$ is a smooth, closed curve in the S - V plane, but its projection has cusps; its interior is the region in which the isentropes are multivalues. The number of isentropes that intersect in the P - V plane depends on the number of folds in the EOS surface: for the surface of Fig. 15, the region where

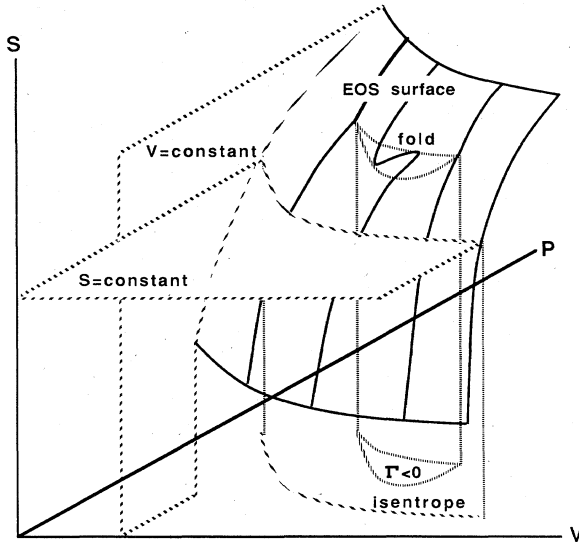


FIG. 15. Anomalous equation of state surface in P - V - S space ($\Gamma > 0$ is violated). The surface exhibits the topology of a fold catastrophe.

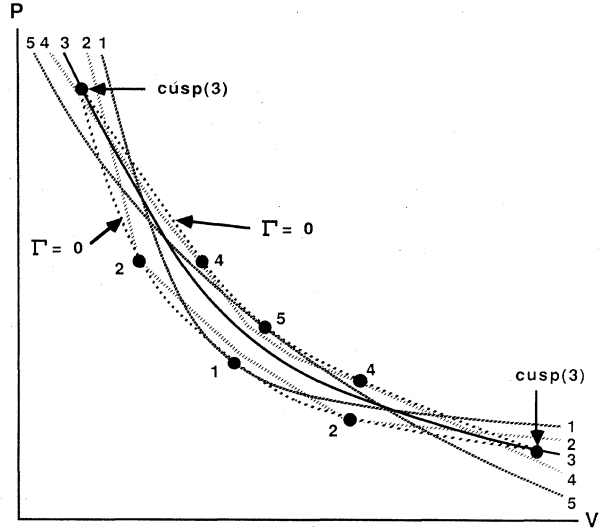


FIG. 16. Isentropes when $\Gamma > 0$ is violated. It is possible for different isentropes to pass through each cusp.

$\Gamma < 0$ is crescent shaped, and up to three isentropes may intersect.

Remark. Notice that when $\Gamma < 0$ on a bounded set, there must be a region of state space in which the sound speed decreases with increasing entropy. To see this, consider the temperature as a function of volume along an isentrope; notice that $\Gamma = -(V/T)\partial T/\partial V|_S$ and that the sign of $\mathcal{H} = (2\gamma T)^{-1}\partial c^2/\partial S|_V$ determines the convexity of this function, according to Eq. (4.45). If the isentrope passes through the region where $\Gamma < 0$, then convexity of T cannot be maintained all along it, so that the sound speed must decrease somewhere.

Suppose that a Hugoniot locus passes through a region where $\Gamma < 0$. Then the change in sign of Γ affects the manner in which the Hugoniot locus, the isentrope, and the Rayleigh line intersect, as illustrated in Fig. 17. At a

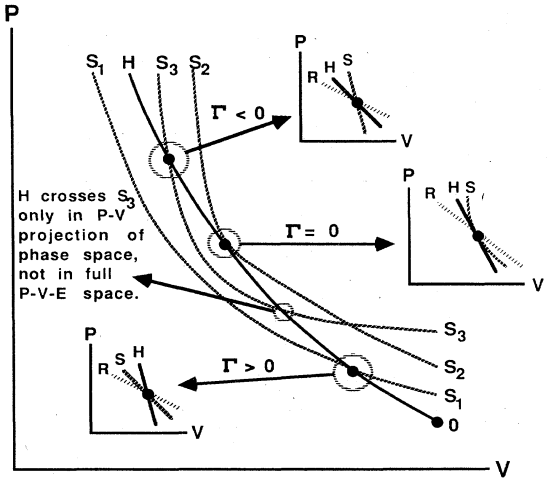


FIG. 17. Hugoniot locus and isentropes for an anomalous equation of state (Γ crosses zero).

point where $\Gamma=0$, the Hugoniot locus and the isentrope are tangent, as seen from the identity $V dP = -\gamma P dV + \Gamma T dS$. Nevertheless, it does not follow that the entropy is a local extremum, in contrast to the normal case when $\Gamma \neq 0$; thus the Rayleigh line is not necessarily tangent to the isentrope, and the shock wave is not necessarily sonic (cf. Theorem 4.2).

E. Summary of anomalies

The results of this section show that the assumption $\mathcal{G} > 0$ is necessary for the standard theory. This assumption excludes real physical phenomena that occur in nature, namely, phase transitions. The theory of elementary waves can be generalized to avoid this assumption by considering split shock waves, composite waves, and shock waves that rarefy the fluid. Nonuniqueness of solutions caused by branching of the wave curve is resolved by requiring the existence of viscous shock profiles. As a consequence, the entropy does not decrease along the wave curve as the wave strength increases. (In particular, the entropy may increase on the expansive branch because of shock waves that rarefy the fluid.) The wave curve may be used in the standard manner to analyze the existence and uniqueness of solutions of the Riemann problem. Existence of a solution follows from the asymptotics of the EOS, while uniqueness depends on monotonicity of the wave curve as drawn in the P - u plane. Anomalous wave structures have been observed experimentally (see the references in Zel'dovich and Raizer, 1966; Thompson *et al.*, 1986; Kutateladze *et al.*, 1987). There is no anomaly in the wave curve when the other assumption of the standard theory $\Gamma > 0$ is violated.

Remarks. (1) We have not analyzed the conditions on the equation of state that guarantee the composite portion of the wave curve to be monotonic; this is an open question.

(2) The anomalous structure of the wave curve has implications for numerical algorithms. Clearly, methods based on Riemann solvers (Godunov methods, the random choice method, and front tracking) need to account for the anomalous wave structure; but finite difference methods, which rely on artificial viscosity to capture shock waves, are also affected. For example, the artificial viscous pressure usually is nonzero only in compression. When $\mathcal{G} < 0$ and shock waves that rarefy the fluid occur, artificial viscous pressure is needed instead for expansive waves.

VI. SHOCK INSTABILITIES AND NONUNIQUENESS OF SOLUTIONS

In previous sections we have studied wave configurations in one spatial dimension. Such waves arise from physical waves in three spatial dimensions by imposing the constraint of planar symmetry. This constraint may preclude modes of instability for the waves that are fundamentally multidimensional. Thus a one-

dimensional wave may be stable with respect to one-dimensional perturbations of the flow and yet be unstable when embedded in three dimensions. In this section we survey some results about stability of shock waves with respect to multidimensional perturbations. The stability conditions may be related to the monotonicity properties of the Hugoniot locus, and thereby to nonuniqueness of solutions of the one-dimensional Riemann problem.

Shock-tube experiments have shown that typically a planar shock front is very stable (see, e.g., Van Moorhem and George, 1975). Physically the reason is as follows (Whitham, 1974). If the shock front is perturbed, the leading or convex part of the disturbance behaves like a diverging wave, while the lagging or concave part of the disturbance behaves like a converging wave. For an ideal gas a similarity solution was derived by Guderley (1942). This solution has the property that converging shock waves strengthen and speed up, whereas diverging shock waves weaken and slow down; moreover, energy considerations suggest that this property is very general. For a perturbed shock front, this mechanism implies that the leading disturbance moves more slowly and that the lagging disturbance moves more quickly. Thus the shock front tends to recover from any perturbations: the front is stable.

More generally we may ask whether multidimensional stability is related to thermodynamic properties of the equation of state and the shape of the Hugoniot locus. For an arbitrary EOS, a linear stability analysis for a planar shock front was performed by D'yakov (1954) and Erpenbeck (1962). They found that the shock front is stable if and only if

$$-1 \leq R \leq 1 + 2M, \quad (6.1)$$

where M is the Mach number of the flow behind the shock, relative to the front, and R is a quantity analogous to $-M^2$ that is related to the Hugoniot locus:

$$-M^2 = m^2 / (\partial P / \partial V|_S), \quad (6.2)$$

$$R = m^2 / (\partial P / \partial V|_h), \quad (6.3)$$

with the mass flux m being defined in Eq. (3.35). Geometrically, M^2 is the ratio of the slope of the Rayleigh line to the slope of the isentrope, and $-R$ is the ratio of the slope of the Rayleigh line to the slope of the Hugoniot. Fowles and Houwing (1984) have pointed out that the same condition is obtained from Whitham's rule (Whitham, 1974) for a shock moving in a tube of varying area, in that these inequalities are equivalent to having shock waves slow down when they diverge and speed up when they converge.

Remarks. By Eq. (4.24) the ratio R is

$$R = \frac{V}{P} \frac{\Delta P}{\Delta V} \frac{1 + \frac{1}{2}\Gamma\Delta V/V}{\gamma - \frac{1}{2}\Gamma\Delta P/P}. \quad (6.4)$$

Thus $-R$ approaches 1 in the limit of weak shock waves as does M^2 ; moreover, the difference between $-R$ and M^2 vanishes as the square of the shock strength. The ar-

gments of Sec. IV.C show that for most materials R approaches 0 in the strong shock limit.

The first inequality relates the slope of the Hugoniot curve to the slope of the Rayleigh line. It is equivalent to part (e) of Theorem 5.4 and, thereby, to having the entropy increase with shock strength and to having subsonic flow behind the shock (at points on the compression branch where the weak condition holds). As discussed in previous sections, this condition may be violated near phase transitions, leading to splitting of shock waves and branching of wave curves. In this case a shock wave is subject to multidimensional instabilities when the flow behind it is supersonic, independently of one-dimensional admissibility criteria. In general, Eq. (4.28), together with Eqs. (4.23) and (4.26), shows the first inequality in (6.1) to be equivalent to

$$\Delta P \frac{dm}{dP} \Big|_h \geq 0 , \quad (6.5)$$

so that the shock speed must increase with pressure along the compression branch.

In a similar fashion, Eq. (4.28), combined with Eqs. (4.23), (4.27), and $dP/du|_S = m/M$, shows that the second inequality is equivalent to

$$\frac{\partial u}{\partial P} \Big|_h \geq -\frac{\partial u}{\partial P} \Big|_S . \quad (6.6)$$

In particular, this inequality can be violated only if the Hugoniot locus is not monotonic in the $P-u$ plane; i.e., the medium condition must be violated. Gardner (1963) and Erpenbeck (1963) pointed out that when inequality (6.6) is violated the single shock wave can split into alternative wave configurations, which consist of a shock wave accompanied by another wave moving in the opposite direction. This second wave may be either (a) a shock wave or (b) a rarefaction wave, as illustrated in Fig. 18. We show in Appendix C that it is possible to have viscous profiles for the shock waves in each of the three alternative wave configurations, so that the nonuniqueness of solutions of the Riemann problem cannot be resolved on this basis. On one hand, the configuration with two shock waves exhibits a peak in the pressure profile similar to that in Fig. 9, and the propagation speed of the shock wave is maximal. On the other hand, the configuration with a shock wave and a rarefaction wave minimizes the entropy production. We have no criterion for deciding which of the configurations is preferred in nature, but numerical experiments of Wendroff (1988) indicate that the configuration with two shock waves is more stable.

A more restrictive condition for shock stability,

$$-1 \leq R \leq 1 , \quad (6.7)$$

was obtained by Fowles (1976) by considering the reflection of acoustic waves that overtake a shock wave in one dimension. These inequalities result from requiring that the acoustic reflection coefficient should not

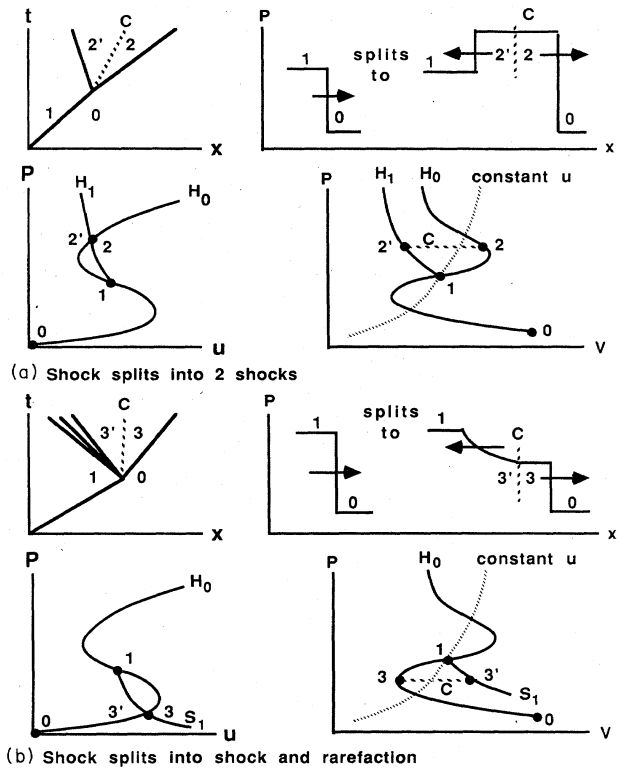


FIG. 18. Shock splitting when $\partial P / \partial u|_S > -\partial P / \partial u|_h$.

exceed unity. The second inequality in (6.7) is fulfilled if and only if

$$\frac{\partial u}{\partial P} \Big|_h \geq 0 , \quad (6.8)$$

as follows in the same manner as inequality (6.6). Thus uniqueness of solutions of the Riemann problem is lost when one-dimensional acoustic waves are amplified upon reflection from a shock wave.

A more elaborate multidimensional analysis by Kortorovich (1958) and Fowles (1981) leads to an even more restrictive condition for shock stability. This condition can be expressed as bounds on the slope of the Hugoniot locus in the $P-V$ plane,

$$-1 \leq R \leq \frac{1 - M^2 - (V_0/V)M^2}{1 - M^2 + (V_0/V)M^2} , \quad (6.9)$$

or in the $P-u$ plane,

$$m \leq \frac{\partial P}{\partial u} \Big|_h \leq \frac{m}{(V_0/V)M^2} \left[1 + \left(\frac{V_0}{V} - 1 \right) M^2 \right] . \quad (6.10)$$

[The pair of inequalities (6.9) is equivalent to the pair (6.10), but the first inequality in (6.9) is equivalent to the first in (6.10) only when $dP/du|_h \geq 0$.] Fowles obtained this result by computing when the amplification coefficient for reflection of oblique acoustic waves becomes singular. This implies that an infinitesimal pertur-

bation in the flow behind the shock wave causes a finite disturbance; in other words, acoustic waves can occur spontaneously. Thus a shock is unstable to the formation of transverse waves along its front when the bounds in (6.10) are violated.

The stability inequality (6.9) may be understood heuristically from the point of view of two-dimensional elementary waves (Glimm *et al.*, 1985). Such waves are steady two-dimensional flow fields consisting of oblique shock waves, contact/slip discontinuities, and Prandtl-Meyer fans centered at a point of interaction, which is called the node. Elementary waves may be constructed and classified (Glimm *et al.*, 1985) with the aid of shock polar diagrams (Courant and Friedrichs, 1948), in which the turning angle θ of the flow is plotted as a function of the pressure behind an oblique shock wave (Grove, 1988):

$$\tan^2 \theta = \left[\frac{\Delta P}{\rho_0 q_0^2 - \Delta P} \right]^2 \left[\frac{q_0^2}{U_s^2} - 1 \right], \quad (6.11)$$

where q_0 is the magnitude of the flow speed ahead of the stationary shock wave, and U_s is the normal propagation speed of the shock wave in the laboratory frame ($\rho_0^2 U_s^2 = -\Delta P / \Delta V$). The general form of a shock polar diagram is shown in Fig. 19. Notice that there is a maximum angle θ_{\max} through which the flow can turn, and that there is a distinguished point at which the flow behind the shock wave is sonic.

The multidimensional stability criterion (6.9) may be shown to be equivalent to having the sonic point occur

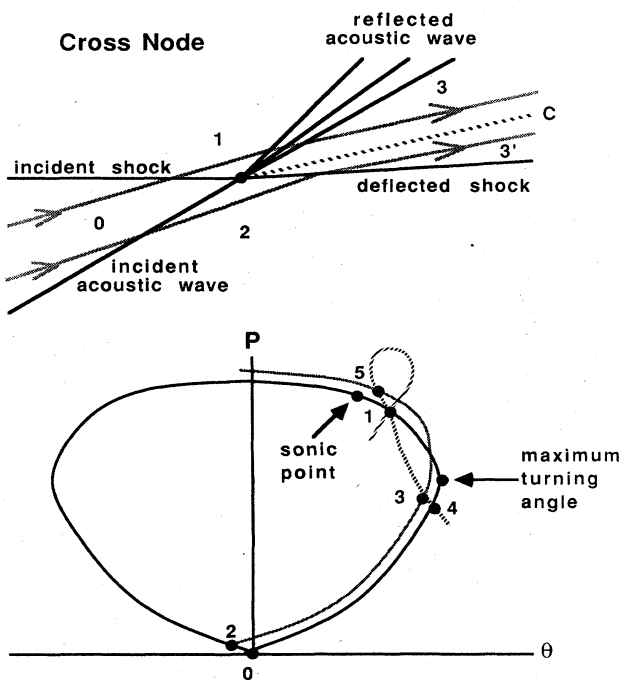


FIG. 19. Shock polar diagram and the corresponding two-dimensional wave pattern when the multidimensional stability criterion is violated.

on the shock polar diagram at a lower pressure than does the maximum turning angle; this follows from Eq. (6.11) and some tedious algebra. When the stability bound is violated, i.e., the sonic point occurs above the point with maximum turning angle, the instability modes may be determined from the geometry of shock polar diagrams. Consider a weak (i.e., acoustic) shock wave impinging on a strong shock front from ahead; Fig. 19 depicts this situation. The intersection point of these waves is termed a cross node (Glimm *et al.*, 1985). State 0 is ahead of the strong shock and state 1 is behind it, while state 2 is behind the acoustic wave; the shock polar diagram is drawn for the reference frame in which the intersection point is stationary. The interaction can result in a strong transmitted shock wave from state 2 to state 3 and in a reflected rarefaction wave from state 1 to state 3'. A reflected rarefaction wave is possible only when state 1 both lies above the point of maximum turning angle and is supersonic, which requires the violation of the stability bound. Furthermore, as the strength of the acoustic wave diminishes (state 2 approaches state 0), state 3 approaches state 4 and the wave configuration becomes a Mach configuration with a reflected rarefaction wave of nonzero strength; the reflection coefficient is infinite. Thus a weak perturbation of the strong shock wave can result in a significantly different wave pattern. Since an arbitrarily small perturbation causes the Mach node to form, the transition can occur spontaneously and the shock is unstable as a two-dimensional front. Thus a two-dimensional instability is realized as a weak rarefaction propagating transversely along the shock front. Similarly, an acoustic wave overtaking a strong shock wave from behind (forming an overtake node) also excites this instability.

Remarks. (1) The qualitative picture described above has been demonstrated by Majda and Rosales (1983, 1984) using a nonlinear asymptotic perturbation analysis. They show that when the stability condition is violated, arbitrarily small, smooth disturbances evolve dynamically into the Mach configuration described by the shock polar analysis.

(2) The higher-pressure solution corresponding to state 5 in Fig. 19 is possible, but experiments indicate that the lower-pressure solution occurs physically (cf. Henderson, 1966, 1967). The lower-pressure solution causes the infinite reflection; nevertheless, this solution may form continuously in the following manner. Consider the development of the interaction as the angle between the acoustic wave and the shock wave varies. Changing the angle changes the node velocity and, thereby, the incident Mach number, which determines the shock polar analysis for the incident shock wave. For some angle, the sonic point occurs at the maximum turning angle, so that the strength of the reflected wave vanishes. As the angle is changed, this wave strength increases continuously from zero.

(3) The rarefaction curve is guaranteed to intersect the incident shock polar analysis if state 1 is sufficiently close to the sonic point. This follows because

$$dP/d\theta = \rho c^2 M^2 (M^2 - 1)^{-1/2} \rightarrow \infty \quad (6.12)$$

as $M \searrow 1$ at the initial point on the reflected wave curve, so that the rarefaction portion of this curve starts inside the shock polar.

(4) The wave configuration shown in Fig. 19 answers a question left open by Glimm *et al.* (1985): a cross node with a reflected rarefaction is indeed possible, provided that the equation of state violates the Kontorovich bound. This possibility was not demonstrated to occur by Glimm *et al.* (1985) because only the polytropic gas equation of state was used to construct examples.

The second inequality in (6.9) is equivalent to

$$\Delta P \frac{dm}{dP} \Big|_h \frac{\gamma - (\Gamma + 1)\Delta P/P}{\gamma + \Delta P/P} \geq 0. \quad (6.13)$$

Therefore compressive multidimensional shock fronts are stable (Fowles, 1981) if and only if the flow is subsonic behind the front and

$$\gamma \geq (\Gamma + 1)(1 - P_0/P). \quad (6.14)$$

Notice that sufficiently weak shock waves ($P \approx P_0$) are stable.

Let us introduce the thermodynamic condition

$$\Gamma \leq \gamma - 1 \text{ (stability condition).}$$

This condition is the basis for a result analogous to Theorems 4.5 and 4.6.

Theorem 6.1. *The stability condition is sufficient for multidimensional stability of compressive shock waves and for monotonicity of u along Hugoniot loci. Furthermore, if $P_0 \rightarrow 0$ as $S_0 \rightarrow 0$ along the backward Hugoniot of a state (V, S) , then the stability condition is also necessary for multidimensional stability of all shock waves that connect to this state.*

Proof. The stability condition implies Eq. (6.14) and, therefore, multidimensional shock stability, provided that $P \geq P_0$. It also implies the medium condition, so that u varies monotonically along Hugoniot loci. If the stability condition is violated and the backwards Hugoniot extends to $P_0 = 0$, then there is an initial state (V_0, S_0) such that Eq. (6.14) is violated; in this case the shock wave connecting (V_0, S_0) to (V, S) is unstable as a multidimensional front. \square

We also point out that the multidimensional stability condition precludes bifurcations on the compressive branch of the Hugoniot locus:

$$2\gamma > \gamma \geq (\Gamma + 1)\Delta P/P > \Gamma \Delta P/P, \quad (6.15)$$

so that the bifurcation condition Eq. (4.8) cannot hold. This holds irrespective of the value of \mathcal{G} .

The stability condition is very stringent. In particular it is stronger than the medium condition, so that it guarantees uniqueness of solutions of the Riemann problem when $\mathcal{G} > 0$. It is possible, however, for the stability inequality (6.10) to be violated even if $\mathcal{G} > 0$, the particle velocity increases monotonically along the Hugoniot

locus, and the shock wave admits a viscous profile. We infer from this result that shock instability becomes a problem before multiple solutions of the Riemann problem occur, and that the existence of a shock profile is not sufficient as an admissibility condition. Notice, however, that the linear stability analysis leading to the criterion (6.10) approximates the shock front as being infinitely thin. A more satisfactory analysis would examine stability of traveling-wave solutions of the viscous equations with respect to multidimensional perturbations.

Remarks. (1) For a polytropic gas the stability condition is an equality. In the limit of high temperatures, the EOS approximates a polytropic gas EOS. Numerical errors in the EOS may cause the stability condition to be violated to a slight extent. This would cause the Hugoniot loci to approach the maximum compression ratio from below, instead of from above as it should (see Sec. IV.C). In numerical algorithms, the multidimensional instability may be controlled by smoothing operations, such as artificial viscosity in finite difference schemes, or redistribution of the front points in front tracking methods.

(2) A mathematically rigorous perturbation analysis of shock instability for general hyperbolic partial differential equations has been performed by Majda (1983). One-dimensional viscous profiles for weak shock waves have been shown to be nonlinearly stable by Liu (1986).

(3) A similar transverse instability is known to occur in detonation waves; the transverse wave takes the form of a standard Mach configuration (with a reflected shock wave) (Strehlow, 1970; Fickett and Davis, 1979; Majda, 1987). The instability mode can be understood heuristically by adapting the shock polar analysis that was discussed for shock instability. Consider perturbing a detonation front by an acoustic wave. Because of the dynamics in the reaction zone, the higher-pressure solution in the wave curve analysis may occur (state 5 in Fig. 19). For a supersonic point (state 4) whose pressure is slightly below the pressure at the maximum turning angle, the higher-pressure solution converges to a Mach configuration with a reflected shock when the strength of the acoustic wave vanishes. Again the reflection coefficient is infinite, and the node can appear spontaneously.

(4) In the shock polar diagram of the standard Mach configuration, the reflected wave curve leads from a point below the sonic point to a point above the maximum turning angle. When the sonic point is below the maximum turning angle, the minimum strength (i.e., pressure difference) for the reflected wave is nonzero. As the sonic point approaches the maximum turning angle, the threshold strength for the reflected wave decreases, so that a smaller perturbation can trigger the formation of a Mach configuration. In this case, the shock front may be linearly stable to infinitesimal perturbation, but unstable to finite perturbations that exceed a small threshold.

(5) As reported by Thompson *et al.* (1986), recent experiments on shock waves in fluids with large heat capacities show evidence for transverse instability near phase

transitions. In addition, experiments have observed transverse instability of shock waves in gases (Griffiths *et al.*, 1975; Glass and Liu, 1978); here the instability appears to be associated with the ionization and relaxation processes behind strong shock waves, i.e., nonequilibrium effects.

(6) Analogous stability results for shock waves in relativistic fluid dynamics have been obtained by Russo and Anile (1987).

(7) The transverse instability was not discovered by the linear analyses of D'yakov and Erpenbeck because the normal modes and boundary conditions that they considered are not compatible with outgoing planar acoustic waves.

Finally, we mention additional questions concerning the Riemann problem. Very little is known about the solution of the Riemann problem in more than one dimension. A classification of stable configurations (elementary waves) under reasonable assumptions was obtained by Glimm *et al.* (1985). This work may be generalized to weaken the physical assumptions and to include the additional wave types that occur because of phase transitions. Moreover, nonuniqueness of fluid flow occurs in other situations. In two dimensions, a well-known case is a shock reflecting off a wedge; for some initial conditions, both regular and Mach reflections are possible (Hornung, 1986). Understanding the two-dimensional Riemann problem is a step toward determining what additional information is needed to resolve this and other cases of nonuniqueness in fluid flow.

VII. A MODEL EQUATION OF STATE

In numerical calculations of fluid flow, the EOS can be specified by an analytical formula, an empirical fit, or a table. When the flow enters a region of state space outside the range of validity of the numerical EOS, the computation can become unstable or give unphysical results, through no fault of the computer code. Thus the EOS should be regarded as input data whose correctness must be assured.

Because of experimental difficulties, data for the equation of state are available in only a limited region in state space. As a result, the range of validity of a numerical EOS is known only approximately. The domain of an EOS can be delimited by checking for thermodynamic consistency. However, this approach is insufficient when only an incomplete EOS is specified, as is frequently the case for ideal fluid flow. Thus it is important to understand the wave structure in order to discern potential difficulties in numerical computations. In this section we illustrate, with a simple analytic example, the anomalous shock behavior that can arise from a seemingly reasonable numerical EOS.

We consider a model for a metal consisting of a Grüneisen EOS together with a linear fit for the shock velocity as a function of the particle velocity (Rice *et al.*, 1958). A Grüneisen EOS reduces a function of two vari-

ables to linear corrections about a reference curve parametrized by one variable. Using the definition (2.47) for the Grüneisen coefficient, a first-order Taylor expansion in the internal energy about the reference curve yields

$$P(V, E) = P_{\text{ref}}(V) + \frac{\Gamma}{V}[E - E_{\text{ref}}(V)]. \quad (7.1)$$

This is an adequate approximation when in the flow the state of the fluid is near the reference curve. For example, in the absence of viscosity, heat conduction, and shock waves, the reference curve may be taken as an isentrope.

The reference curve is chosen frequently to match experimental data. High-pressure data that are available for solids lie along a single shock Hugoniot for which the initial state is at standard temperature and pressure. For many metals, the shock and particle velocity are observed to be related linearly up to a pressure of several megabars:

$$\sigma = c_0 + su. \quad (7.2)$$

We assume that $s > 1$ in order that $\sigma > u$ for all u , as required by mass conservation. The shock state is then determined from the Hugoniot jump conditions to be

$$P_h(V) = P_0 + \frac{c_0^2(V_0 - V)}{[V_0 - s(V_0 - V)]^2}, \quad (7.3)$$

$$E_h(V) = E_0 + \frac{1}{2}[P_h(V) + P_0](V_0 - V), \quad (7.4)$$

where V_0 , E_0 , and P_0 are the initial-state conditions. At the initial state, a good approximation (Rice *et al.*, 1958) is

$$\Gamma = 2s - 1. \quad (7.5)$$

We consider the EOS in which Γ is a constant independent of V and E .

This model EOS has the following limitations:

(A) The reference curve is based on a single shock curve, which has a maximum compression ratio of

$$\frac{V_0}{V} = \frac{s}{s-1}. \quad (7.6)$$

Hence Eqs. (7.3) and (7.4) are only meaningful for

$$\frac{s-1}{s} V_0 < V \leq V_0. \quad (7.7)$$

Remark. As V approaches the maximum compression, P_h and E_h approach infinity. For V beyond the maximum compression, Eqs. (7.1), (7.3), and (7.4) lead to a negative compressibility.

(B) The sound speed is given by

$$c^2(V, E) = c_h^2(V) + \Gamma(\Gamma+1)[E - E_h(V)], \quad (7.8a)$$

where the sound speed along the Hugoniot curve is determined from

$$\left[\frac{c_h(V)}{V} \right]^2 = \frac{dP}{dV} \Big|_h \left[(V_0 - V) \frac{\Gamma}{2V} - 1 \right] + (P_h - P_0) \frac{\Gamma}{2V}. \quad (7.8b)$$

Thus if one extrapolates E too far below E_h , the sound speed becomes imaginary, which means that the compressibility is negative and hence unphysical.

In general, for the Grüneisen EOS, it is useful to express the sound speed along the Hugoniot curve in terms of the particle velocity. From Eqs. (7.3), (7.8b), and the relations

$$\frac{V}{V_0} = \frac{\sigma - u}{\sigma} \quad \text{and} \quad \frac{u}{c_0} = \frac{V_0/V - 1}{s - (s-1)V_0/V}, \quad (7.9)$$

we find that

$$\begin{aligned} \left[\frac{c_h}{c_0} \right]^2 &= \left[1 + (s-1) \frac{u}{c_0} \right] \\ &\times \left[\left[1 + (s-1 - \frac{1}{2}\Gamma) \frac{u}{c_0} \right] \left[1 + 2s \frac{u}{c_0} \right] \right. \\ &\quad \left. + \frac{1}{2}\Gamma \frac{u}{c_0} \right]. \end{aligned} \quad (7.10)$$

Thus c_h^2 is a cubic polynomial in u . Furthermore, Eq. (7.5) implies that $s-1 - \frac{1}{2}\Gamma = -\frac{1}{2}$, so that the coefficient of the cubic term in u/c_0 is negative. A sketch of c_h as a function of u is shown in Fig. 20. The sound speed is imaginary and the adiabatic compressibility is negative when

$$\frac{u}{c_0} > \frac{(3s-1) + [(3s-1)^2 + 4s]^{1/2}}{2s}. \quad (7.11)$$

The corresponding bound on V follows from this inequality and Eq. (7.9).

Remarks. (1) Equation (7.8b) can be used in the other direction: experimental measurements of both the shock

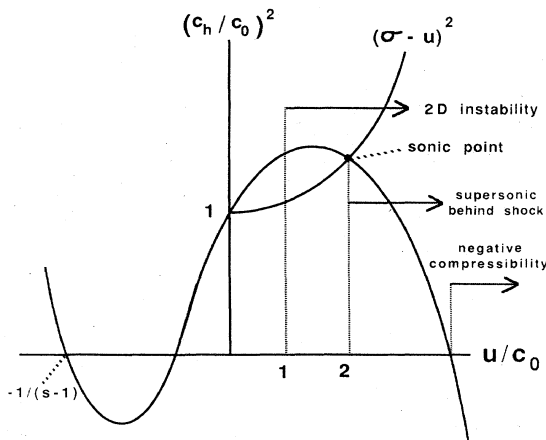


FIG. 20. Sound speed vs particle velocity along the principal Hugoniot locus for the model equation of state.

Hugoniot and the sound speed behind the shock may be used to determine Γ on the shock Hugoniot.

(2) There are two common ways in which $E < E_h(V)$ may occur: first, when a shock wave is followed by adiabatic compression (e.g., when a gas is compressed between two plates that have been set into motion impulsively); second, when numerical errors are caused by insufficient resolution (as in finite difference calculations near boundary layers).

(3) When the flow enters regions outside the range of validity of the EOS, numerical calculations can be expected to yield inaccurate results. In particular, if the flow enters a regime where the sound speed is imaginary, then the numerical algorithm may fail catastrophically. For the model EOS considered here, we see that there are indeed regimes of V and E where this occurs. Before a catastrophic failure occurs, however, the flow may enter a regime where certain wave structures, such as shock waves, are unstable because of the EOS (as in Sec. VI).

(C) For weak shock waves ($u/c_0 \ll 1$), the sound speed is given by

$$c_h = c_0 + (2s-1)u + O(u^2), \quad (7.12)$$

according to Eq. (7.10). Thus c_0 is the sound speed for the initial state; this is consistent with weak shock waves being acoustic waves. Furthermore, the characteristic speed for weak shock waves is greater than the shock velocity:

$$u + c_h = c_0 + 2su + O(u^2) \geq \sigma = c_0 + su. \quad (7.13)$$

That $d(u+c)/d\sigma = 2$ at the initial state is a consequence of the general result that

$$\sigma \approx \frac{1}{2}[(u+c)_{\text{ahead}} + (u+c)_{\text{behind}}] \quad (7.14)$$

for weak shock waves. In addition, the sound speed behind the shock wave is initially greater than the shock velocity:

$$c_h = c_0 + (2s-1)u + O(u^2) \geq \sigma = c_0 + su. \quad (7.15)$$

Remark. The initial behavior or weak shock limit of this model is physically consistent, but it is not a realistic model for a metal because elastic properties have been neglected. Only well above the yield strength does a metal behave as a fluid.

At the point where $c_h = 0$, the characteristic speed is less than the wave speed because $\sigma > u$. Therefore there must be a sonic point on the shock Hugoniot. The sonic point, $u + c_h = \sigma$, occurs at

$$V = \frac{\Gamma}{\Gamma+2} V_0. \quad (7.16)$$

At this point, $u/c_0 = 2$, $c_h/c_0 = 2s-1$, and $\sigma/c_0 = 2s+1$. In addition, because $d(c_h/c_0)^2/d(u/c_0) = -2(2s-1) < 0$, the sonic point occurs after the maximum in the sound speed along the Hugoniot curve. Beyond the sonic point, the flow is supersonic behind the shock wave; thus the Lax characteristic criterion is violated and the shock

wave is unstable.

Furthermore, the sonic point is also a point of secondary bifurcation. In fact, the second branch of the shock Hugoniot is the line in the P - V plane given by Eq. (7.16). Because of the bifurcation, the usual results—that the Rayleigh line and the shock Hugoniot are tangent at the sonic point, and that the flow behind a shock wave is subsonic when the wave speed increases—do not hold.

At the sonic point, $\mathcal{G} < 0$. We will demonstrate this by showing the isentrope to be concave. The second derivative is given by

$$\begin{aligned} \frac{\partial^2 P}{\partial V^2} \Big|_S = & - \frac{d}{dV} \left(\frac{c_h^2(V)}{V^2} \right) + \frac{\Gamma(\Gamma+1)}{V^2} \left[P_h + \frac{dE_h}{dV} \right] \\ & + \frac{\Gamma(\Gamma+1)(\Gamma+2)}{V^2} \left[\frac{E - E_h}{V} \right]. \end{aligned} \quad (7.17)$$

The third term is zero on the reference curve, while the second term is negative because

$$P_h + \frac{dE_h}{dV} = \frac{1}{2} \left[(P_h - P_0) - (V - V_0) \frac{d(P_h - P_0)}{dV} \right] < 0, \quad (7.18)$$

as follows from the convexity of $P_h(V)$. At the sonic point,

$$\sigma = u + c_h = \frac{2s+1}{2s-1} c_h \quad (7.19)$$

and

$$-\frac{dc_h^2}{dV} = \frac{\sigma^2}{V_0} \frac{d(c_h/c_0)^2}{d(u/c_0)} = -\frac{\sigma^2}{V_0} 2(2s-1), \quad (7.20)$$

so that the first term in Eq. (7.17) expands to

$$\begin{aligned} -\frac{d}{dV} \left(\frac{c_h^2}{V^2} \right) &= \frac{1}{V^2} \left[-\frac{d}{dV} c_h^2 + \frac{2c_h^2}{V} \right] \\ &= -4sc_h^2/V^3 < 0. \end{aligned} \quad (7.21)$$

Therefore $\partial^2 P / \partial V^2|_S < 0$ and hence $\mathcal{G} < 0$ at the sonic point.

(D) Before the sonic point is reached, the sound speed has a maximum. The maximum, $dc_h^2/du = 0$, occurs when

$$\frac{u}{c_0} = \frac{3s^2 - 5s + 1 + (9s^4 - 18s^3 + 13s^2 - 4s + 1)^{1/2}}{3s(s-1)}. \quad (7.22)$$

It follows from Eq. (7.8a) that $\partial c^2 / \partial E|_V = \Gamma(\Gamma+1)$; hence $\partial c^2 / \partial S|_V > 0$. Thus when the sound speed is a maximum along the Hugoniot curve, $\partial c^2 / \partial V|_S > 0$, so that $\mathcal{G} < 1$. Although thermodynamics does not preclude having the sound speed decrease with density, it is unusual. It is an indication that this EOS no longer models a simple metal.

(E) Finally, it has been shown by Fowles (1981) for the model EOS that the criterion for two-dimensional stability, Eq. (6.10), is violated for

$$V > \frac{s}{s+1} V_0. \quad (7.23)$$

This occurs when $u/c_0 > 1$. Because

$$\frac{d(c_h/c_0)^2}{d(u/c_0)} \Big|_{u=c_0} = 3s(s-1) > 0, \quad (7.24)$$

the two-dimensional instability occurs before the maximum in c_h . It thus provides the most stringent limit on when the model is unphysical. The limit occurs when $c = \sqrt{2}sc_0$, $\sigma = (s+1)c_0$, and $P_h = P_0 + (s+1)c_0^2/V_0$. At this point, the adiabatic exponent is $\gamma = 2s(s+1)\gamma_0/[1+(s+1)\gamma_0]$, where $\gamma_0 = c_0^2/(P_0 V_0)$. Beyond this point, numerical instabilities in two-dimensional calculations are expected.

Remarks. (1) For a typical metal like steel (Marsh, 1980), $\rho_0 = 7.91 \text{ g/cm}^3$, $c_0 = 0.462 \text{ cm}/\mu\text{s}$, $s = 1.42$, and $P_0 = 10^{-6} \text{ Mbar}$. At the initial point, the EOS is very stiff, with $\gamma_0 = 1.7 \times 10^6$. The model EOS breaks down at $\sigma = 1.12, \text{ cm}/\mu\text{s}$ and $P = 4.1 \text{ Mbar}$.

(2) The strong, medium, and weak conditions of Sec. IV are all violated because $\gamma \rightarrow 0$ and Γ is a constant. As a result, it is possible to describe a foamed metal (Mader, 1970) by choosing an initial specific volume V'_0 greater than the normal initial volume V_0 .

(3) Another way to understand the anomalous behavior of this incomplete EOS is to try to determine a consistent entropy and temperature function. To do this, we write the fundamental thermodynamic identity as

$$T dS = dE + P dV. \quad (7.25)$$

The solution of this equation is given as follows. Let

$$\begin{aligned} \alpha &= V^\Gamma E + \int dV V^\Gamma \left[P_h(V) - \frac{\Gamma}{V} E_h(V) \right] \\ &= V^\Gamma [E - E_0 - P_0(V_0 - V)] \\ &\quad + c_0^2 \int dV V^\Gamma \left[1 - \frac{\Gamma}{2} \left(\frac{V_0 - V}{V} \right) \right] \\ &\quad \times \frac{V_0 - V}{[V_0 - s(V_0 - V)]^2}. \end{aligned} \quad (7.26)$$

[Note that if Γ is an integer, the integral is a sum of terms of the form $\int dx x^m/(x+a)^2$, which may be calculated analytically.] Then

$$S = f(\alpha), \quad (7.27)$$

$$T = V^{-\Gamma} / f'(\alpha), \quad (7.28)$$

where f is an arbitrary function. The simplest choice $f(\alpha) = \alpha$ results in T being independent of E . This leads to $C_V = \infty$, which is unphysical; it also violates the third law of thermodynamics, that the $T=0$ isotherm and the

$S=0$ isentrope coincide. Thus more information is needed to determine a complete EOS, e.g., $T_h(V)$. However, thermodynamics further restricts f . The dimensionless specific heat at constant volume is

$$g = \frac{PV}{T^2} \frac{\partial T}{\partial S} \Big|_V = -\frac{f''}{f'} PV^{\Gamma+1}. \quad (7.29)$$

In order that $T > 0$ and $g > 0$, we require that f be increasing and concave: $f' > 0$ and $f'' < 0$. If one solves Eq. (7.1) for E in terms of P and substitutes the resulting expression into Eq. (7.26), one obtains an expression for the isentropes in the P - V plane, as parametrized by α . However, if one analyzes the asymptotic behavior as V approaches the maximum compression ratio, one finds that the isentropes end at $P=0$ with a positive slope, as illustrated in Fig. 21. This behavior results because $E_h(V)$ grows much faster than the energy as V decreases along an isentrope. Consequently, the large energy extrapolation for the pressure in Eq. (7.1) leaves the range of validity of the model. In addition, we note that before γ becomes negative, the inequalities (2.32) for thermodynamic stability are violated. The anomalous behavior of the model EOS is a consequence of the loss of convexity and positive slope of the isentropes as V approaches the maximum compression ratio.

(4) When variations in the density are small, the Grüneisen EOS may be linearized to obtain a "stiffened gas" EOS (see, e.g., Harlow and Amsden, 1971). More generally, a stiffened gas EOS approximates any equations of state near a reference state (V_0, E_0) :

$$\begin{aligned} P(V, E) &\approx P_0 + (\gamma_0 - \Gamma_0) F_0 V_0 (\rho - \rho_0) + \Gamma_0 \rho_0 (E - E_0) \\ &\approx (P_0 - \Gamma_0 \rho_0 E_0) \\ &\quad + [c_0^2 - \Gamma_0 (E_0 + P_0 V_0)] (\rho - \rho_0) + \Gamma_0 \rho E \end{aligned} \quad (7.30)$$

to within errors that are quadratic in $\rho - \rho_0$ and $E - E_0$.

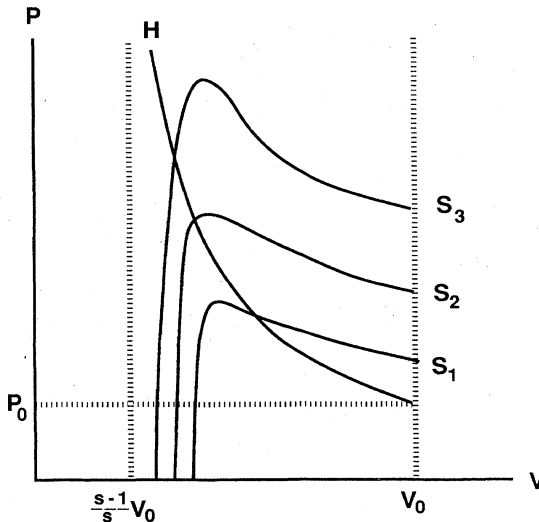


FIG. 21. Principal Hugoniot locus and isentropes for the model equation of state.

If we define $P_\infty = \rho_0 c_0^2 / (\Gamma_0 + 1) - P_0$ and $E_\infty = E_0 + P_0 V_0 - c_0^2 / \Gamma_0$, then the stiffened gas EOS may be expressed simply as

$$P = \Gamma_0 \rho (E - E_\infty) - (\Gamma_0 + 1) P_\infty. \quad (7.31)$$

(Often the energy offset E_∞ is irrelevant, so that the stiffened gas is defined by the two parameters Γ_0 and P_∞ .) We note that the fundamental thermodynamic parameters for a stiffened gas are

$$\Gamma = \Gamma_0, \quad (7.32)$$

$$\gamma = (\Gamma_0 + 1)(1 + P_\infty / P), \quad (7.33)$$

$$\vartheta = 1 + \frac{1}{2} \Gamma_0, \quad (7.34)$$

$$S = f((P + P_\infty) V^{\Gamma_0 + 1}). \quad (7.35)$$

A stiffened gas reduces to a polytropic gas when $P_\infty = 0$ and $E_\infty = 0$. For some materials, however, P_∞ can be quite large; examples are water and metals, for which P_∞ is on the order of megabars. According to Eq. (7.33), $c^2 = (\Gamma_0 + 1)(P + P_\infty)V$; therefore, when P_∞ is large, a stiffened gas models materials with a sound speed that is insensitive to changes in pressure. Despite the extra parameter P_∞ , Riemann problems may be solved for a stiffened gas just as easily as for a polytropic gas (Plohr, 1988a). Therefore the stiffened gas EOS is useful as a simple, analytical approximation to an arbitrary EOS, obtained by locally fitting P and its two first derivatives, γ and Γ . The local wave structure is qualitatively correct provided that ϑ_0 has the same sign as $1 + \frac{1}{2} \Gamma_0$. We mention also that isentropes are given by

$$P_S(V) = -P_\infty + \alpha \Gamma_0 V^{-(\Gamma_0 + 1)}, \quad (7.36a)$$

$$E_S(V) = E_\infty + P_\infty V + \alpha V^{-\Gamma_0}. \quad (7.36b)$$

The isentrope through the initial state corresponds to having $\alpha_0 = c_0^2 V_0^{\Gamma_0} / [\Gamma_0(\Gamma_0 + 1)]$. Thus a stiffened gas represents the first-order expansion of Eq. (7.26).

It is clear why the model EOS breaks down. As the temperature increases with shock strength, the EOS should approach a polytropic gas with $\gamma \rightarrow \frac{s}{3}$ and $\Gamma \rightarrow \frac{2}{3}$. The linear σ - u relation has correction terms, and Γ is not constant. In fact, by choosing $\Gamma = (V/V_0)\Gamma_0$ with $\Gamma_0 = 2s - 1$, one can show that c_h^2 increases monotonically along the principle Hugoniot curve, that the flow behind the shock wave is subsonic, and that the multidimensional stability condition is satisfied. Therefore this small change in the EOS removes the unphysical anomalies in this example.

Remarks. (1) In numerical finite difference schemes, shock waves are smeared by artificial viscosity. For the model EOS, we can explicitly calculate the shock profile in the presence of viscosity but no heat conduction, following the results of Appendix C. From Eq. (C23) it follows that the shock profile, extending from the initial state V_0 to the final state V_f in the P - V plane, is given by

$$P(V) = P_h(V) + \frac{1}{2} \Gamma \frac{(V_0 - V)^2}{V} \times \left[\frac{P_h(V_f) - P_0}{V_0 - V_f} - \frac{P_h(V) - P_0}{V_0 - V} \right]. \quad (7.37)$$

If the sonic point is beyond the final shock state, this pressure profile is monotonic, and it lies between the Hugoniot curve and the Rayleigh line. Beyond the sonic point, the system of ordinary differential equations for the shock profile has a third critical point caused by the secondary bifurcation in the Hugoniot curve. The shock profile cannot be extended beyond $V/V_0 = \Gamma/(\Gamma+1)$, so that the corresponding shock waves are inadmissible. In numerical calculations with artificial viscosity, the shock profile is not resolved. If Eq. (7.37) is followed, then the peak pressure exceeds the final shock pressure when the EOS breaks down (i.e., when $c^2 < 0$); this is because the slope of the shock profile coincides with that of the isentrope at the final state. Most likely, numerical oscillations occur when a shock profile does not exist.

(2) One common approach to expanding the region of validity of an EOS is to patch together different models. It is important to require more than continuity for $P(V, E)$. If the partial derivatives of P are not continuous, then the isentropes have kinks. This leads to anomalous wave behavior similar to what occurs at phase transitions, as described in Sec. V. In finite difference calculations, the flow may carry the fluid state past these boundaries sufficiently fast that difficulties are avoided. Other methods that rely heavily on Riemann solvers may have difficulty with the anomalous wave structure caused by artificial kinks in the numerical EOS. Similarly, for tabular equations of state, simple linear interpolation is not sufficient: the interpolation scheme must enforce that P and its derivatives be continuous in order to avoid numerical difficulties with Riemann solvers.

VIII. SUMMARY

The wave structure in fluid flow depends crucially on the equation of state characterizing the material. This dependence is reflected in solutions of one-dimensional Riemann problems. Such solutions are constructed using wave curves, which parametrize stable, scale-invariant elementary waves. For real fluid materials, the class of elementary waves includes composite and split waves in addition to shock and rarefaction waves. Existence of solutions for the Riemann problem depends on global properties of wave curves, while uniqueness of solutions depends on monotonicity properties. In turn, the structure and behavior of wave curves is determined by properties of the equation of state.

The equation of state affects wave curves through its influence on isentropes and Hugoniot loci. Global properties of wave curves follow from physically reasonable assumptions about the asymptotic behavior of the equation of state, while the influence on local structure is

characterized by three dimensionless parameters: the adiabatic exponent γ , the Grüneisen coefficient Γ , and the fundamental derivative \mathcal{G} . Thermodynamic consistency and stability place some restrictions on these parameters, but preclude neither anomalous wave structure nor nonuniqueness of solutions of the Riemann problem.

When \mathcal{G} is assumed to be positive, the wave curve consists solely of shock and rarefaction waves. This standard assumption breaks down when the fluid undergoes phase transitions. As a result, the wave propagation speed fails to vary monotonically along wave curves, leading to the formation of composite and split waves. When anomalous waves occur, the physical admissibility of solutions is no longer determined by the increase of thermodynamic entropy; other more refined criteria, such as the existence of viscous profiles for shock waves, must be employed. Monotonicity properties along the Hugoniot loci, which affect uniqueness of solutions of the Riemann problem, depend on the relationship between γ and Γ . Uniqueness is also related to whether shock waves define stable solutions of the fluid equations in physical three-dimensional space; multidimensional stability may be formulated as a condition on the equation of state.

Fluid dynamics provides an enlightening example in the study of systems of hyperbolic conservation laws. When the standard mathematical assumptions on the equation of state are relaxed, solutions exhibit a rich wave structure that reflects the spectrum of phenomena occurring in general systems. These phenomena are observed experimentally; indeed, phase transitions are a generic property of real materials, not mathematical pathologies. They are important also for numerical simulation of fluid flow. The equation of state is input data for a numerical computation, so it must correctly model the behavior of the material; otherwise solutions that are wrong both quantitatively and qualitatively will result.

There are several interesting open questions.

(1) A general multidimensional Riemann problem is an initial value problem with initial data that are constant along rays. Because the equations are scale invariant, one expects the solution to be scale invariant, so that the space and time variables may be replaced by fewer scaled variables (see, e.g., Jones *et al.*, 1951). The reduced system has source terms and is of mixed type: far from the origin the system is hyperbolic, but elliptic regions may occur near the origin. Solutions are expected to consist of several interacting elementary waves together with outgoing radiation waves.

Focusing on the elementary waves reduces the dimensionality of the problem further; for instance, elementary waves for two-dimensional Riemann problems are constructed by solving one-dimensional Riemann problems in which rarefaction waves correspond to Prandtl-Meyer fans, shock waves to oblique shock waves, Hugoniot loci to shock polar diagrams. This approach was used by Glimm *et al.* (1985) to classify the elementary wave configurations for polytropic gases. Such solutions are

particularly important for numerical calculations using front tracking (Chern *et al.*, 1985; Glimm *et al.*, 1985).

The interaction and bifurcation of elementary waves is determined by solving multidimensional Riemann problems. Here an analogy with particle scattering is helpful (Glimm and Sharp, 1986). This analogy can be extended to shock formation, which corresponds to pair production, and to metastable interactions of waves (an example being double Mach reflection), which are similar to bound states. Other examples occur when incident shock waves reflect from contact discontinuities; for experimental data illustrating this phenomenon, see, e.g., Abd-El-Fattah and Henderson (1976). Thus solving multidimensional Riemann problems would illuminate the physical structure and interaction of waves, in addition to serving to improve numerical algorithms.

(2) A question that is related to multidimensional Riemann problems is the effect of curvature of a detonation front on its propagation speed. This has been partially analyzed by Bdzil and Stewart (1986), Jones (1987, 1989), and Bukiet (1989).

(3) For higher-order numerical algorithms (e.g., Godunov schemes), it is important to generalize the Riemann problem to include initial value problems in one dimension with piecewise linear initial data. It is also important to analyze the Riemann problem for conservation equations with source terms (e.g., those accounting for geometrical effects). Several authors have addressed these issues for one-dimensional problems (see, e.g., Liu, 1979; Le Floch and Raviart, 1988).

(4) Understanding the nonuniqueness of solutions of the Riemann problem is an important problem. This is expected to involve additional physics. Fluid dynamics is well suited to this task because the additional physics is understood, and because it is possible to verify theory with experiments. The additional physics may involve viscosity and heat conduction, or perhaps nonequilibrium relaxation phenomena.

(5) Two important aspects of real materials have been neglected in this study. First, phase transitions involve nonequilibrium or relaxation effects that are similar to chemical reactions (see, e.g., Rabie *et al.*, 1979; Chaves *et al.*, 1985). Second, material strength must be considered when the material is solid. The Riemann problem for elastic materials is partially understood (see, e.g., Tang and Ting, 1987; Plohr and Sharp, 1989). Accounting for these phenomena is of great interest.

ACKNOWLEDGMENTS

We would like to thank Professor James Glimm for his continual encouragement concerning this work. We are also grateful to Dr. John Grove for proofreading early versions of this manuscript and for helpful discussions, especially in regard to stability of multidimensional shock fronts. This work was supported by the U.S. Department of Energy, the National Science Foundation, and the U.S. Army Research Office.

APPENDIX A: THERMODYNAMIC IDENTITIES

To formulate the thermodynamic constraints on the equation of state, we have used various results from classical thermodynamics. In this appendix we summarize these results.

The principle thermodynamic potential is the specific internal energy $E = E(V, S)$ expressed in terms of the specific volume V and the specific entropy S . The fundamental thermodynamic identity (which follows from the first and second laws of thermodynamics) defines the pressure P and the temperature T as derivatives of E :

$$dE = T dS - P dV ; \quad (A1)$$

P and T are assumed to be positive, continuous functions. Moreover, thermodynamic stability requires E to be convex, as discussed below.

Three other thermodynamic potentials are related to E through Legendre transformations:

$$F(V, T) = \text{specific Helmholtz free energy}$$

$$= \inf_S \{E(V, S) - TS\} , \quad (A2)$$

$$G(P, T) = \text{specific Gibbs free energy}$$

$$= \inf_{V, S} \{E(V, S) - TS + PV\} , \quad (A3)$$

$$H(P, S) = \text{specific enthalpy}$$

$$= \inf_V \{E(V, S) + PV\} . \quad (A4)$$

These thermodynamic potentials correspond to parametrizing the space of equilibrium states with different independent variables. When the changes of variables are locally invertible (i.e., away from phase transitions), the potentials are simply

$$F = E - TS, \quad G = E - TS + PV, \quad H = E + PV . \quad (A5)$$

In terms of these potentials, the fundamental thermodynamic identity is expressed as

$$dF = -S dT - P dV , \quad (A6)$$

$$dG = -S dT + V dP , \quad (A7)$$

$$dH = T dS + V dP . \quad (A8)$$

Notice, also that the specific entropy S may be expressed in terms of the specific volume and specific energy, $S = S(V, E)$, since $T = \partial E / \partial S|_V > 0$.

The fundamental measurable quantities are

$$C_V = \text{specific heat at constant volume}$$

$$= T \partial S / \partial T|_V , \quad (A9)$$

$$C_P = \text{specific heat at constant pressure}$$

$$= T \partial S / \partial T|_P , \quad (A10)$$

$$K_T = \text{isothermal compressibility}$$

$$= -(1/V) \partial V / \partial P|_T , \quad (A11)$$

K_S = isentropic compressibility

$$= -(1/V) \partial V / \partial P|_S , \quad (\text{A12})$$

β = coefficient of thermal expansion

$$= (1/V) \partial V / \partial T|_P . \quad (\text{A13})$$

They are related by the two identities

$$\frac{K_S}{K_T} = 1 - \frac{\beta^2 V T}{C_P K_T} = \frac{C_V}{C_P} . \quad (\text{A14})$$

As a result, they can be expressed in terms of the three dimensionless quantities

γ = adiabatic exponent

$$= 1/(PK_S) , \quad (\text{A15})$$

Γ = Grüneisen coefficient

$$= \beta V / (C_V K_T) , \quad (\text{A16})$$

g = dimensionless specific heat

$$= PV / (C_V T) , \quad (\text{A17})$$

as follows:

$$C_V = \frac{PV}{T} \frac{1}{g} , \quad (\text{A18})$$

$$C_P = \frac{PV}{T} \frac{\gamma}{\gamma g - \Gamma^2} , \quad (\text{A19})$$

$$K_T = \frac{1}{P} \frac{g}{\gamma g - \Gamma^2} , \quad (\text{A20})$$

$$K_S = \frac{1}{P} \frac{1}{\gamma} , \quad (\text{A21})$$

$$\beta = \frac{1}{T} \frac{\Gamma}{\gamma g - \Gamma^2} . \quad (\text{A22})$$

All second derivatives of the thermodynamic potentials may be expressed in terms of the fundamental measurable quantities. These identities are derived by algebraic manipulations of differential calculus formulas relating changes of pairs of independent variables: let x, y and z, y be pairs of independent variables; then

$$\left. \frac{\partial}{\partial z} \right|_y = \left. \frac{\partial x}{\partial z} \right|_y \left. \frac{\partial}{\partial x} \right|_y \quad (\text{chain rule}),$$

$$\left. \frac{\partial}{\partial y} \right|_z = \left. \frac{\partial x}{\partial y} \right|_z \left. \frac{\partial}{\partial x} \right|_y + \left. \frac{\partial}{\partial y} \right|_x \quad (\text{chain rule}),$$

$$\left. \frac{\partial x}{\partial y} \right|_z \left. \frac{\partial y}{\partial z} \right|_x \left. \frac{\partial z}{\partial x} \right|_y = -1 \quad (\text{cyclic rule}).$$

The identities are as follows:

$$\begin{aligned} \partial T / \partial V|_S &= \partial^2 E / \partial V \partial S = -\partial P / \partial S|_V \\ &= -\beta T / (C_V K_T) = -(T/V)\Gamma , \end{aligned} \quad (\text{A23})$$

$$-\partial S / \partial V|_T = \partial^2 F / \partial V \partial T = -\partial P / \partial T|_V$$

$$= -\beta / K_T = -(P/T)\Gamma/g , \quad (\text{A24})$$

$$-\partial S / \partial P|_T = \partial^2 G / \partial P \partial T = \partial V / \partial T|_P$$

$$= \beta V = (V/T)\Gamma / (\gamma g - \Gamma^2) , \quad (\text{A25})$$

$$\partial T / \partial P|_S = \partial^2 H / \partial P \partial S = \partial V / \partial S|_P$$

$$= \beta TV / C_P = (T/P)\Gamma / \gamma , \quad (\text{A26})$$

$$\partial^2 E / \partial V^2|_S = -\partial P / \partial V|_S = 1/(VK_S)$$

$$= (P/V)\gamma , \quad (\text{A27})$$

$$\partial^2 E / \partial S^2|_V = \partial T / \partial S|_V = T / C_V$$

$$= (T^2/PV)g , \quad (\text{A28})$$

$$\partial^2 F / \partial V^2|_T = -\partial P / \partial V|_T = 1/(VK_T)$$

$$= (P/V)(\gamma g - \Gamma^2)/g , \quad (\text{A29})$$

$$\partial^2 F / \partial T^2|_V = -\partial S / \partial T|_V = -C_V / T$$

$$= -(PV/T^2)/g , \quad (\text{A30})$$

$$\partial^2 G / \partial P^2|_T = \partial V / \partial P|_T = -VK_T$$

$$= -(V/P)g / (\gamma g - \Gamma^2) , \quad (\text{A31})$$

$$\partial^2 G / \partial T^2|_P = -\partial S / \partial T|_P = -C_P / T$$

$$= -(PV/T^2)\gamma / (\gamma g - \Gamma^2) , \quad (\text{A32})$$

$$\partial^2 H / \partial P^2|_S = \partial V / \partial P|_S = -VK_S$$

$$= -(V/P)1/\gamma , \quad (\text{A33})$$

$$\partial^2 H / \partial S^2|_P = \partial T / \partial S|_P = T / C_P$$

$$= (T^2/PV)(\gamma g - \Gamma^2)/\gamma . \quad (\text{A34})$$

It is also useful to note the relations

$$\partial \log P / \partial \log V|_S = -\gamma , \quad (\text{A35})$$

$$\partial \log P / \partial \log V|_T = -(\gamma g - \Gamma^2)/g , \quad (\text{A36})$$

$$\partial \log P / \partial \log T|_S = \gamma / \Gamma , \quad (\text{A37})$$

$$\partial \log T / \partial \log V|_S = -\Gamma , \quad (\text{A38})$$

$$\partial \log T / \partial \log V|_P = (\gamma g - \Gamma^2)/\Gamma . \quad (\text{A39})$$

For example, from Eqs. (A35) and (A36) and the inequalities (A46) below, it follows that isentropes intersect isotherms in the P - V plane with greater negative slope.

In terms of the independent variables V and S , the differential relations may be summarized as

$$dE = -P dV + T dS , \quad (\text{A40})$$

$$V dP = -\gamma P dV + \Gamma T dS , \quad (\text{A41})$$

$$(PV/T)dT = -\Gamma P dV + gT dS . \quad (\text{A42})$$

When P and V are chosen as independent variables (which is possible, locally, in regions where $\Gamma \neq 0$), the differential relations may be written

$$\Gamma dE = (\gamma - \Gamma)P dV + V dP , \quad (A43)$$

$$\Gamma T dS = \gamma P dV + V dP , \quad (A44)$$

$$\Gamma(PV/T)dT = (\gamma g - \Gamma^2)P dV + gV dP . \quad (A45)$$

The differential relations for other choices of independent variables may be obtained from those above by simple algebraic manipulations.

Thermodynamic stability requires that the specific internal energy E be jointly convex in V and S ; i.e., the Hessian matrix of second derivatives is non-negative. This translates into the inequalities

$$g \geq 0, \quad \gamma \geq 0, \quad \gamma g \geq \Gamma^2 , \quad (A46)$$

or equivalently

$$C_V^{-1} \geq C_P^{-1} \geq 0 , \quad (A47)$$

$$K_S^{-1} \geq K_T^{-1} \geq 0 . \quad (A48)$$

In particular, $\frac{1}{2}(\gamma + g) \geq |\Gamma|$, since the arithmetic mean bounds the geometric mean. The other thermodynamic potentials are related to E through Legendre transformations, so they also have convexity properties. For instance, G is jointly concave in P and T ; in fact, G is strictly concave because E is continuously differentiable. In addition, F and H are convex (or concave) in each argument separately, but not jointly, since they are only partial Legendre transformations of E . Furthermore, thermodynamic stability is equivalent to joint concavity of the entropy $S = S(V, E)$.

A pure state is an equilibrium state that cannot be decomposed as a convex combination of other equilibrium states. A pure state is therefore an extremal point on the convex energy surface; i.e., the inequalities (A46) are strict. A mixed state, on the other hand, may be written

$$V = (1-\alpha)V_0 + \alpha V_1, \quad S = (1-\alpha)S_0 + \alpha S_1 , \quad (A49)$$

$$E = (1-\alpha)E_0 + \alpha E_1 ,$$

for some α , $0 < \alpha < 1$, in terms of distinct equilibrium states 0 and 1. Since the energy surface is convex, all states on the line segment given by Eq. (A49) with arbitrary α , $0 < \alpha < 1$, lie in the manifold of equilibrium states. In the mixed-phase region, therefore, the energy surface has zero curvature in at least one direction, so that the determinant of the Hessian matrix vanishes: $\gamma g = \Gamma^2$. All points on such a line segment (i.e., an edge in the energy surface) correspond, under the Legendre transformation, to the same value of P , T , and G . A two-phase state is a mixed state that has a unique decomposition in terms of two pure states. In a two-phase region, g and γ may vanish (although not simultaneously). A two-phase region maps to a coexistence curve in the P - T plane, along which G has jump discontinuities in its derivatives. A three-phase state has a unique decomposition in terms of three pure states. An open region in the V - S plane, throughout which E is linear (i.e., a face in the energy surface), lies in a three-phase region and corresponds to a triple point in the P - T plane. The Hessian

matrix is identically zero in a three-phase region: $g = \gamma = \Gamma = 0$.

Although the derivatives of G , viz., V and S , are discontinuous across a coexistence curve, the quantity $dG/dT|_{\text{coex}} = -S + V dP/dT|_{\text{coex}}$ is continuous, so that the Clausius-Clapeyron relation

$$\left. \frac{dP}{dT} \right|_{\text{coex}} = \frac{\Delta S}{\Delta V} \quad (A50)$$

holds (with Δ denoting the jump across the phase transition). The latent heat of the phase transition is $L = \Delta H = T \Delta S$.

A boundary of a mixed-phase region, as drawn in the P - V plane, is called a saturated phase boundary or, simply, a saturation boundary. Since V and T are continuous across a saturation boundary,

$$0 = \Delta(dT/dP|_{\text{coex}}) = \Delta(\partial T/\partial S|_P) dS/dP|_{\text{sat}} + \Delta(\partial T/\partial P|_S) , \quad (A51)$$

$$0 = \Delta(dV/dP|_{\text{sat}}) = \Delta(\partial V/\partial S|_P) dS/dP|_{\text{sat}} + \Delta(\partial V/\partial P|_S) . \quad (A52)$$

After expressing the partial derivatives in these equations in terms of dimensionless parameters and noting that $\gamma g - \Gamma^2$ vanishes in the mixed phase, Eqs. (A51) and (A52) may be combined to show that

$$\frac{\gamma - \gamma_m}{\gamma_m} = (\gamma g - \Gamma^2) \left[\left. \frac{T}{V} \frac{dS}{dP} \right|_{\text{sat}} \right]^2 \geq 0 , \quad (A53)$$

where the subscript m denotes the mixed phase, and all other quantities are evaluated in the pure phase. Thus at a saturation boundary the sound speed is greater in the pure phase than in the mixed phase. In the same fashion,

$$0 = \Delta(dS/dP|_{\text{sat}}) = \Delta(\partial S/\partial V|_P) dV/dP|_{\text{sat}} + \Delta(\partial S/\partial P|_V) \quad (A54)$$

may be manipulated to demonstrate that

$$\frac{\Gamma_m}{\Gamma} = \frac{\gamma_m - \xi}{\gamma - \xi} > 0 , \quad (A55)$$

where

$$\xi = - \left. \frac{V}{P} \frac{dP}{dV} \right|_{\text{sat}} \quad (A56)$$

measures the slope of the saturation boundary in the P - V plane; the last inequality is true because the isentrope crosses through the saturation boundary.

A dimensionless quantity that characterizes the behavior of isentropes relative to the saturation boundary is the retrogradicity r , which is defined by

$$r = \left. \frac{\partial T}{\partial V} \right|_P \left. \frac{dS}{dP} \right|_{\text{sat}} . \quad (A57)$$

Because mixtures of two pure states lie along an isobar,

the Clausius-Clapeyron equation may be written $dP/dT|_{\text{coex}} = (\partial S/\partial V)_P m$; as a result, Eqs. (A25) and (A26) show that

$$r = \frac{\Gamma_m}{\Gamma} \frac{\gamma g - \Gamma^2}{\gamma_m} \frac{T^2}{PV} \frac{dS}{dT} \Big|_{\text{sat}} \quad (\text{A58})$$

has the same sign as the slope of the saturation boundary, as drawn in the S - T plane. Similarly, the identity $dS = \partial S/\partial T|_P dT + \partial S/\partial P|_T dP$ and Eq. (A55) imply that

$$r = \frac{\partial P/\partial T|_S}{\partial P/\partial T|_{\text{coex}}} - 1 = \frac{\gamma/\Gamma}{\gamma_m/\Gamma_m} - 1 = \frac{\gamma - \gamma_m}{\gamma_m} \frac{\xi}{\xi - \gamma}. \quad (\text{A59})$$

Consider a point on the saturation boundary where the mixed phase has higher density than the pure phase at the same pressure (such as at the saturated vapor boundary). Then geometrical considerations show that $0 \leq \xi \leq \gamma$, i.e., $r \leq 0$, if and only if the isentrope through this point crosses from the mixed phase to the pure phase as the density increases. This is the normal situation, but some phase transitions, such as vaporization in fluids with high heat capacity and polymorphic transitions in solids, cause isentropes to cross in the opposite direction, which is called retrograde behavior.

APPENDIX B: WAVE CURVES FOR GENERAL CONSERVATION LAWS

In this appendix we consider the properties of rarefaction, shock, and composite curves for a general system of conservation laws. In particular, we prove the Bethe-Wendroff theorem. (For more details see, e.g., Wendroff, 1972; Smoller, 1982; Isaacson, Marchesin, and Plohr, 1988b.)

The equations we consider are of the form

$$h(u)_t + f(u)_x = 0, \quad (\text{B1})$$

where u belongs to a domain $\mathcal{D} \subseteq \mathbb{R}^n$, and h and f take values in \mathbb{R}^n . This system is assumed to be strictly hyperbolic; i.e., there are n distinct eigenvalues $\lambda_i(u)$ and corresponding right and left eigenvectors $r_i(u)$ and $l_i(u)$, $i = 1, \dots, n$, satisfying

$$[-\lambda_i(u)h'(u) + f'(u)]r_i(u) = 0, \quad (\text{B2})$$

$$l_i(u)[- \lambda_i(u)h'(u) + f'(u)] = 0. \quad (\text{B3})$$

A smooth, scale-invariant solution u of Eq. (B1) depends on t and x only through the combination $\xi = x/t$; it therefore must satisfy

$$[-\xi h'(u) + f'(u)]u_\xi = 0. \quad (\text{B4})$$

This can be achieved by solving the initial value problem for the differential equations

$$u_\xi = r_i(u), \quad (\text{B5})$$

$$u(\xi_0) = u_0, \quad (\text{B6})$$

providing that $r_i(u)$ and ξ_0 are chosen such that

$$\lambda'_i(u)r_i(u) = 1, \quad (\text{B7})$$

$$\lambda_i(u_0) = \xi_0. \quad (\text{B8})$$

Indeed, Eqs. (B5) and (B7) say that $\lambda_i(u)|_{\xi=1} = 1$; thus the initial conditions, Eqs. (B6) and (B8), give that $\lambda_i(u(\xi)) = \xi$. Therefore Eq. (B4) follows from Eq. (B2). Integral curves of Eq. (B5) define the rarefaction curves of the i th family. The states u on the rarefaction curve starting at u_0 comprise a rarefaction wave solution, which may be realized in space-time by inverting the equation $x/t = \lambda_i(u)$. Note, however, that it is not possible to satisfy Eq. (B7) at points u where

$$\lambda'_i(u)r_i(u) = 0. \quad (\text{B9})$$

We refer to this locus as the inflection locus (of the i th family); rarefaction waves cannot contain a point of inflection. Away from the inflection locus the i th family is said to be genuinely nonlinear.

Example. We consider one-dimensional gas dynamics in Lagrangian coordinates. The quantities appearing in Eq. (B1) are

$$u = \begin{bmatrix} V \\ v \\ E \end{bmatrix}, \quad h(u) = \begin{bmatrix} V \\ v \\ \frac{1}{2}v^2 + E \end{bmatrix}, \quad f(u) = \begin{bmatrix} -v \\ P(V, E) \\ vP(V, E) \end{bmatrix}, \quad (\text{B10})$$

where V is specific volume, v is particle velocity, and E is specific energy. Then we find

$$h'(u) = \begin{bmatrix} 1 & 0 & 0 \\ 0 & 1 & 0 \\ 0 & v & 1 \end{bmatrix} \quad (\text{B11})$$

and

$$f'(u) = \begin{bmatrix} 0 & -1 & 0 \\ P_V & 0 & P_E \\ vP_V & P & vP_E \end{bmatrix},$$

where

$$P_V = \partial P/\partial V|_E = -(\gamma - \Gamma)P/V,$$

and

$$P_E = \partial P/\partial E|_V = \Gamma/V.$$

The eigenvalues and eigenvectors for this system are

$$\lambda_1 = -c/V, \quad \lambda_2 = 0, \quad \lambda_3 = c/V, \quad (\text{B12})$$

$$r_i = (-1, \lambda_i, P)^T, \quad (\text{B13})$$

$$l_i = (P_V, \lambda_i - vP_E, P_E), \quad (\text{B14})$$

with $c/V = (-P_V + PP_E)^{1/2} = (\gamma P/V)^{1/2}$. Furthermore, $\lambda'_2 r_2 = 0$ and

$$\lambda'_i r_i = - \left[\frac{\partial}{\partial V} \left|_E \right. - P \frac{\partial}{\partial E} \left|_V \right. \right] \lambda_i = \pm g_c / V^2 \quad (\text{B15})$$

for $i=3$ and 1, respectively. Thus the $i=2$ family is linearly degenerate; it corresponds to contact discontinuities. The other two families are genuinely nonlinear when $g \neq 0$; they correspond to sound waves.

A scale-invariant solution u of Eq. (B1) in which a jump discontinuity occurs at velocity $\xi=\sigma$ must satisfy the Rankine-Hugoniot conditions

$$-\sigma \Delta h(u) + \Delta f(u) = 0 \quad (\text{B16})$$

across the jump. We use the notation ΔA for the jump $\Delta A = A - A_0$ in a quantity A , where A_0 and A are the limiting values on the two sides of the discontinuity. (Later we will consider A_0 to be fixed as A varies.) The Hugoniot locus $\mathcal{H}(u_0)$ through u_0 comprises states u satisfying Eq. (B16) for some σ .

The Hugoniot locus $\mathcal{H}(u_0)$ can be constructed by finding the zero-set of the function H_{u_0} defined by

$$H_{u_0}: \mathcal{D} \times \mathbb{R} \rightarrow \mathbb{R}^n$$

$$:(u, \sigma) \mapsto -\sigma[h(u) - h(u_0)] + f(u) - f(u_0). \quad (\text{B17})$$

The projection of this zero-set into \mathcal{D} gives $\mathcal{H}(u_0)$. Notice that if $h(u_*) \neq h(u_0)$ for some $u_* \in \mathcal{H}(u_0)$, then the corresponding speed σ_* is uniquely determined; thus the projection is one to one at such points.

Suppose that $H_{u_0}(u_*, \sigma_*) = 0$ for some u_* and σ_* . Then the implicit function theorem guarantees that the zero-set of H_{u_0} is a one-dimensional manifold in a neighborhood of (u_*, σ_*) , provided that $H'_{u_0}(u_*, \sigma_*)$ has rank n . Otherwise, the zero-set bifurcates at (u_*, σ_*) . Since

$$dH_{u_0}(u_*, \sigma_*) = -[h(u_*) - h(u_0)]d\sigma + [-\sigma_* h'(u_*) + f'(u_*)]du, \quad (\text{B18})$$

$H'_{u_0}(u_*, \sigma_*)$ has rank n if either (1) σ_* does not coincide with any eigenvalue $\lambda_i(u_*)$, or (2) $\sigma_* = \lambda_i(u_*)$ for some i , but

$$l_i(u_*)[h(u_*) - h(u_0)] \neq 0. \quad (\text{B19})$$

Furthermore, Eq. (B18) implies that the u component of the tangent vector must be nonzero if $h(u_*) \neq h(u_0)$. Therefore the Hugoniot locus $\mathcal{H}(u_0)$, which is the projection of the zero-set, is a one-dimensional manifold in a

$$\dot{\sigma}|_{u=u_0} = \frac{l_i(u_0)[-\lambda_i(u_0)h''(u_0) + f''(u_0)] \cdot (\dot{u}|_{u=u_0})^2}{l_i(u_0)h'(u_0)\dot{u}|_{u=u_0}}. \quad (\text{B24})$$

This may be compared with the formula obtained by differentiating Eq. (B2):

$$-\lambda'_i(u)\dot{u}h'(u)r_i(u) + [-\lambda_i(u)h''(u) + f''(u)] \cdot \dot{u}r_i(u) + [-\lambda_i(u)h'(u) + f'(u)](r_i(u)) = 0, \quad (\text{B25})$$

so

$$\lambda'_i(u_0)\dot{u}|_{u=u_0} = \frac{l_i(u_0)[-\lambda_i(u_0)h''(u_0) + f''(u_0)] \cdot \dot{u}|_{u=u_0} r_i(u_0)}{l_i(u_0)h'(u_0)r_i(u_0)} \quad (\text{B26})$$

neighborhood of u_* unless conditions (1) and (2) fail.

Example. For Lagrangian gas dynamics, $H_{u_0}(u, \sigma) = 0$ reduces to the standard Rankine-Hugoniot conditions. If u is a point on the Hugoniot locus through u_0 , then $\sigma = \lambda_i(u)$ and $l_i(u)[h(u) - h(u_0)] = 0$ if and only if

$$-\frac{V}{P} \frac{\Delta P}{\Delta V} = \gamma = \frac{1}{2} \Gamma \frac{\Delta P}{P}. \quad (\text{B20})$$

Condition (B19) was identified by Wendroff (1972), who assumed it to be true in his application to gas dynamics. [He assumes the sufficient conditions $\gamma > \Gamma > 0$; cf. Eq. (B20).] It is violated in certain models of immiscible three-phase flow (Shearer *et al.*, 1987), where it is called secondary bifurcation [the name primary bifurcation being reserved for the bifurcation of $\mathcal{H}(u_0)$ at the trivial solution, $u = u_0$ and $\sigma = \lambda_i(u_0)$ for some i]. We therefore define the secondary bifurcation locus to comprise pairs of states (u, u_0) such that $u \neq u_0$, $H_{u_0}(u, \sigma) = 0$ with $\sigma = \lambda_i(u)$ for some i , and

$$l_i(u)[h(u) - h(u_0)] = 0. \quad (\text{B21})$$

Although the secondary bifurcation locus is a prominent feature for some systems of conservation laws, it seems to be the empty set in the case of fluid flows of real materials.

Remark. Secondary bifurcation does occur in the example of Sec. VII. This is one of its unphysical features.

The structure of the Hugoniot locus $\mathcal{H}(u_0)$ for u close to u_0 is well known (Lax, 1957): there are n branches of solutions u , which emanate from u_0 in the directions tangent to $r_i(u)$, $i=1, \dots, n$. Away from bifurcation points, $\mathcal{H}(u_0)$ may be parametrized by a single variable, for instance, arc length; we let an overdot denote differentiation with respect to this parameter. Then differentiating Eq. (B16) yields

$$-\dot{\sigma}\Delta h(u) + [-\sigma h'(u) + f'(u)]\dot{u} = 0; \quad (\text{B22})$$

similarly,

$$-\ddot{\sigma}\Delta h(u) - 2\dot{\sigma}h'(u)\dot{u} + [-\sigma h''(u) + f''(u)]\cdot\dot{u}^2 + [-\sigma h'(u) + f'(u)]\ddot{u} = 0. \quad (\text{B23})$$

Consider taking the limit as u approaches u_0 . Equation (B22) implies that $\sigma = \lambda_i(u_0)$ and $\dot{u}|_{u=u_0}$ is a multiple of $r_i(u_0)$ for some i . From Eq. (B23) multiplied by $l_i(u_0)$, one finds that

Consequently,

$$\dot{\sigma}|_{u=u_0} = \frac{1}{2} \lambda'_i(u_0) \dot{u}|_{u=u_0}. \quad (\text{B27})$$

For weak shock waves, therefore, $\sigma \approx \frac{1}{2} [\lambda_i(u_0) + \lambda_i(u)]$.

Such a relation between wave and characteristic speeds is conveniently illustrated in a wave speed diagram, which shows the shock speed $\sigma(u; u_0)$ and the characteristic speed $\lambda_i(u)$ as a function along a portion of the Hugoniot locus (schematically depicted as the u axis). Figure 22 indicates the situation for u near u_0 .

When $u \neq u_0$, Eq. (B22) shows that if $\dot{\sigma} = 0$, then $\sigma = \lambda_i(u)$ for some i . Moreover, multiplying Eq. (B22) by $l_i(u)$ yields

$$-\dot{\sigma} l_i(u) \Delta h(u) + [\lambda_i(u) - \sigma] l_i(u) h'(u) \dot{u} = 0. \quad (\text{B28})$$

Thus if $\sigma = \lambda_i(u)$, then $\dot{\sigma} = 0$, provided (u, u_0) is not a point of secondary bifurcation. In either case, \dot{u} is a multiple of $r_i(u)$, so that the Hugoniot locus is tangent to a rarefaction curve. By induction, $\lambda_i(u) - \sigma$ and $\dot{\sigma}$ vanish to the same order at such a point, as seen by differentiating Eq. (B28) multiple times. These results, which generalize a theorem of Bethe (1942), were demonstrated by Wendroff (1972). We refer to this result as the Bethe-Wendroff theorem. The relation between wave and characteristic speeds is indicated in Fig. 23.

Not all solutions of the Rankine-Hugoniot conditions correspond to physically realizable shock waves; thus a criterion must be supplied to define admissible solutions. For this purpose, Lax (1957) introduced a mathematical analog of the thermodynamic entropy that supplies an admissibility criterion for gas dynamics. A conservation law

$$U(u)_t + F(u)_x = 0 \quad (\text{B29})$$

is satisfied by all smooth solutions of Eq. (B1) if and only if

$$F'(u) = U'(u)[h'(u)]^{-1} f'(u). \quad (\text{B30})$$

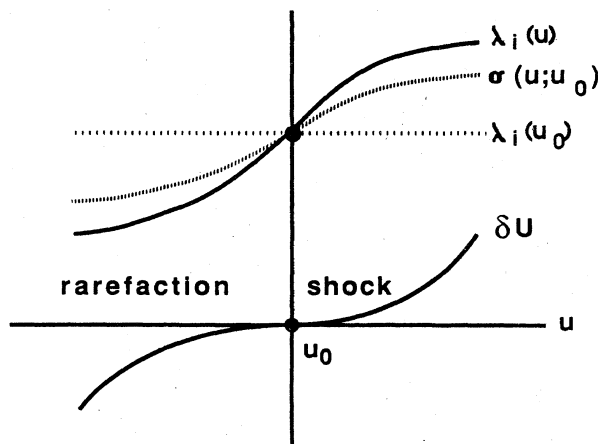


FIG. 22. Shock speed, characteristic velocity, and entropy change along a Hugoniot locus for states u near u_0 . The i th family wave speed is assumed to be genuinely nonlinear at u_0 .

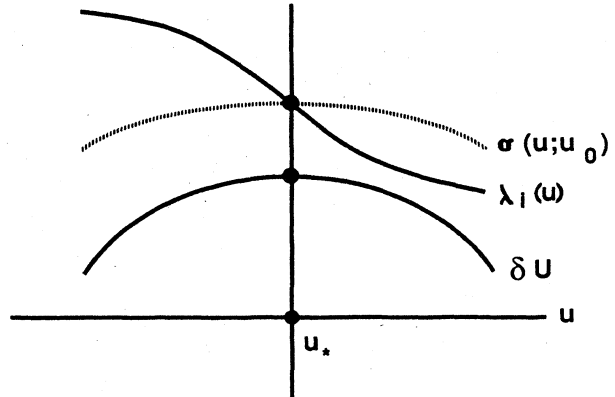


FIG. 23. Shock speed, characteristic velocity, and entropy change along a Hugoniot locus for states u near u_* , where $\sigma(u_*; u_0) = \lambda_i(u_*)$. The i th family wave speed is assumed to be genuinely nonlinear at u_* . The shock speed and entropy also may have a local maximum instead of the local minimum shown.

A mathematical entropy consists of such a conservation law, consistent with Eq. (B1), that satisfies an additional assumption that

$$U''(u) - U'(u)[h'(u)]^{-1} h''(u) > 0 \quad (\text{B31})$$

as a quadratic form. [In the common situation in which $h(u) = u$, this assumption reduces to $U''(u) > 0$, i.e., strict convexity of U .] Whereas the Rankine-Hugoniot conditions [Eq. (B16)] are satisfied across a discontinuous solution, the entropy change δU , defined by

$$\delta U = -\sigma \Delta U(u) + \Delta F(u), \quad (\text{B32})$$

need not vanish; its sign will be used to determine admissibility.

Example. For Lagrangian gas dynamics one takes $U(u) = -S(V, E)$ and $F(u) = 0$, where S is the thermodynamic entropy. Inequality (B31) requires that S be strictly concave in V and E , and that $\partial S / \partial E|_V = 1/T > 0$. The quantity $-\delta U$ is the jump in S multiplied by the mass flux.

Differentiating Eq. (B32) along the Hugoniot locus gives

$$\begin{aligned} (\delta U)' &= -\dot{\sigma} \Delta U(u) + [-\sigma U'(u) + F'(u)] \dot{u} \\ &= -\dot{\sigma} \Delta U(u) \\ &\quad + U'(u)[h'(u)]^{-1} [-\sigma h'(u) + f'(u)] \dot{u}, \end{aligned} \quad (\text{B33})$$

so Eq. (B22) shows that

$$(\delta U)' = -\dot{\sigma} \{ \Delta U(u) - U'(u)[h'(u)]^{-1} \Delta h(u) \}. \quad (\text{B34})$$

Thus

$$\begin{aligned} (\delta U)'' &= -\dot{\sigma} \{ \Delta U(u) - U'(u)[h'(u)]^{-1} \Delta h(u) \} \\ &\quad + \dot{\sigma} (U'[h']^{-1})'(u) \cdot \dot{u} \Delta h(u). \end{aligned} \quad (\text{B35})$$

The limits of Eqs. (B34) and (B35) yield $(\delta U)'|_{u=u_0} = 0$

and $(\delta U)''|_{u=u_0}=0$. In addition, differentiating Eq. (B35) once more and evaluating at $u=u_0$ shows that

$$\begin{aligned} & (\delta U)'''|_{u=u_0} \\ &= \dot{\sigma}|_{u=u_0} \{ U''(u) - U'(u)[h'(u)]^{-1}h''(u) \} \cdot (\dot{u}|_{u=u_0})^2. \end{aligned}$$

Based on inequality (B31), we conclude that the entropy change δU has cubic behavior near a genuinely nonlinear point u_0 ; this is illustrated in the wave speed diagram, Fig. 22.

Furthermore, the convexity condition (B31) guarantees that the quantity in curly brackets in Eq. (B34) is strictly positive when $u \neq u_0$. Consequently, $(\delta U)'=0$ if and only if $\dot{\sigma}=0$, and an induction argument shows that $(\delta U)'$ and $\dot{\sigma}$ vanish to the same order (cf. the Bethe-Wendroff theorem). This behavior is illustrated in Fig. 23.

Similar results may be obtained for waves that are composites of discontinuous and smooth waves. A simple composite wave consists of a rarefaction wave bordered by a jump discontinuity that propagates at characteristic speed. Let the states in the rarefaction portion of the composite wave be $u_0(\xi)$ for ξ between ξ_0 and η , where u_0 satisfies $(u_0)_\xi = r_i(u_0)$ with $\lambda'(u_0)r_i(u_0)=1$, as in Eqs. (B5) and (B7). Let u denote the state on the opposite side of the discontinuity from $u_0(\eta)$. Then $\lambda_i(u_0(\eta))$ is the propagation speed of the discontinuity in the composite wave, and the Rankine-Hugoniot conditions are satisfied across the discontinuity:

$$-\sigma(\eta)[h(u)-h(u_0(\eta))] + f(u) - f(u_0(\eta)) = 0 \quad (B37)$$

with

$$\sigma(\eta) = \lambda_i(u_0(\eta)).$$

Given the rarefaction curve on which the composite wave is based, the composite is specified by u and η satisfying Eq. (B37). We therefore define the composite locus based on the given rarefaction curve to consist of states u such that Eq. (B37) holds for some η . The composite locus may be obtained by finding the zero-set of the function that appears on the left-hand side of Eq. (B37) and projecting it into \mathcal{D} .

Notice that the differential of the left-hand side of Eq. (B37) is

$$\begin{aligned} & -[h(u)-h(u_0(\eta))] \sigma'(\eta) d\eta \\ & + [-\sigma(\eta)h'(u) + f'(u)] du \quad (B38) \end{aligned}$$

because $[-\lambda_i(u_0)h'(u_0) + f'(u_0)](u_0)_\xi = 0$. By the implicit function theorem, then, the zero-set is a one-dimensional manifold, except when $\sigma(\eta) = \lambda_j(u)$ for some j and either $\lambda_j(u)[h(u)-h(u_0(\eta))] = 0$ or $\sigma'(\eta) = \lambda'_i(u_0(\eta))r_i(u_0(\eta)) = 0$. (In general, j may be different from i ; in gas dynamics, however, j must be the same as i .) To phrase this another way, define a two-sided contact discontinuity to be a solution (u_-, u_+) of the Rankine-Hugoniot conditions such that the speed

$\sigma(u_-, u_+)$ satisfies $\lambda_i(u_-) = \sigma(u_-, u_+) = \lambda_j(u_+)$; i.e., the discontinuity propagates at characteristic speed with respect to both its left and right states. Then the zero-set bifurcates only if $(u, u_0(\eta))$ is a two-sided contact and either $(u, u_0(\eta))$ is a point of secondary bifurcation or $u_0(\eta)$ is a point of inflection.

Additionally, Eq. (B38) implies that the u component of the tangent vector to the zero-set must be nonzero if $h(u_*) \neq h(u_0)$. [We assume that the rarefaction curve on which the composite locus is based does not cross the inflection locus, so that $\sigma'(\eta) \neq 0$.] Therefore the composite locus, which is the projection of the zero-set, is a one-dimensional manifold except at bifurcation points.

Away from points of bifurcation, the composite locus may be parametrized by a single variable. Differentiating Eq. (B37) with respect to this variable reproduces Eq. (B22), again because u_0 lies along a rarefaction curve and $\sigma = \lambda_i(u_0)$. Similarly, if δU corresponds to the discontinuity in the composite wave, then Eq. (B34) holds. By the same arguments as before, the conclusions of the Bethe-Wendroff theorem extend to composite loci. We summarize these arguments by stating the following.

Theorem B.1 (Bethe-Wendroff). Consider the Hugoniot locus through a state u_0 or a composite locus based on a rarefaction of the i th family. Assume that the locus does not bifurcate at a point u . Then the following are equivalent: (a) $\dot{\sigma}=0$; (b) $\lambda_j(u)=\sigma$ for some j ; (c) $(\delta U)'=0$. In this instance, $\lambda_j(u)-\sigma$, $\dot{\sigma}$, and (δU) all vanish to the same order, and the locus is tangent to a rarefaction curve of the j th family.

This theorem, and its depiction using wave speed diagrams, are basic tools for constructing wave curves for general systems of conservation laws (Isaacson, Marchesin, and Plohr, 1988b).

APPENDIX C: SHOCK PROFILES AND ADMISSIBILITY CONDITIONS

Nonuniqueness of solutions of the Riemann problem can be resolved in some cases by requiring that shock waves arise as limits of solutions of more complete equations. When heat conduction and viscosity are included, physical shock waves are limits of traveling-wave profiles. Here we recount the analysis by Weyl (1949) and Gilbarg (1951) of shock profiles for fluid dynamics.

The equations of motion are

$$\partial_t \rho + \nabla \cdot (\rho \mathbf{u}) = 0, \quad (C1)$$

$$\partial_t (\rho \mathbf{u}) + \nabla \cdot (\rho \mathbf{u} \mathbf{u}) + \nabla P = \nabla \cdot \Sigma, \quad (C2)$$

$$\partial_t (\rho \mathcal{E}) + \nabla \cdot (\rho \mathcal{E} \mathbf{u}) + \nabla \cdot (P \mathbf{u}) = \nabla \cdot (\Sigma \cdot \mathbf{u}) - \nabla \cdot \mathbf{q}, \quad (C3)$$

where the heat flux is

$$\mathbf{q} = -\kappa \nabla T \quad (C4)$$

and the extra stress arises from viscosity:

$$\Sigma_{ij} = \zeta (\nabla \cdot \mathbf{u}) \delta_{ij} + \eta [\partial_i u_j + \partial_j u_i - \frac{2}{3} (\nabla \cdot \mathbf{u}) \delta_{ij}]; \quad (C5)$$

ζ , η , and κ are the coefficients of bulk viscosity, shear viscosity, and thermal conductivity, respectively, which are assumed to be non-negative.

For one-dimensional flows, these equations become

$$\rho_t + (\rho u)_x = 0, \quad (C1')$$

$$(\rho u)_t + (\rho u^2 + P)_x = (\mu' u_x)_x, \quad (C2')$$

$$(\frac{1}{2}\rho u^2 + \rho E)_t + [u(\frac{1}{2}\rho u^2 + \rho E + P)]_x = (\mu' uu_x)_x + (\kappa T_x)_x, \quad (C3')$$

where $\mu' = \zeta + \frac{4}{3}\eta$ is the dynamic viscosity. In addition, the energy equation (C3') may be replaced by the equation

$$(\rho S)_t + \left[\rho u S + \frac{-\kappa T_x}{T} \right]_x = \frac{\mu'}{T} (u_x)^2 + \kappa \left[\frac{T_x}{T} \right]^2 \quad (C3'')$$

for the entropy. The right-hand side represents the entropy production; it is non-negative, in accordance with the Clausius-Duhem inequality.

Let the state variables be denoted by $Z = (V, T, u)$. The shock profile is determined by a traveling-wave solution, which takes the form $Z = Z(x - \sigma t)$. As $x = \pm\infty$, the solution tends to the states on the left and right of the shock wave; let Z_0 denote the left (or initial) state, and let Z_∞ denote the right (or final) state. Substituting $\partial_t = -\sigma \partial_x$ into Eqs. (C1')–(C3') and integrating from $-\infty$ to x , we obtain the ordinary differential equations for the shock profile:

$$\rho(u - \sigma) = \mp m = \text{const}, \quad (C6)$$

$$\mp m \mathbf{J}[u] + \mathbf{J}[P] = \mu' \frac{du}{dx}, \quad (C7)$$

$$\mp m \mathbf{J}[\frac{1}{2}u^2 + E] + \mathbf{J}[uP] = \mu' u \frac{du}{dx} + \kappa \frac{dT}{dx}, \quad (C8)$$

where we use the notation $\mathbf{J}[A] = A - A_0$ for the jump in a quantity A . The constant $m > 0$ will be seen to be the mass flux. Moreover, Eq. (C3'') becomes

$$\frac{d}{dz} \left[\mp m S - \frac{\kappa}{T} \frac{dT}{dx} \right] = \frac{\mu'}{T} \left[\frac{du}{dx} \right]^2 + \kappa \left[\frac{1}{T} \frac{dT}{dx} \right]^2. \quad (C9)$$

The final state Z_∞ , as well as the initial state Z_0 , is a critical point of these equations; taking the limit as $x \rightarrow \infty$ we obtain

$$\rho_\infty(u_\infty - \sigma) = \mp m = \rho_0(u_0 - \sigma), \quad (C10)$$

$$\mp m \Delta u + \Delta P = 0, \quad (C11)$$

$$\mp m \Delta(\frac{1}{2}u^2 + E) + \Delta(uP) = 0, \quad (C12)$$

where $\Delta A = A_\infty - A_0$. Thus Z_∞ and Z_0 satisfy the Rankine-Hugoniot relations for the wave speed σ , and m is the mass flux. The upper (lower) choice of sign corresponds to right-facing (left-facing) shock waves. Because $-m^2$ is the slope of the Rayleigh line, critical points for the ordinary differential equations are intersections of the Hugoniot locus with the Rayleigh line.

It is convenient to change variables from u and T to V and T , since the equation of state is independent of u . Straightforward manipulations of Eqs. (C6)–(C8) lead to the equations

$$\mp m \mu' \frac{dV}{dx} = \mathbf{J}[P + m^2 V], \quad (C13)$$

$$\mp \frac{\kappa}{m} \frac{dT}{dx} = \mathbf{J}[E - \frac{1}{2}m^2 V^2 + V(P_0 + m^2 V_0)]. \quad (C14)$$

To analyze this system, it is important to characterize its critical points. Near a critical point (V_c, T_c) , Eqs. (C13) and (C14) may be expanded to first order to yield

$$\frac{d}{dx} \begin{bmatrix} \tilde{V} \\ \tilde{T} \end{bmatrix} = \mathbf{A} \begin{bmatrix} \tilde{V} \\ \tilde{T} \end{bmatrix}, \quad (C15)$$

where $\tilde{V} = (V - V_c)/V_c$, $\tilde{T} = (T - T_c)/T_c$, and

$$\mathbf{A} = \mp \begin{bmatrix} \frac{1}{m\mu'} \left[m^2 - \frac{\gamma g - \Gamma^2}{g} \frac{P}{V} \right] & \frac{1}{m\mu'} \frac{\Gamma P}{gV} \\ \frac{m}{\kappa} \frac{\Gamma PV}{gT} & \frac{m}{\kappa} \frac{PV}{gT} \end{bmatrix} \quad (C16)$$

with all matrix elements evaluated at the critical point.

Two important quantities are

$$\mp \text{Tr } \mathbf{A} = \frac{1}{m\mu'} \left[m^2 - \frac{\gamma g - \Gamma^2}{g} \frac{P}{V} \right] + \frac{m}{\kappa} \frac{PV}{gT}, \quad (C17)$$

$$\det \mathbf{A} = \frac{1}{\mu' \kappa} \frac{PV}{gT} \left[m^2 - \frac{\gamma P}{V} \right]. \quad (C18)$$

Simple algebraic manipulations show the discriminant of \mathbf{A} to be positive:

$$\begin{aligned} \text{disc } \mathbf{A} &= (\text{Tr } \mathbf{A})^2 - 4 \det \mathbf{A} \\ &= \left[\frac{1}{m\mu'} \left[m^2 - \frac{\gamma g - \Gamma^2}{g} \frac{P}{V} \right] - \frac{m}{\kappa} \frac{PV}{gT} \right]^2 \\ &\quad + \frac{4}{\mu' \kappa} \frac{\Gamma^2 P^2}{g^2 T} \geq 0. \end{aligned} \quad (C19)$$

Therefore the eigenvalues of \mathbf{A} are real.

In Eq. (C18), the bracketed quantity may be expressed as

$$m^2 - \frac{\gamma P}{V} = \rho^2 [(u - \sigma)^2 - c^2]. \quad (C20)$$

Thus $\det \mathbf{A}$ is positive or negative according to whether the flow at the critical point is supersonic or subsonic relative to the wave speed σ . For subsonic flow, $\det \mathbf{A} < 0$ and the eigenvalues of \mathbf{A} have opposite signs: a subsonic critical point is a saddle point. Similarly, the bracketed quantity in Eq. (C17) may be expressed as

$$m^2 - \frac{\gamma g - \Gamma^2}{g} \frac{P}{V} = \rho^2 \left[(u - \sigma)^2 - c^2 \left[1 - \frac{\Gamma^2}{\gamma g} \right] \right]. \quad (C21)$$

Because thermodynamics requires that $\gamma g \geq \Gamma^2$, $\mp \text{Tr } \mathbf{A} > 0$ and the eigenvalues of \mathbf{A} are both negative

(positive) when the flow is supersonic and the wave is right-facing (left-facing). Thus a supersonic critical point is an attractive (repulsive) node. To summarize, we have proved the following.

Theorem C.1 (Weyl, 1949). Suppose that the shock layer is caused by viscosity and heat conduction. Then the ordinary differential equations for the shock profile with a given wave speed have the following properties: (a) The critical points are the intersections of the Hugoniot locus with the Rayleigh line. (b) A subsonic critical point is a saddle point. (c) A supersonic critical point is an attractive (repulsive) node for a shock wave that faces right (left).

Remark. In the proof given by Weyl, two assumptions are made on the EOS: $\Gamma > 0$ and $\mathcal{G} > 0$. The first, $\Gamma > 0$, is for convenience; it allows the use of P and V as independent variables, but it is not crucial. The second, $\mathcal{G} > 0$, guarantees that Eqs. (C13) and (C14) have exactly two critical points. We emphasize that Theorem C.1 holds for any EOS and for any number of critical points. Of course, the EOS affects the existence and nature of critical points.

Let us first consider the standard case $\mathcal{G} > 0$, in which the negative slope of the Rayleigh line, m^2 , increases monotonically with shock strength. Then the ordinary differential equations for the shock profile have only two critical points. For a left-facing shock wave, the initial shock state is a repelling node, while the final shock state is a saddle point. Because the ordinary differential equations are autonomous, the shock profile defines a trajectory in the V - T plane. If a smooth vector field on the whole plane has only two critical points, a repulsive node and a saddle point, then topological considerations show that a trajectory exists connecting the critical points. In the present application, the domain is the subset of the plane defined by the physical constraints $V > 0$ and $T \geq 0$; thus more analysis is required to demonstrate the existence of a shock profile. The existence of connecting orbits for Eqs. (C13) and (C14) may be proved using the arguments of Gilbarg (1951). This proof assumes that only two critical points occur but the following discussion shows how it may be generalized to the situation where the Rayleigh line intersects the Hugoniot locus at more points.

The principal idea is to exploit the curves \mathcal{C}_V and \mathcal{C}_T along which dV/dx and dT/dx vanish, respectively. Thus \mathcal{C}_V satisfies the Rayleigh line equation

$$P = P_0 + m^2(V_0 - V) \quad (\text{C22})$$

and

$$E = E_0 + (V_0 - V)[P_0 + \frac{1}{2}m^2(V_0 - V)] \quad (\text{C23})$$

along \mathcal{C}_T . These curves intersect precisely at the critical points.

The tangents to these curves may be calculated using thermodynamic identities to express dP and dE in terms of dV and dT :

$$\frac{\Gamma P}{g T} dT + \left[m^2 - \frac{\gamma g - \Gamma^2}{g} \frac{P}{V} \right] dV = 0 \quad (\text{C24})$$

and

$$\frac{PV}{gT} dT + \left[\left(\frac{\Gamma}{g} - 1 \right) P + P_0 + m^2(V_0 - V) \right] dV = 0 \quad (\text{C25})$$

along \mathcal{C}_V and \mathcal{C}_T , respectively. Assuming that $\Gamma > 0$, we see that the coefficients of dT in Eqs. (C24) and (C25) are positive, so that \mathcal{C}_V and \mathcal{C}_T can be parametrized by V . Thus

$$-\frac{dT}{dV} \Big|_{\mathcal{C}_V} = \Gamma \frac{T}{V} + \frac{gT}{\Gamma P} \Bigg[\left(m^2 - \frac{\gamma P}{V} \right) \Bigg] \quad (\text{C26})$$

and

$$-\frac{dT}{dV} \Big|_{\mathcal{C}_T} = \Gamma \frac{T}{V} + \frac{gT}{\Gamma P} [P_0 + m^2(V_0 - V) - P]. \quad (\text{C27})$$

At a critical point, $-dT/dV|_{\mathcal{C}_T} = \Gamma T/V > 0$; furthermore, $-dT/dV|_{\mathcal{C}_V} > -dT/dV|_{\mathcal{C}_T}$ if the critical point is a supersonic ($m^2 > \gamma P/V$), and the opposite inequality holds if it is subsonic.

Consider the case of a left-facing compressive shock wave, with the subsonic state 0 ahead (on the left) of it. Let state 1 be the first critical point with $V_1 < V_0$. We assume that this state is not sonic, so that it must be supersonic. According to the inequalities above, \mathcal{C}_T is seen to lie below \mathcal{C}_V for $V_1 < V < V_0$ in both the V - T and P - V planes. In particular, $P < P_0 + m^2(V_0 - V)$ along \mathcal{C}_T , so $-dT/dV|_{\mathcal{C}_T} > 0$ between states 0 and 1; i.e., \mathcal{C}_T may be parametrized by T . Furthermore, the signs of dV/dx and dT/dx , which are determined by the sectors defined by \mathcal{C}_V and \mathcal{C}_T , dictate that the vector field point in the positive T direction on \mathcal{C}_V and in the negative V direction on \mathcal{C}_T . Thus the vector field points out of the region \mathcal{R} bounded by \mathcal{C}_V and \mathcal{C}_T between V_0 and V_1 . The analysis of Gilbarg now demonstrates that a trajectory connecting state 0 to state 1 exists and lies in the region \mathcal{R} .

Observe that the argument makes no assumption about \mathcal{G} and that it applies even if there are more than two critical points, as in Fig. 24. The Rayleigh line provides a natural ordering for the critical points. Because the curves \mathcal{C}_V and \mathcal{C}_T are parametrized by V , they pass through the critical points in accordance with this ordering; moreover, the critical points alternate between being saddle points and nodes. Notice that $dV/dx > 0$ above \mathcal{C}_V and $dT/dx < 0$ below \mathcal{C}_T , so that it is impossible for a trajectory leaving state 0 to connect to any other critical point with smaller specific volume and higher temperature than state 0. Furthermore, the final shock temperature is higher than the initial shock temperature; this is because isentropes intersect isotherms with larger negative slopes in the P - V plane (assuming that $\Gamma > 0$), and because shock waves increase the entropy. Consequently, state 0 is connected by a trajectory only to the first criti-

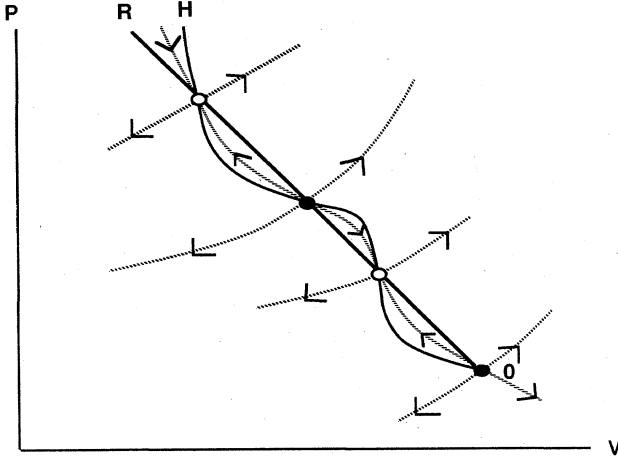


FIG. 24. Topology of trajectories for the shock profile equations in the P - V plane when the Rayleigh line intersects the Hugoniot locus at four points.

cal point with smaller volume.

Summarizing these results, we have the following.

Theorem C.2 (Gilbarg, 1951). Suppose that state 1 lies on the compressive branch of the Hugoniot locus for state 0, with the flow supersonic at state 0 and subsonic at state 1. Assume that any other intersection of the Rayleigh line with the compressive branch occurs at higher pressure than state 1; also assume that $\Gamma > 0$. Then there exists a unique shock profile connecting state 0 to state 1. Furthermore, state 0 is not connected to any other higher-pressure critical point.

Remarks. (1) Liu (1976) has proved a version of this theorem that allows $\mathcal{G} > 0$ to be violated: a (unique) viscous shock profile exists if and only if the Liu-Oleinik admissibility criterion holds (i.e., for each state on the Hugoniot locus between the initial and final shock state, the Rayleigh line lies entirely above the Hugoniot locus in the P - V plane). His proof assumes that there is no heat conduction. When both viscosity and heat conduction are present, Gilbarg's result has been extended to this case by Pego (1986).

(2) This result is consistent with, but more general than, the Lax characteristic criterion (Lax, 1957). This criterion, which requires the flow to be supersonic ahead and subsonic behind, excludes only one of the two inadmissible final states in Fig. 24.

(3) Let us label the four critical points along the Rayleigh line as 0, 1, 2, and 3. The triple shock rule, Proposition 5.5, implies that states 2 and 3 are connected by a shock wave, and Theorem C.2 implies that this shock wave has a viscous profile. Thus trajectories connect alternate pairs of critical points. We emphasize that the theorem does not require that $\mathcal{G} > 0$; it requires only that the critical points alternate along the Rayleigh line between being saddle points and nodes.

(4) Since the trajectory lies in region \mathcal{R} , the components of the vector field do not change sign. Therefore

V decreases and T increases monotonically along the shock profile. It then follows from Eq. (A45) that P increases monotonically along the shock profile, and from Eq. (C6) that u varies monotonically. We will see below that S varies monotonically if the viscosity is large, whereas it does not if the heat conduction is large. If, in addition, $\mathcal{G} > 1$ and $\mathcal{H} > 0$ in region \mathcal{R} , then c increases monotonically along the profile. This, in turn, implies that the characteristic speed $u - c$ varies monotonically.

(5) Any point along the Hugoniot locus satisfies Eq. (C23), provided that $-m^2$ is reinterpreted as the slope of the line connecting it to state 0 in the P - V plane. Consequently, for each V between V_0 and V_1 , E is larger on \mathcal{C}_T than it is on the Hugoniot locus; this is because the Hugoniot locus lies below the Rayleigh line to state 1. Therefore \mathcal{C}_T lies above the Hugoniot locus in the T - V plane (independently of the sign of Γ). In particular, the proof of Theorem C.2 shows that the shock profile lies between the Hugoniot locus and the Rayleigh line in the P - V plane, provided that $\Gamma > 0$.

(6) The present analysis depends crucially on the form of the vector field in the shock profile ordinary differential equations. Here the parabolic terms result physically from viscosity and heat conduction. Other forms have been used in connection with van der Waals EOS by Shearer (1983) and Slemrod (1983). The allowable form for the "viscosity" terms that give rise to shock profiles has been analyzed by Pego (1984).

(7) The existence of viscous shock profiles for strictly hyperbolic, genuinely nonlinear systems of conservation law satisfying an entropy condition has been proved by Mock (1980).

(8) For a shock wave to occur physically, its viscous profile must be stable under perturbations. One-dimensional viscous profiles for weak shock waves have been shown to be nonlinearly stable by Liu (1986). A further requirement for the profile is that it be stable as a multidimensional front (cf. Sec. IV).

We conclude by discussing two special cases. Equations (C13) and (C14) show that dT/dV , and therefore the shock profile, depends on μ' and κ only in the ratio μ'/κ . A dimensionless form of this ratio is the Prandtl number:

$$Pr = \mu' C_V / \kappa. \quad (C28)$$

The extreme cases are $Pr = 0$, when there is heat conduction but no viscosity, and $Pr = \infty$, when there is viscosity but no heat conduction.

When $Pr = 0$, the shock profile lies along \mathcal{C}_V , i.e., along the Rayleigh line. At the initial state 0, which is supersonic, $m^2 > -\partial P/\partial V|_S$, whereas the reverse inequality holds at the subsonic state 1. Therefore the isentrope must be tangent to the Rayleigh line at some intermediate point, and there is an entropy maximum in the interior of the shock profile. However, the limit $Pr \rightarrow 0$ is generally singular. In fact, $dT/dV|_{\mathcal{C}_V}$ may vanish at a point where the right-hand side of Eq. (C14) does not, in which case a continuous shock profile would not exist.

(See Gilbarg, 1951; Zel'dovich and Raizer, 1966.) This occurs, for instance, for sufficiently strong shock waves in polytropic gases with $1 < \gamma < 3$. If a continuous profile for $Pr = 0$ fails to exist, then for small, nonzero values of Pr we expect the profile to consist of a thin viscous profile with a wide thermal precursor. Thus there would be two distinct length scales: a short length scale determined by viscosity and a long length scale determined by heat conduction.

In the other extreme, $Pr \rightarrow \infty$, the shock profile lies along \mathcal{C}_T . Equation (C9) shows that the entropy increases monotonically, $m dS/dx \geq 0$, so that the shock profile remains between the initial and final isentropes in the P - V plane. In addition, the differential of Eq. (C23), combined with various thermodynamic identities, shows that

$$-dP/dV = \gamma P/V + \Gamma [P_0 + m^2(V_0 - V) - P]/V. \quad (\text{C29})$$

If $\Gamma > 0$, then the shock profile lies below the Rayleigh line, so that $-dP/dV > 0$; i.e., the pressure varies monotonically along the profile. Furthermore, $dP/dV = -\gamma P/V$ at critical points: the shock profile is tangent to the isentropes at the initial and final states.

Finally, we note that Pego (1986) has constructed an equation of state with an unusual property. For this EOS, isentropes are nonconvex, so that the wave curve includes shock waves that rarefy the fluid. Pego proves the existence of such an expansive shock wave that has a unique profile when Pr is sufficiently large (i.e., when viscosity dominates) but fails to have a profile when Pr is sufficiently small (i.e., when heat conduction dominates). However, no attempt was made, in constructing this example, to ensure that thermodynamic stability ($\gamma g \geq \Gamma^2$) holds.

REFERENCES

- Adb-El-Fattah, A., and L. Henderson, 1976, "Precursor Shock Waves at a Slow-Fast Gas Interface," *J. Fluid Mech.* **76**, 157.
- Adamson, T., Jr., and J. Nicholls 1959, "On the Structure of Jets from Highly Underexpanded Nozzles into Still Air," *J. Aerosp. Sci.* **26**, 16.
- Bdzil, J., and D. Stewart, 1986, "Time-Dependent Two-Dimensional Detonation: the Interaction of Edge Rarefactions with Finite-Length Reaction Zones," *J. Fluid Mech.* **171**, 1.
- Bethe, H., 1942, "The Theory of Shock Waves for an Arbitrary Equation of State" (Clearinghouse for Federal Scientific and Technical Information, U. S. Department of Commerce, Washington, D.C.), Report No. PB-32189.
- Bukiet, B., 1989, "The Effect of Curvature on Detonation Speed," *SIAM J. Appl. Math.* (in press).
- Chaves, H., H. Lang, G. Meier, and H.-D. Speckmann, 1985, "Adiabatic Phase Transitions and Wavesplitting in Fluids of High Specific Heat", in *Flow of Real Fluids*, edited by G. Meier and F. Obermeier, Lecture Notes in Physics No. 235, (Springer, New York), p. 115.
- Chern, I-L., and P. Colella, 1987, "A Conservation Front Tracking Method for Hyperbolic Conservation Laws," Lawrence Livermore National Laboratory Report No. UCRL-97200.
- Chern, I-L., J. Glimm, O. McBryan, B. Plohr, and S. Yaniv, 1985, "Front Tracking for Gas Dynamics," *J. Comput. Phys.* **62**, 83.
- Chorin, A., 1976, "Random Choice Solutions of Hyperbolic Systems," *J. Comput. Phys.* **22**, 517.
- Colella, P., 1985, "A Direct Eulerian MUSCL Scheme for Gas Dynamics," *SIAM J. Sci. Stat. Comput.* **6**, 104.
- Colella, P., and H. Glaz, 1985, "An Efficient Solution Algorithm for the Riemann Problem for Real Gases," *J. Comput. Phys.* **59**, 264.
- Collella, P., and P. Woodward, 1984, "The Piecewise Parabolic Method (PPM) for Gas-Dynamical Simulation," *J. Comput. Phys.* **54**, 174.
- Courant, R., and K. Friedrichs, 1948, *Supersonic Flow and Shock Waves* (Interscience, New York).
- Cowan, R., 1958, "Properties of the Hugoniot Function," *J. Fluid Mech.* **3**, 531.
- Cowperthwaite, M., 1968, "Properties of Some Hugoniot Curves Associated with Shock Instabilities," *J. Franklin Inst.* **285**, 275.
- Cramer, M., and R. Sen, 1987, "Exact Solution for Sonic Shocks in van der Waals Gases," *Phys. Fluids* **30**, 377.
- Davis, W., 1985, "Equation of State for Detonation Products," in *Eighth International Detonation Symposium*, edited by J. Short (Naval Surface Weapons Center, White Oak, Silver Springs, MD), p. 785.
- Dukowicz, J., 1985, "A General, Non-Iterative Riemann Solver for Godunov's Method," *J. Comput. Phys.* **61**, 119.
- Duvall, G., and R. Graham, 1977, "Phase Transitions under Shock-Wave Loading," *Rev. Mod. Phys.* **49**, 523.
- D'yakov, S., 1954, "On the Stability of Shock Waves," *Zh. Eksp. Teor. Fiz.* **27**, 288.
- Erpenbeck, J., 1962, "Stability of Step Shocks," *Phys. Fluids* **5**, 1181.
- Erpenbeck, J., 1963, "Reply to Comments by Gardner," *Phys. Fluids* **6**, 1368.
- Fickett, W., and W. Davis, 1979, *Detonation* (University of California, Berkeley).
- Fowles, G., 1976, "Conditional Stability of Shock Waves—A Criterion for Detonation," *Phys. Fluids* **19**, 227.
- Fowles, G., 1981, "Stimulated and Spontaneous Emission of Acoustic Waves from Shock Fronts," *Phys. Fluids* **24**, 220.
- Fowles, G., and A. Houwing, 1984, "Instabilities of Shock and Detonation Waves," *Phys. Fluids* **27**, 1982.
- Gardner, C., 1963, "Comment on 'Stability of Step Shocks,'" *Phys. Fluids* **6**, 1366.
- Gelfand, I., 1959, "Some Problems in the Theory of Quasilinear Equations," *Usp. Mat. Nauk* **14**, 87 [Am. Math. Soc. Transl., Ser. 2, **29**, 295 (1963)].
- Gilbarg, D., 1951, "The Existence and Limit Behavior of the One-Dimensional Shock Layer," *Am. J. Math.* **73**, 256.
- Gilmore, R., 1981, *Catastrophe Theory for Scientists and Engineers* (Wiley-Interscience, New York), Secs. 10.4–10.6.
- Glass, I., and W. Liu, 1978, "Effects of Hydrogen Impurities on Shock Structure and Stability in Ionizing Monatomic Gases," *J. Fluid Mech.* **84**, 55.
- Glimm, J., 1965, "Solutions in the Large for Nonlinear Hyperbolic Systems of Equations," *Commun. Pure Appl. Math.* **XVIII**, 697.
- Glimm, J., C. Klingenberg, O. McBryan, B. Plohr, D. Sharp, and S. Yaniv, 1985, "Front Tracking and Two Dimensional Riemann Problems," *Adv. Appl. Math.* **6**, 259.
- Glimm, J., and D. Sharp, 1986, "An S-Matrix Theory for Clas-

- sical Nonlinear Physics," *Found. Phys.* **16**, 125.
- Godunov, S., 1959, "A Difference Method for Numerical Calculation of Discontinuous Solutions of the Equations of Hydrodynamics," *Mat. Sb.* **47**, 271.
- Griffiths, R., R. Sandeman, and H. Hornung, 1975, "The Stability of Shock Waves in Ionizing and Dissociating Gases," *J. Phys. D* **8**, 1681.
- Grove, J., 1988, "Front Tracking and Shock-Contact Interactions," in *Advances in Computer Methods for Partial Differential Equations*, edited by R. Vichnevetsky and R. Stepleman (Rutgers University, New Brunswick) (in press).
- Guderley, G., 1942, "Starke kugelige und zylindrische Verdichtungsstöße in der Nähe des Kugelmittelpunktes bzw der Zylinderachse," *Luftfahrt-Forsch.* **19**, 302.
- Harlow, Francis, and Anthony A. Amsden, 1971, *Fluid Dynamics*, Monograph LA-4700 (Los Alamos Scientific Laboratory, Los Alamos, N. Mex.).
- Hayes, Wallace D., 1958, "The Basic Theory of Gasdynamic Discontinuities," in *Fundamentals of Gas Dynamics*, edited by Howard W. Emmons, High Speed Aerodynamics and Jet Propulsion, Vol. 3 (Princeton University, Princeton, NJ), p. 416.
- Henderson, L., 1966, "The Refraction of a Plane Shock Wave at a Gas Interface," *J. Fluid Mech.* **26**, 607.
- Henderson, L., 1967, "The Reflection of a Shock Wave at a Rigid Wall in the Presence of a Boundary Layer," *J. Fluid Mech.* **30**, 699.
- Hornung, H., 1986, "Regular and Mach Reflection of Shock Waves," *Annu. Rev. Fluid Mech.* **18**, 33.
- Isaacson, E., D. Marchesin, and B. Plohr, 1988a, "Transitional Waves for Conservation Laws," (Center for the Mathematical Sciences, University of Wisconsin-Madison), Technical Report No. 89-20.
- Isaacson, E., D. Marchesin, and B. Plohr, 1988b, "Construction of Nonlinear Waves for Conservation Laws," in preparation.
- Isaacson, E., D. Marchesin, B. Plohr, and J. B. Temple, 1988, "The Riemann Problem Near a Hyperbolic Singularity: the Classification of Quadratic Riemann Problems I," *SIAM J. Appl. Math.* **48**, 1009.
- Isaacson, E., and J. B. Temple, 1988a, "The Riemann Problem Near a Hyperbolic Singularity II," *SIAM J. Appl. Math.* (in press).
- Isaacson, E., and J. B. Temple, 1988b, "The Riemann Problem Near a Hyperbolic Singularity III," *SIAM J. Appl. Math.* (in press).
- Jones, D., P. Martin, and C. Thornhill, 1951, "A Note on the Pseudo-Stationary Flow Behind a Strong Shock Diffracted or Reflected at a Corner," *Proc. R. Soc. London Ser. A* **209**, 238.
- Jones, J., 1987, "Asymptotic Analysis of an Expanding Detonation," Ph.D. Thesis (New York University).
- Jones, J., 1989, "Spherical Detonation," *Adv. Appl. Math.* (in press).
- Kontorovich, V., 1958, "Concerning the Stability of Shock Waves," *Zh. Eksp. Teor. Fiz.* **33**, 1525 [Sov. Phys. JETP **6**, 1179 (1958)].
- Kutateladze, S., V. Nakoryakov, and A. Borisov, 1987, "Rarefaction Waves in Liquid and Gas-Liquid Media," *Annu. Rev. Fluid Mech.* **19**, 577.
- Landau, L., and E. Lifshitz, 1958, *Statistical Physics* (Addison-Wesley, Reading, MA), Sec. 74.
- Landau, L., and E. Lifshitz, 1959, *Fluid Mechanics* (Addison-Wesley, Reading MA).
- Lax, P., 1957, "Hyperbolic Systems of Conservation Laws II," *Commun. Pure Appl. Math.* **X**, 537.
- Lax, P., 1972, *Hyperbolic Systems of Conservation Laws and the Mathematical Theory of Shock Waves*, Regional Conference Series Lectures in Applied Mathematics, Vol. 11 (Society for Industrial and Applied Mathematics, Philadelphia).
- Le Floch, P., and P. Raviart, 1988, "An Asymptotic Expansion for the Solution of the Generalized Riemann Problem," *Nonlinear Analysis, Ann. Inst. Henri Poincaré* (in press).
- Lieb, Elliott H., 1976, "The Stability of Matter," *Rev. Mod. Phys.* **48**, 553.
- Liu, T.-P., 1975, "The Riemann Problem for General Systems of Conservation Laws," *J. Diff. Eq.* **18**, 218.
- Liu, T.-P., 1976, "The Entropy Condition and the Admissibility of Shocks," *J. Math. Anal. Appl.* **53**, 78.
- Liu, T.-P., 1979, "Quasilinear Hyperbolic Systems," *Commun. Math. Phys.* **68**, 141.
- Liu, T.-P., 1986, "Shock Waves for Compressible Navier-Stokes Equations are Stable," *Commun. Pure Appl. Math.* **39**, 565.
- Mader, C., 1970, "An Equation of State for Shocked Copper Foam," Los Alamos National Laboratory Report No. LA-4381.
- Majda, A., 1983, "The Stability of Multi-dimensional Shock Fronts," *Mem. Am. Math. Soc.* **41**, 275.
- Majda, A., 1987, "Criteria for Regular Spacing of Reacting Mach Stems," *Proc. Natl. Acad. Sci. U.S.A.* **84**, 6011.
- Majda, A., and R. Rosales, 1983, "A Theory for Spontaneous Mach Stem Formation in Reacting Shock Fronts: I. The Basic Perturbation Analysis," *SIAM J. Appl. Math.* **43**, 1310.
- Majda, A., and R. Rosales, 1984, "A Theory of Spontaneous Mach Stem Formation in Reacting Shock Fronts: II. Steady-Wave Bifurcations and the Evidence for Breakdown," *Stud. Appl. Math.* **71**, 117.
- Malkus, D., J. Nohel, and B. Plohr, 1988, "Dynamics of Shear Flow of a Non-Newtonian Fluid" (Center for the Mathematical Sciences, University of Wisconsin-Madison), Technical Report No. 89-14.
- Marsh, S., 1980, Ed., *LASL Shock Hugoniot Data* (University of California, Berkeley).
- Meier, G., and P. Thompson, 1985, "Real Gas Dynamics of Fluids with High Specific Heat," in *Flow of Real Fluids*, edited by G. Meier and F. Obermeier, Lecture Notes in Physics, No. 235 (Springer, New York), p. 103.
- Mock, M., 1980, "A Topological Degree for Orbits Connecting Critical Points of Autonomous Systems," *J. Diff. Eq.* **38**, 176.
- Moler, C., and J. Smoller, 1970, "Elementary Wave Interactions in Quasilinear Hyperbolic Systems," *Arch. Ration. Mech. Anal.* **37**, 309.
- More, R., K. Warren, D. Young, and G. Zimmerman, 1988, "A New Quotidion Equation of State (QEOS) for Hot Dense Matter," *Phys. Fluids* **31**, 3059.
- Oleinik, O., 1959, "Uniqueness and Stability of the Generalized Solution of the Cauchy Problem for a Quasi-linear Equation," *Usp. Mat. Nauk* **14**, 165 [Am. Math. Soc. Transl. Ser. 2, **33**, 285 (1964)].
- Oleinik, O., 1965, "Discontinuous Solutions of Non-linear Differential Equations," in *Seminari 1962/63 Analisi, Algebra, Geometria e Topologia*, Vol. 1, edited by A. Cremonese (Ist. Naz. Alta Mat., Rome), p. 404.
- Pego, R., 1984, "Stable Viscosities and Shock Profiles for Systems of Conservation Laws," *Trans. Am. Math. Soc.* **282**, 749.
- Pego, R., 1986, "Nonexistence of a Shock Layer in Gas Dynamics with a Nonconvex Equation of State," *Arch. Ration. Mech. Anal.* **94**, 165.
- Plohr, B., 1988a, "Shockless Acceleration of Thin Plates Modeled by a Tracked Random Choice Method," *AIAA J.* **26**, 470.

- Plohr, B., 1988b, "Instabilities in Shear Flow of Viscoelastic Fluids with Fading Memory," in *Workshop on Partial Differential Equations and Continuum Models of Phase Transitions . . .* Nice, 1988, edited by D. Serre, Lecture Notes in Mathematics (Springer, New York) (in press).
- Plohr, B., and D. Sharp, 1989, "A Conservative Eulerian Formulation of the Equations for Elastic Flow," *Adv. Appl. Math.* (in press).
- Rabie, R., G. Fowles, W. Fickett, 1979, "The Polymorphic Detonation," *Phys. Fluids* **22**, 422.
- Reichl, L., 1980, *A Modern Course in Statistical Physics* (University of Texas, Austin).
- Rice, M., R. McQueen, and J. Walsh, 1958, "Compression of Solids by Strong Shock Waves," in *Solid State Physics, Vol. 6*, edited by F. Seitz and D. Turnbull (Academic, New York), p. 1.
- Riemann, B., 1860, "Über die Fortpflanzung ebener Luftwellen von endlicher Schwingungsweite," in *Collected Works of Bernhard Riemann*, 1953, edited by H. Weber (Dover, New York), p. 157.
- Russo, G., and A. Anile, 1987, "Stability Properties of Relativistic Shock Waves: Basic Results," *Phys. Fluids* **30**, 2406.
- Shearer, M., 1983, "Admissibility Criteria for Shock Wave Solutions of a System of Conservation Laws of Mixed Type," *Proc. R. Soc. Edinburgh, Sec. A* **93**, 233.
- Shearer, M., 1988, "Loss of Strict Hyperbolicity of the Buckley-Leverett Equations for Three Phase Flow in a Porous Medium," in *IMA Volumes in Mathematics and its Applications* **11**, edited by M. Wheeler (Springer, New York), p. 263.
- Shearer, M., D. Schaeffer, D. Marchesin, and P. Paes-Leme, 1987, "Solution of the Riemann Problem for a Prototype 2×2 System of Non-Strictly Hyperbolic Conservation Laws," *Arch. Ration. Mech. Anal.* **97**, 299.
- Sidorenko, A., 1982, "Wave Adiabatic Curves for Media with Arbitrary State Equation," *Prikl. Mat. Mekh.* **46**, 241 [J. Appl. Math. Mech. **46**, 180 (1982)].
- Slemrod, M., 1983, "Admissibility Criteria for Propagating Phase Boundaries in a van der Waals Fluid," *Arch. Ration. Mech. Anal.* **81**, 303.
- Smith, R., 1979, "The Riemann Problem in Gas Dynamics," *Trans. Am. Math. Soc.* **249**, 1.
- Smoller, J., 1982, *Shock Waves and Reaction-Diffusion Equations* (Springer, New York).
- Strehlow, R., 1970, "Multi-Dimensional Detonation Wave Structure," *Astronaut. Acta* **15**, 345.
- Tang, Z., and T. Ting, 1987, "Wave Curves for Riemann Problems of Plane Waves in Simple Isotropic Elastic Solids," *Int. J. Eng. Sci.* **25**, 1343.
- Thompson, P., 1971, "A Fundamental Derivative of Gas Dynamics," *Phys. Fluids* **14**, 1843.
- Thompson, P., 1972, *Compressible-Fluid Dynamics* (McGraw-Hill, New York), Sec. 5.2.
- Thompson, P., G. Carafano, and Y.-G. Kim, 1986, "Shock Waves and Phase Changes in a Large-Heat-Capacity Fluid Emerging from a Tube," *J. Fluid Mech.* **166**, 57.
- van Leer, B., 1979, "Towards the Ultimate Conservative Difference Scheme. V. A Second-Order Sequel to Godunov's Method," *J. Comput. Phys.* **32**, 101.
- Van Moorhem, W., and A. George, 1975, "On the Stability of Plane Shocks," *J. Fluid Mech.* **68**, 97.
- Wendroff, B., 1972, "The Riemann Problem for Materials with Non-Convex Equations of State: I, Isentropic Flow; II, General Flow," *J. Math. Anal. Appl.* **38**, 454 and 640.
- Wendroff, B., 1988, private communication.
- Weyl, H., 1949, "Shock Waves in Arbitrary Fluids," *Commun. Pure Appl. Math.* **II**, 103.
- Whitham, G., 1974, *Linear and Nonlinear Waves* (Wiley, New York), Secs. 8.1 and 8.8.
- Wightman, A. S. 1979, "Convexity and the Notion of Equilibrium State in Thermodynamics and Statistical Mechanics," introduction to *Convexity in the Theory of Lattice Gases*, by Robert B. Israel (Princeton University, Princeton, N.J.).
- Zel'dovich, Ya., and Yu. Raizer, 1966, *Physics of Shock Waves and High-Temperature Hydrodynamic Phenomena* (Academic, New York).